

CLARKSON UNIVERSITY

Modeling Reactive Distillation Dynamics

A Dissertation

by

Richard Baur

Department of Chemical Engineering

Submitted in partial fulfillment of the requirements

for the degree of Doctor of Philosophy

(Chemical Engineering)

7 April, 2000

Accepted by the Graduate School

Date

Dean

**The undersigned have examined the dissertation
entitled: “Modelling Reactive Distillation Dynamics”
presented by Richard Baur, a candidate for the degree
of Doctor of Philosophy in Chemical Engineering, and
hereby certify that it is worthy of acceptance.**

Date

Prof. R. Taylor, Advisor

Prof. G. A. Campbell

Prof. R. S. Subramanian

Prof. R. J. McCluskey

Prof. D. Powers

Abstract

In this thesis a nonequilibrium (NEQ) cell model is developed to describe the dynamic operation of reactive distillation (RD) tray columns. The features of the model are: (1) use of the Maxwell-Stefan equations for describing mass transfer between fluid phases, (2) chemical reactions are assumed to take place only in the liquid phase, (3) coupling between mass transfer and chemical reactions within the diffusion layer is accounted for, and (4) the use of multiple well-mixed cells in the liquid and vapour flow directions accounts for staging in either fluid phase. When the chemical reactions are suppressed, the model describes the dynamic behaviour of conventional distillation columns. We demonstrate the utility of the dynamic NEQ cell model by means of several cases studies: (a) synthesis of methyl tert-butyl ether (MTBE), (b) metathesis of 2-propene, (c) hydration of ethylene oxide to ethylene glycol, and (d) distillation of methanol – *iso*-propanol – water.

An extensive model comparison between commonly used equilibrium models, non-equilibrium models and multiple cell models reveals a *qualitatively* different steady state behavior with regard to conversion and selectivity. Increasing mass transfer resistance tends to narrow the region of steady state multiplicity. The qualitative differences of the model predications are also reflected in their dynamic behavior. For a process exhibiting multiple steady states, the models can lead to qualitatively different responses to feed flow disturbances. Due to differences in the hold-up of packed and tray columns the dynamic responses of an RD column are sensitive to the hardware choice. Furthermore, the introduction of staging in the liquid and vapour phases not only influences the steady state performance, by increasing reaction conversion and separation capability, but also has an significant influence on the column dynamics.

The overall conclusion of this thesis is that nonequilibrium dynamic model, taking proper account interphase mass transfer and of liquid and vapour staging in a column, are essential for developing the proper description of RD column dynamics and for developing appropriate control strategies.



Acknowledgements

I would like to thank all the people who supported my research and me during the past three and half years. Foremost have been my advisors Prof. R. Taylor at Clarkson University and Prof. R. Krishna at the University of Amsterdam. I appreciated very much their guidance, suggestions, their manner of carrying out research and their intriguing way of working and thinking. I also would like to thank my research colleagues Arnoud, Jasper and Rohit who have always been of great help in any regard. Special thanks belong to Dr. Harry Kooijman for his valuable advice and ideas.

Looking back, my stay in Potsdam and Amsterdam was a unique opportunity and experience, which wouldn't have been so joyful without all my friends: Lu, Ioana, Andreas, Sven, Jen, Rich, Fred, Pericles, Bart and Julia. I also would like to thank my parents and my sister, Bettina, for supporting me throughout my Ph.D.

BP-Amoco Chemicals are gratefully acknowledged for their support of this research and Hyperotech Inc (now AEA Technology, UK). for their partial support

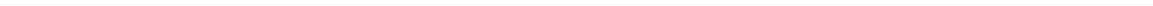
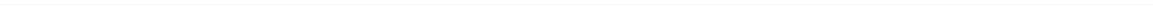


Table of Contents

Abstract	v
Acknowledgements	vii
Table of Contents	ix
List of Tables	xi
List of Figures	xiii
Nomenclature	xxi
<i>Chapter 1</i> Introduction	1
Part I. Steady-state models for reactive distillation	
<i>Chapter 2</i> Comparison of Equilibrium and Nonequilibrium Stage Models	17
<i>Chapter 3</i> Influence of Column Hardware on the Performance.....	41
<i>Chapter 4</i> Mass Transfer Efficiencies in Reactive Distillation.....	47
<i>Chapter 5</i> Influence of Mass Transfer on Distillation Trajectories	59
Part II. Dynamic models for reactive distillation	
<i>Chapter 6</i> Development of a Dynamic Nonequilibrium Stage Model.....	69
<i>Chapter 7</i> Development of a Dynamic Nonequilibrium Cell Model	95
Conclusions	121
References	123



List of Tables

Chapter 2

Table 1. Thermodynamic, physical property and mass transfer models incorporated into the reactive distillation program.	23
Table 2. Tray Specifications for the rectifying and stripping sections in the MTBE column.	28
Table 3. Sieve tray specification for ethylene glycol reactive distillation column.....	34
Table 4. Steady-states for ethylene glycol column, using EQ model.....	37

Chapter 4

Table 1. Sieve tray specification for ethylene glycol reactive distillation column.....	51
Table 2. Sieve tray specification for metathesis RD column	56

Chapter 5

Table 1. NRTL parameters for the mixtures methanol- iso-propanol-water and benzene - iso-propanol- n-propanol	61
Table 2. Specification of sieve tray column used in the simulations.	62

Chapter 6

Table 1. Hydrodynamics and mass transfer correlations for sieve trays and packings incorporated in our dynamic NEQ model for RD columns	78
Table 2. Model equations for single stage nonequilibrium model	79

Chapter 7

Table 1. Model equations for dynamic nonequilibrium cell model.....	102
Table 2. Specification of sieve tray columns used in case studies.....	105

List of Figures

Chapter 1

Figure 1. Processing schemes for a reaction sequence $A+B \rightleftharpoons C+D$ where C and D are both desired products.	2
Figure 2. Processing schemes for the production of methyl acetate.	3
Figure 3. (a) Reactive distillation concept for synthesis of MTBE. (b) Reactive distillation concept for the hydration of ethylene oxide to ethylene glycol. (c) Reactive distillation concept for reaction between benzene and propene to form cumene. (d) Reactive distillation concept for reaction production of propylene oxide from propylene chlorohydrin and lime.	4
Figure 4. Hydrodesulphurisation of gas oil carried out in (a) co-current trickle bed reactor and (b) counter-current RD unit.	5
Figure 5. Counter-current vapour-liquid contacting in trayed columns.	7
Figure 6. Counter-current vapour-liquid contacting in packed columns.	7
Figure 7. Flow regimes on trays.	8
Figure 8. Various “tea-bag” configurations. Catalyst particles need to be enveloped in wire gauze packings and placed inside RD columns.	9
Figure 9. Horizontally disposed (a) wire gauze gutters and (b) wire gauze tubes containing catalyst.	10
Figure 10. Catalyst bales licensed by Chemical Research and Licensing.	10
Figure 11. Structured catalyst-sandwiches.	11
Figure 12. Catalytically active Raschig ring. Adapted from Sundmacher (1995).	11
Figure 13. Catalyst envelopes placed along the liquid flow path	13
Figure 14. Counter-current vapour-liquid-catalyst contacting in trayed column.	13

Figure 15. Transport processes in RD. (a) homogeneous liquid phase reaction, and (b) heterogeneous catalysed reactions. Adapted from Sundmacher (1995).	14
Figure 16. Length and time scales in RD. Adapted from Sundmacher (1995).	15

Chapter 2

Figure 1. Typical configuration of a reactive distillation tray column.	19
Figure 2. Schematic representation of the nonequilibrium model describing interphase mass transfer, with liquid phase chemical reaction.	21
Figure 3. Schematic of the nonequilibrium cell model.	24
Figure 4. Configuration of the MTBE synthesis column, following Jacobs and Krishna (1993).	27
Figure 5. High and low conversion branches obtained by EQ and NEQ simulations.	29
Figure 6. The <i>iso</i> -butene consumption rates for the (a) high and (b) low conversion branches obtained by EQ and NEQ simulations.	31
Figure 7. Bifurcation diagram for the EQ and models NEQ (both Maxwell-Stefan and equal diffusivities) with the bottoms product flow rate as continuation parameter.	32
Figure 8. Configuration of reactive distillation column for hydration of ethylene oxide to ethylene glycol.	33
Figure 9. Equilibrium model calculations for the ethylene glycol process.	35
Figure 10. Nonequilibrium model calculations for the ethylene glycol process for a column of diameter 1.7 m.	35
Figure 11. Nonequilibrium model calculations for the ethylene glycol process for a column of diameter 3.0 m.	36
Figure 12. Formation of by-product DEG versus formation of EG for various tray configurations, specified in Table 3 and for various mixing model assumptions .37	

Figure 13. Hydrodynamic and mass transfer parameters for various tray configurations 1,3,4 and 5 specified in Table 3. 38

Chapter 3

Figure 1. Catalyst configurations in (a) packed column and (b) tray column. 43

Figure 2. Tray configurations 43

Figure 3. Bifurcation diagrams for tray and packed columns for various operating. 45

Figure 4. Bifurcation diagrams for tray column (a) influence of liquid flow passes. (b) influence of staging of the liquid phase..... 46

Chapter 4

Figure 1. (a) Configuration of reactive distillation column for hydration of ethylene oxide to ethylene glycol. (b) Equivalent configuration of a non-reactive column..... 49

Figure 2. Component efficiencies for EO, water, EG and DEG for reactive and non-reactive operation 50

Figure 3. Configuration of the MTBE synthesis column, following Jacobs and Krishna (1993). The column consists of 17 stages. 52

Figure 4. (a) Five-liquid-pass sieve tray configuration. (b) and (c) The reactive section consists of catalyst envelopes placed along the liquid flow path. 53

Figure 5. Bifurcation diagram for sieve tray MTBE RD column calculated with NEQ model..... 53

Figure 6. Component efficiencies for iso-butene, MeOH, MTBE and n-butene for reactive and non-reactive operations. 54

Figure 7. Configuration of the RD column for metathesis of 2-pentene. 55

Figure 8. Component efficiencies for 2-pentene, 2-butene and 3-hexene in RD column calculated with NEQ 1×1 cell and 3×3 cell models.	57
--	----

Chapter 5

Figure 1. Residue curve maps for the systems (a) methanol- <i>iso</i> -propanol-water and (b) benzene - <i>iso</i> -propanol- <i>n</i> -propanol.	61
Figure 2. Composition trajectories for the system methanol- <i>iso</i> -propanol-water....	63
Figure 3. Component vapour phase Murphree tray efficiencies for the system methanol- <i>iso</i> -propanol-water.....	64
Figure 4. Composition trajectories for the system benzene- <i>iso</i> -propanol - <i>n</i> -propanol in a 40-stage sieve tray column.	65
Figure 5. Component vapour phase Murphree tray efficiencies for the system benzene- <i>iso</i> -propanol - <i>n</i> -propanol.	66

Chapter 6

Figure 1. Schematic representation of a NEQ stage	74
Figure 2. Composition and temperature profiles within the “films”.....	75
Figure 3. Condenser and reboiler model configurations.....	80
Figure 4. Configuration of the MTBE synthesis column, following Jacobs and Krishna (1993). The column consists of 17 stages.	81
Figure 5. Bifurcation diagram for sieve tray configuration for three different model implementations, EQ, NEQ and Equal Efficiencies.....	82
Figure 6. Dynamic response to a 5% increase in the MeOH feed flow. (a) response of EQ model and (b) response of NEQ model.....	83

Figure 7. Dynamic response to a 5% increase in the MeOH feed flow. Responses of EQ, NEQ and Equal Efficiency models.	84
Figure 8. Dynamic response to a (a) 10% increase or (b) 10% decrease in the MeOH feed flow.	85
Figure 9. MTBE production rates for (a) EQ model and (b) NEQ model for +10 % MeOH feed flow perturbation.	86
Figure 10. Dynamic response to a (a) 10% increase or (b) 15% decrease in the iso-butene feed flow.	87
Figure 11. Dynamic response to a (a) 15% decrease or (b) 15% increase in the n-butene feed flow, 1 h after column start-up and lasting for 1 h.	88
Figure 12. Bifurcation diagrams for sieve tray and packed column configurations for MTBE synthesis.	89
Figure 13. Dynamic response to a (a) 7% increase or (b) 7 % decrease in the MeOH feed flow, 1 h after column start-up and lasting for 1 h.	90
Figure 14. Dynamic response to a (a) 3% increase or (b) 15% decrease in the iso-butene feed flow, 1 h after column start-up and lasting for 1 h.	91
Figure 15. Dynamic response to a (a) 5% decrease or (b) 15% increase in the n-butene feed flow, 1 h after column start-up and lasting for 1 h.	92

Chapter 7

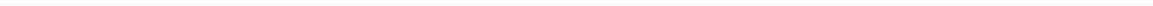
Figure 1. (a) Schematic representation of a NEQ cell model for a stage j. (b) Balance relations for a representative cell. (c) Composition and temperature profiles within the vapour and liquid “films”	97
Figure 2. Configuration of the 2-propene metathesis RD column.	104
Figure 3. Dynamic response of metathesis RD column to feed perturbations. Comparison of the response of NEQ 1×1 and NEQ 3×3 models.	106
Figure 4. Residue curve map for methanol – <i>iso</i> -propanol - water.	107

Figure 5. Configuration of sieve tray column for separating methanol – <i>iso</i> -propanol - water.....	108
Figure 6. Steady state column composition trajectories for distillation of methanol (1) – <i>iso</i> -propanol (2) – water (3). Comparison of the response of EQ, NEQ 1 × 1 and NEQ 3 × 3 models.	109
Figure 7. Response to step disturbance in feed composition for distillation of methanol (1) – <i>iso</i> -propanol (2) – water (3). Comparison of the responses of EQ, NEQ 1 × 1 and NEQ 3 × 3 models.	109
Figure 8. Tray-12 composition response to pulse and step disturbance in feed composition for distillation of methanol (1) – <i>iso</i> -propanol (2) – water (3). Comparison of the responses of EQ, NEQ 1 × 1 and NEQ 3 × 3 models.	110
Figure 9. Configuration of the MTBE synthesis column, following Jacobs and Krishna (1993).	111
Figure 10. Bifurcation diagram for three different model implementations, NEQ 1 × 1, NEQ 2 × 2 and NEQ 3 × 3 models. (a) and (b) are drawn to different scales.	112
Figure 11. Comparison of the bifurcation diagram for NEQ 3 × 3 cell model with EQ model. (a) and (b) are drawn to different scales.	113
Figure 12. Dynamic response obtained with the NEQ 3 × 3 cell model for MeOH feed flow perturbations (+3%, +5% and +7%), 1 h after column start-up.....	114
Figure 13. Dynamic response obtained with the EQ, NEQ 2 × 2 and NEQ 3 × 3 models to MeOH feed flow perturbations of (a) +3%, (b) +5% and (c) +7%....	114
Figure 14. Dynamic response obtained with the EQ and NEQ 3 × 3 models to a -15% feed flow perturbations of n-butene, 1 h after column start-up.	115
Figure 15. Configuration of RD column for hydration of ethylene oxide to ethylene glycol.....	116
Figure 16. Dynamic response to a 10% increase in the water feed	117
Figure 17. Composition phase portraits obtained during feed perturbations of EO (to all stages 2,3,4,5,6) and H ₂ O (to stage 2) to various extents.	117

Figure 18. Production rates of EG and DEG along the reactive stages at time $t = 0$ and $t = 1.5$ h. Response to a -10% perturbation of EO feed to all reactive stages. NEQ model with $m = 1$ and $n = 1$ 118

Figure 19. Dynamic responses of the temperature, EG mole fraction, DEG mole fraction of the bottom product stream to a 10% decrease in the EO feed. 119

Figure 20. Composition phase portraits (DEG vs EG composition in bottom product) during transient response to a 10% decrease in the EO feed flow 119



Nomenclature

a	interfacial area per unit volume, m^{-1}
A	interfacial area, m^2
A_{bub}	active (bubbling) area on tray, m^2
A_{ij}	NRTL parameters, J/mol
c	number of components, dimensionless
c_t	total concentration, mol m^{-3}
$D_{i,k}$	Maxwell-Stefan diffusivity, $\text{m}^2 \text{ s}^{-1}$
D_L	Fick diffusivity for binary liquid phase mixture, m^2/s
E	energy transfer rate, J s^{-1}
E_i^{MV}	overall Murphree tray efficiency, dimensionless
HETP	Height equivalent to a theoretical plate, m
f	component feed stream, mol s^{-1}
F	Feedstream, mol s^{-1}
h_{cl}	clear liquid height, m
h_t	tray spacing, m
h_w	weir height, m
h	heat transfer coefficient, $\text{W m}^{-2} \text{ K}^{-1}$
H	molar enthalpy, J mol^{-1}
k_G	vapour phase mass transfer coefficient, m/s
k_L	liquid phase mass transfer coefficient, m/s
K	vapour-liquid equilibrium constant, dimensionless
K_{eq}	metathesis reaction equilibrium constant
L	Liquid flow rate, mol s^{-1}
L_M	interchange liquid flow rate between horizontal rows of cells, mol s^{-1}
m	number of cells along the liquid flow direction
M_j	molar hold-up on stage j , mol

$M_{i,j}$	molar hold-up of component i on stage j , mol
n	number of cells along the vapour flow direction
nL	number of grid cells in liquid diffusion film
nV	number of grid cells in vapour diffusion film
N	Mass transfer rate, mol s ⁻¹
p_j	stage pressure, Pa
Q	Heat duty, J s ⁻¹
Q_L	liquid flow rate across tray, m ³ /s
r	number of reactions, dimensionless
$R_{m,j}$	Reaction rate, mol m ⁻³ s ⁻¹
R	Gas constant, J mol ⁻¹ K ⁻¹
T	Temperature, K
V	Vapour flowrate, mol s ⁻¹
W	weir length, m
x	mole fraction in the liquid phase, dimensionless
y	mole fraction in the vapour phase, dimensionless
$\overline{y_{iL}}$	average composition of the vapour leaving the tray, dimensionless
y_{iE}	composition of the vapour entering the tray, dimensionless
y_i^*	composition of the vapour in equilibrium with the liquid leaving the tray, dimensionless
z	mole fraction in the feed stream, dimensionless

Greek

α	non-randomness parameter in NRTL equation, dimensionless
e	volumetric hold-up of phase, m ³
d	diffusion film thickness, m
h	dimensionless coordinate, dimensionless
k	mass transfer coefficient, m s ⁻¹
m	Chemical potential, J mol ⁻¹

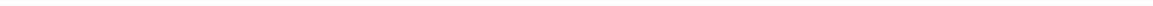
r_G	density of gas mixture, kg/m ³
n	stoichiometric coefficient, dimensionless

subscripts

i	component index
in	stream entering cell
I	Referring to interface
j	stage index
k	index
m	reaction index
mm	index for cells in a row
nn	index for cells in a column
t	total

superscripts

F	Referring to feed stream
I	Referring to interface
L	Referring to liquid phase
Lf	Referring to liquid diffusion film
V	Referring to vapour phase
Vf	Referring to vapour diffusion film



Chapter 1

Introduction

The addition of an in-situ separation function in a reactor offers the promise of improved conversion and selectivity, and, for this reason, there is considerable academic and industrial interest in the area of reactive distillation. The term catalytic distillation is also used for such systems where a catalyst (homogeneous or heterogeneous) is used to accelerate the reaction. In this thesis we use the generic name reactive distillation, with the acronym RD, to cover both catalysed or uncatalysed reactions systems.

Before the objectives of the thesis can be laid out, let us examine the specific benefits of RD.

Why RD?

Let us begin by considering a reversible reaction scheme $A+B \rightleftharpoons C+D$ where the boiling points of the components follow the sequence A, C, D and B. The traditional flow-sheet for this process consists of a reactor followed by a sequence of distillation columns; see Fig. 1 (a). The mixture of A and B is fed to the reactor, where the reaction takes place in the presence of a catalyst and reaches equilibrium. A distillation train is required to produce pure products C and D. The unreacted components, A and B, are recycled back to the reactor. In practice the distillation train could be much more complex than the one portrayed in Fig. 1 (a) if one or more azeotropes are formed in the mixture. The alternative RD configuration is shown in Fig.1 (b). The RD column consists of a reactive section in the middle with non-reactive rectifying and stripping sections at the top and bottom. The task of the rectifying section is to recover reactant B from the product stream C. In the stripping section, the reactant A is stripped from the product stream D. In the reactive section the products are separated in-situ, driving the equilibrium to the right and preventing any undesired side reactions between the reactants A (or B) with the product C (or D). For a properly designed RD column, virtually 100% conversion can be achieved.

The most spectacular example of the benefits of RD is in the production of methyl acetate. The acid catalysed reaction $\text{MeOH} + \text{AcOH} \rightleftharpoons \text{MeOAc} + \text{H}_2\text{O}$ was traditionally carried out using the processing scheme shown in Fig. 2 (a), which consists of one reactor and a train of nine distillation columns. In the RD implementation (see Fig 2 (b)) only one column is required and nearly 100 % conversion of the reactant is achieved. The capital and operating costs are significantly reduced.

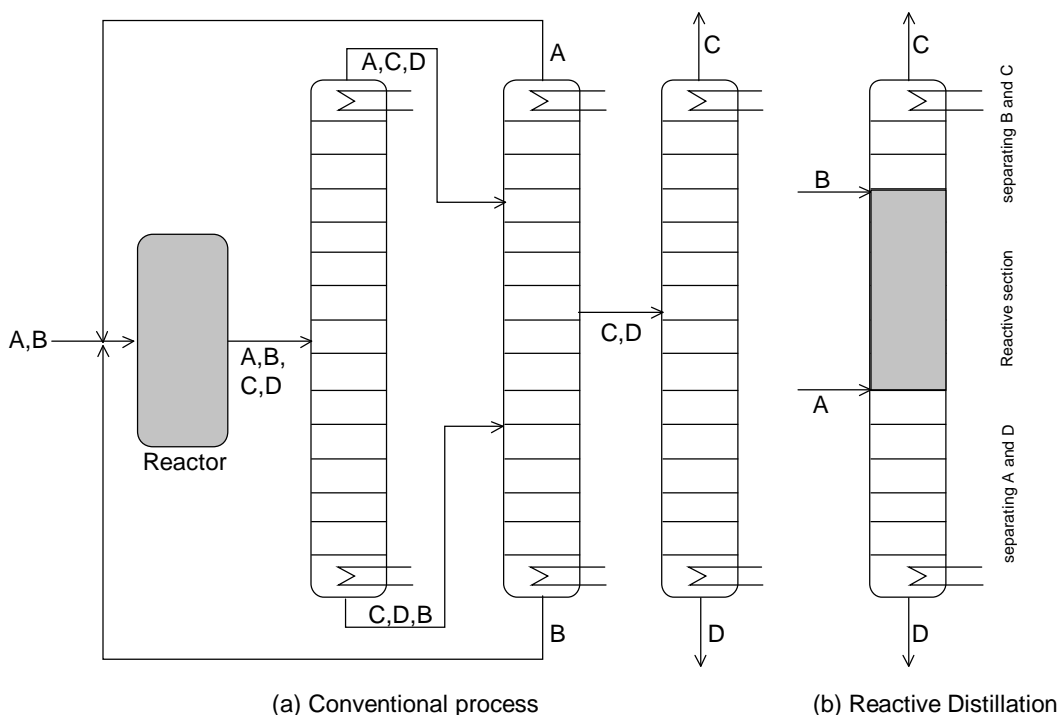


Figure 1. Processing schemes for a reaction sequence $A + B \rightleftharpoons C + D$ where C and D are both desired products. (a) Typical configuration of a conventional process consisting of a reactor followed by a distillation train. (b) The reactive distillation configuration. The components A , C , D and B have increasing boiling points. The reactive sections are indicated by grid lines. Adapted from Stichlmair and Frey (1999).

For the acid catalysed reaction between iso-butene and methanol to form methyl tert-butyl ether, $\text{isobutene} + \text{MeOH} \rightleftharpoons \text{MTBE}$, the traditional reactor-followed-by-distillation concept is particularly complex because the reaction mixture leaving the reactor forms three minimum boiling azeotropes. The RD implementation requires only one column to which the butenes feed (consisting of a mixture of n-butene, which is non-reactive, and iso-butene which is reactive) and methanol are fed near the bottom of the reactive section. The RD concept shown in Fig. 3 (a) is capable of achieving close to 100% conversion of iso-butene and methanol, along with suppression of the formation of the unwanted dimethyl ether (Sundmacher, 1995). Also, some of the azeotropes in the mixture are “reacted away” (Doherty and Buzad, 1992).

For the hydration of ethylene oxide to mono-ethylene glycol, $\text{EtO} + \text{H}_2\text{O} \rightarrow \text{EG}$, the RD concept, shown in Fig. 3 (b) is advantageous for two reasons (Ciric and Gu, 1994). Firstly, the side reaction $\text{EtO} + \text{EG} \rightarrow \text{DEG}$ is suppressed because the concentration of EtO in the liquid phase is kept low because of its high volatility. Secondly, the high heat of reaction is utilised to vaporise the liquid phase mixtures on the trays. To achieve the same

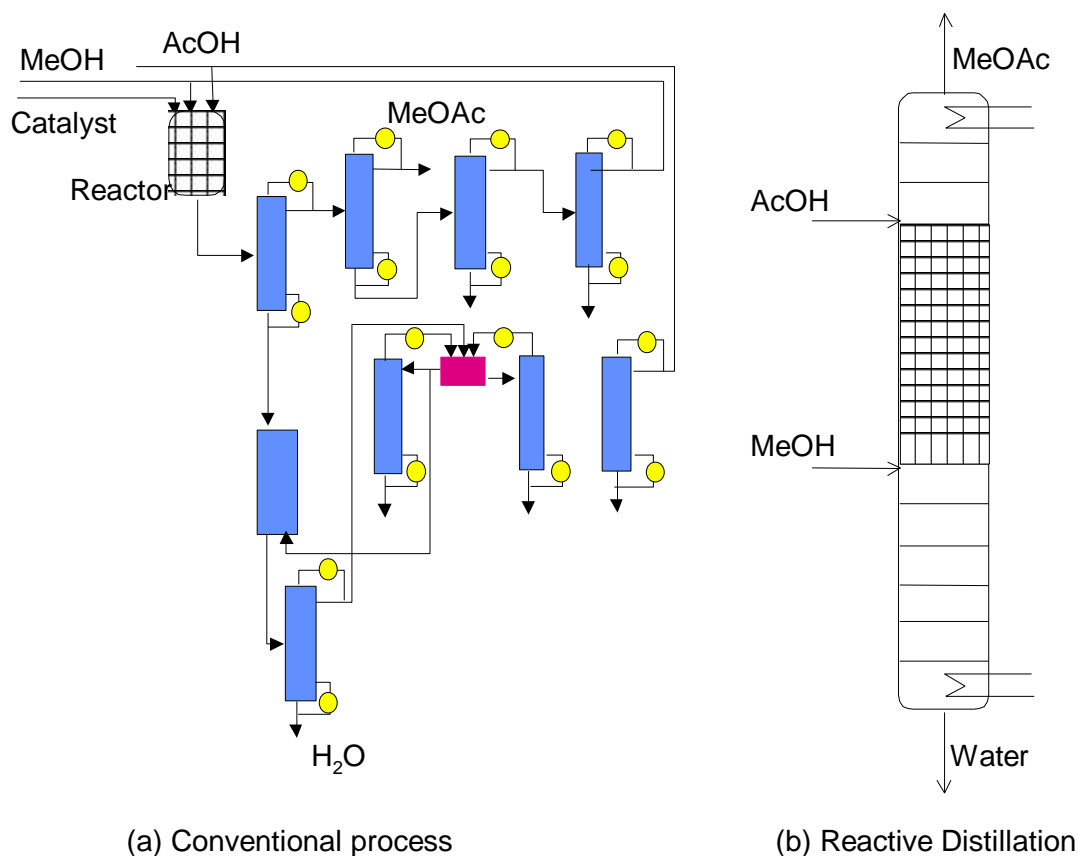


Figure 2. Processing schemes for the esterification reaction $\text{MeOH} + \text{AcOH} \rightleftharpoons \text{MeOAc} + \text{H}_2\text{O}$
 (a) Conventional processing scheme consisting of one reactor followed by nine distillation columns. (b) The reactive distillation configuration. The reactive sections are indicated by grid lines. Adapted from Sirola (1995).

selectivity to EG in a conventional liquid phase plug flow reactor would require the use of 60% excess water (Ciric and Gu, 1994). Similar benefits are also realised for the hydration of iso-butene to tert-butanol (Velo et al., 1988) and hydration of 2-methyl-2-butene to tert-amyl alcohol (Gonzalez and Fair, 1997).

Several alkylation reactions, $\text{Aromatic} + \text{Olefin} \rightleftharpoons \text{Alkylaromatic}$, are best carried out using the RD concept not only because of the shift in the reaction equilibrium due to in-situ separation but also due to the fact that the undesirable side reaction, $\text{AlkylAromatic} + \text{Olefin} \rightleftharpoons \text{Di-Alkylaromatic}$, is suppressed. The reaction of propene with benzene to form cumene, $\text{Benzene} + \text{Propene} \rightleftharpoons \text{Cumene}$ (Shoemaker and Jones, 1987; see Fig. 3 (c)), is advantageously carried out in a RD column because not only is the formation of the undesirable di-isopropylbenzene suppressed, but also the problems posed by high exothermicity of the reaction for operation in a conventional packed bed reactor

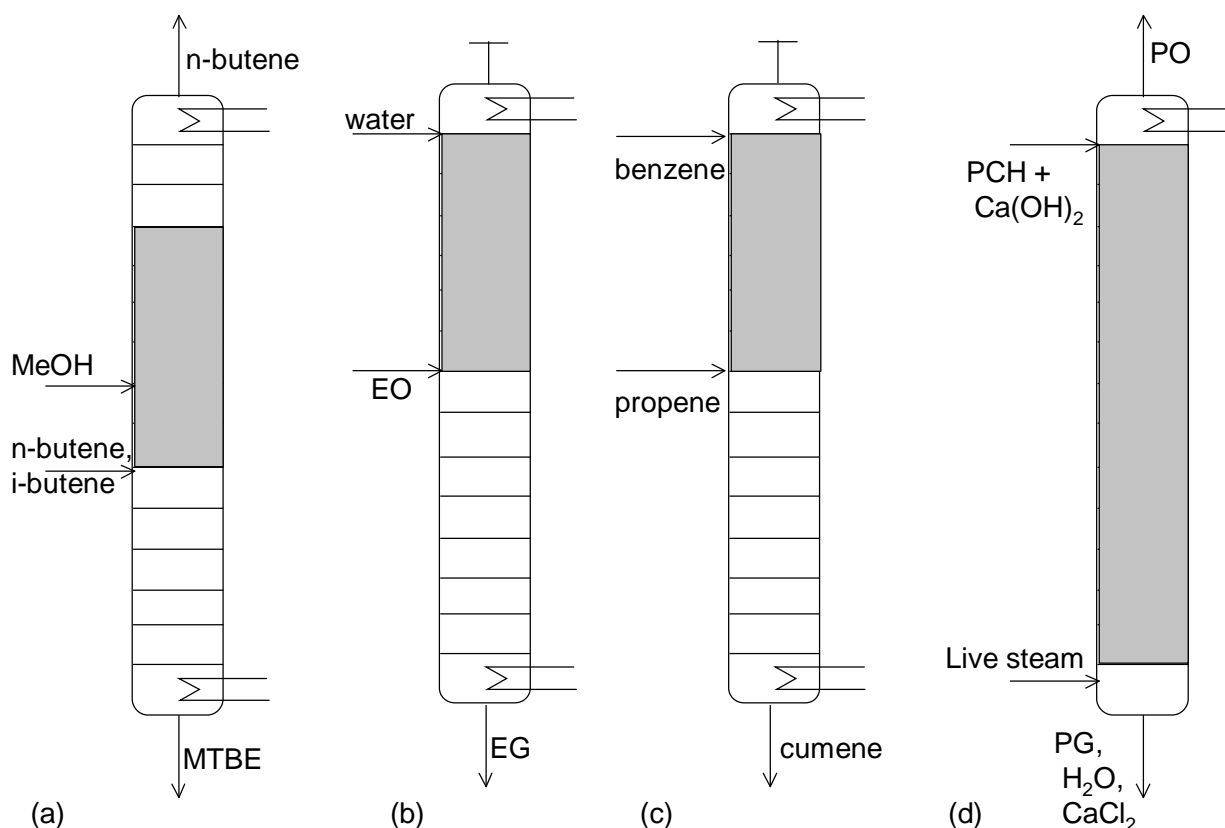


Figure 3. (a) Reactive distillation concept for synthesis of MTBE from the acid catalysed reaction between MeOH and iso-butene. The butene feed is a mixture of reactive iso-butene and non-reactive n-butene. (b) Reactive distillation concept for the hydration of ethylene oxide to ethylene glycol. (c) Reactive distillation concept for reaction between benzene and propene to form cumene. (d) Reactive distillation concept for reaction production of propylene oxide from propylene chlorohydrin and lime. The reactive sections are indicated by grid lines

are avoided. Hot spots and runaway problems are alleviated in the RD concept where liquid vaporisation acts as a thermal flywheel. The alkylation of isobutane to isooctane, $\text{isobutane} + \text{n-butene} \rightleftharpoons \text{isooctane}$, is another reaction that benefits from a RD implementation because in-situ separation of the product prevents further alkylation: $\text{isooctane} + \text{n-butene} \rightleftharpoons \text{C}_{12}\text{H}_{24}$ (Doherty and Buzad, 1992).

The reaction between propylene chlorohydrin (PCH) and Ca(OH)_2 to produce propylene oxide (PO) is best implemented in an RD column, see Fig. 3 (d). Here the desired product PO is stripped from the liquid phase by use of live steam, suppressing hydrolysis to propylene glycol (Bezzo et al., 1999).

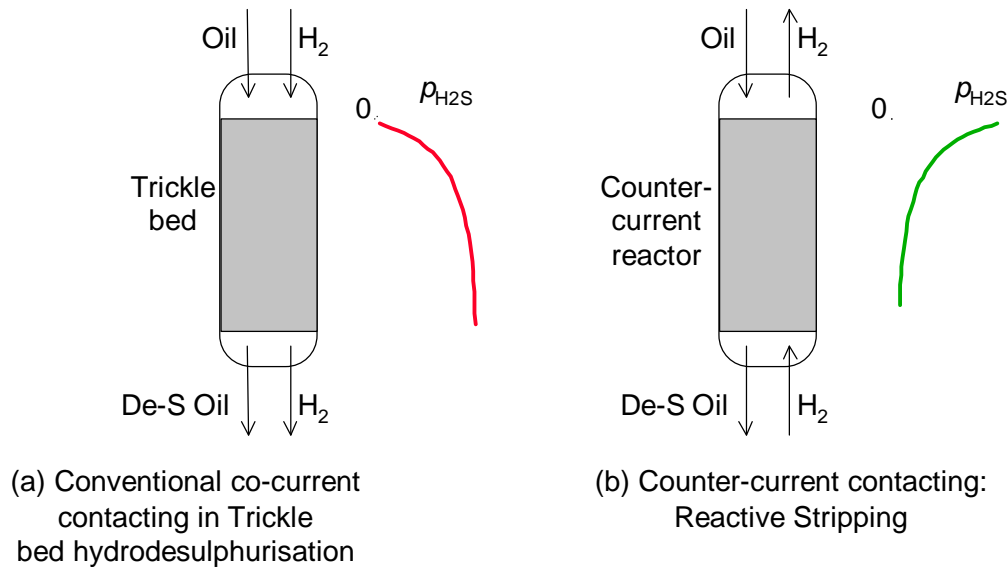


Figure 4. Hydrodesulphurisation of gas oil carried out in (a) co-current trickle bed reactor and (b) counter-current RD unit.

Co-current gas-liquid downflow trickle bed reactors are widely applied for hydroprocessing of heavy oils. This co-current mode of operation is disadvantageous in most hydroprocesses (Krishna and Sie, 1994), and counter-current flow of gas and liquid would be much more desirable (cf. Fig. 4). The counter-current reactor shown in Fig. 4 (b) is essentially a RD column wherein the H_2S is *stripped* from the liquid phase at the bottom and carried to the top. The quantitative advantages of the RD implementation for hydroprocessing are brought out in a design study carried out by Van Hasselt (1999). For a 20,000 bbl/day hydrodesulphurisation unit with a target conversion of 98% conversion of sulphur compounds, the catalyst volume required for a conventional trickle bed reactor is about 600 m^3 . For counter-current RD implementation the catalyst volume is reduced to about 450 m^3 .

From the foregoing examples, the benefits of RD can be summarised as follows:

- Simplification or elimination of the separation system can lead to significant capital savings
- Improved conversion of reactant approaching 100 %. This increase in conversion gives a benefit in reduced recycle costs
- Improved selectivity. Removing one of the products from the reaction mixture or maintaining a low concentration of one of the reagents can lead to reduction of the rates of side reactions and hence improved selectivity for the desired products.
- Significantly reduced catalyst requirement for the same degree of conversion

- (e) Avoidance of azeotropes. RD is particularly advantageous when the reactor product is a mixture of species that can form several azeotropes with each other. RD conditions can allow the azeotropes to be “reacted away” in a single vessel.
- (f) Reduced by-product formation
- (g) Heat integration benefits. If the reaction is exothermic, the heat of reaction can be used to provide the heat of vaporisation and reduce the reboiler duty.
- (h) Avoidance of hot spots and runaways using liquid vaporisation as thermal fly wheel.

The constraints and difficulties in RD implementation

Against the above mentioned advantages of RD, there are several constraints and foreseen difficulties (Towler and Frey, 2000)

- (a) Volatility constraints. The reagents and products must have suitable volatility to maintain high concentrations of reactants and low concentrations of products in the reaction zone.
- (b) Residence time requirement. If the residence time for the reaction is long, a large column size and large tray hold-ups will be needed and it may be more economic to use a reactor-separator arrangement.
- (c) Scale up to large flows. It is difficult to design RD processes for very large flow rates because of liquid distribution problems in packed RD columns.
- (d) Process conditions mismatch. In some processes the optimum conditions of temperature and pressure for distillation may be far from optimal for reaction and vice versa.

Hardware aspects

For homogeneous RD processes, counter-current vapour-liquid contacting, with sufficient degree of staging in the vapour and liquid phases, can be achieved in a multi-tray column (cf. Fig. 5) or a column with random or structured packings (cf. Fig. 6). The hardware design information can be found in the standard sources for conventional distillation design (Fair et al., 1997; Lockett, 1986; Stichlmair and Fair, 1998). The Hatta number for most RD applications is expected to be smaller than about unity (Sundmacher et al., 1994) and the froth regime is usually to be preferred on the trays (cf. Fig. 7) because of the desire to maintain high liquid hold-up on the trays. High liquid hold-ups can be realised by use of bubble caps or reverse flow trays with additional sumps to provide ample tray residence time. In the Eastman process for methyl acetate manufacture specially designed high liquid hold-up trays are used (Agreda et al., 1990).

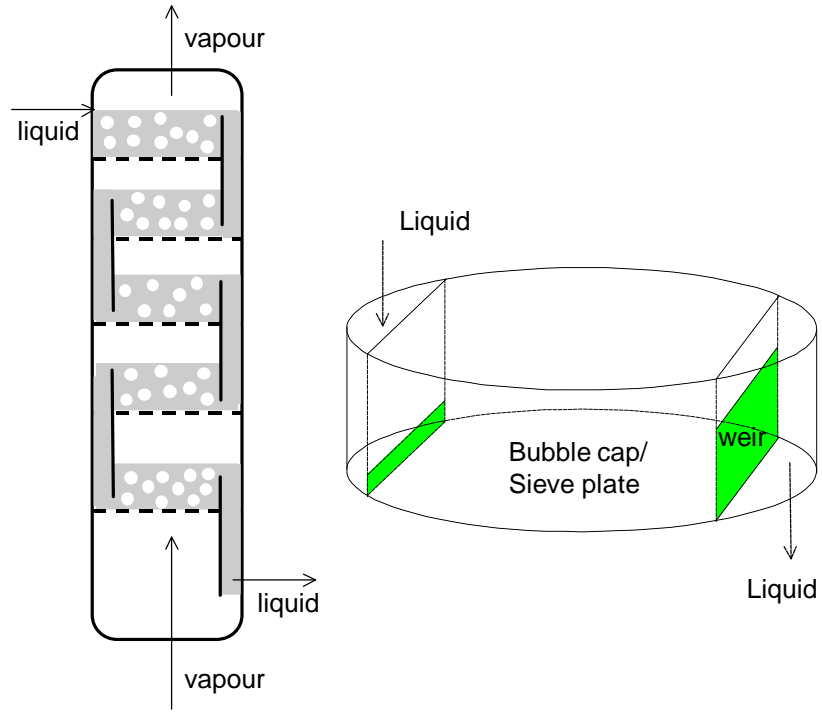


Figure 5. Counter-current vapour-liquid contacting in trayed columns.

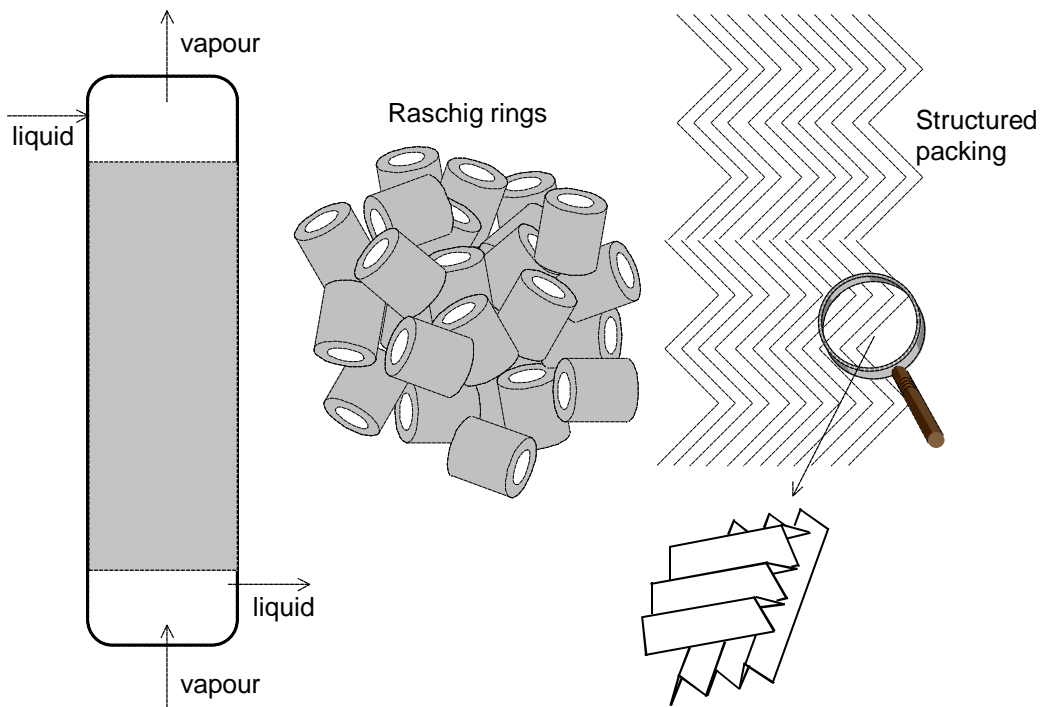


Figure 6. Counter-current vapour-liquid contacting in packed columns.

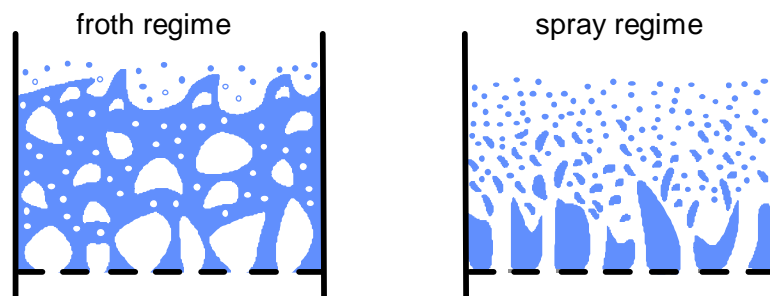


Figure 7. Flow regimes on trays.

Catalytically packed RD columns

For heterogeneously catalysed processes, hardware design poses considerable challenges. The catalyst particle sizes used in such operations are usually in the 1 - 3 mm range. Larger particle sizes lead to intra-particle diffusion limitations. To overcome the limitations of flooding the catalyst particles have to be enveloped within wire gauze envelopes. Most commonly the catalyst envelopes are packed inside the column. Almost every conceivable shape of these catalyst envelopes has been patented; some basic shapes are shown in Figs 10 - 14. These structures are:

1. Porous spheres filled with catalyst inside them (Buchholz et al., 1995; Johnson, 1993); see Fig. 8 (a)
2. Cylindrical shaped envelopes with catalyst inside them (Johnson, 1993); see Fig. 8 (b)
3. Wire gauze envelopes with various shapes: spheres, tablets, doughnuts, etc. (Smith, 1984); see Fig. 8 (c)
4. Horizontally disposed wire-mesh “gutters”, filled with catalyst (Van Hasselt, 1999); see Fig. 9 (a)
5. Horizontally disposed wire mesh tubes containing catalyst (Buchholz et al., 1995; Groten et al., 1998; Hearn, 1993); see Fig. 9 (b).
6. Catalyst particles enclosed in cloth wrapped in the form of bales (Johnson and Dallas, 1994; Smith, 1985). This is the configuration used by Chemical Research & Licensing in their RD technology for etherification, hydrogenation and alkylation of aromatic compounds (Shoemaker and Jones, 1997). The catalyst is held together by fibreglass cloth. Pockets are sewn into a folded cloth and then solid catalyst is loaded into the pockets. The pockets are sewn shut after loading the catalyst and the resulting belt or “catalyst quilt” is rolled with alternating layers of steel mesh to form a cylinder of “catalyst bales” as shown in Fig. 10. The steel mesh creates void volume to allow for vapour traffic and vapour/liquid contacting.]

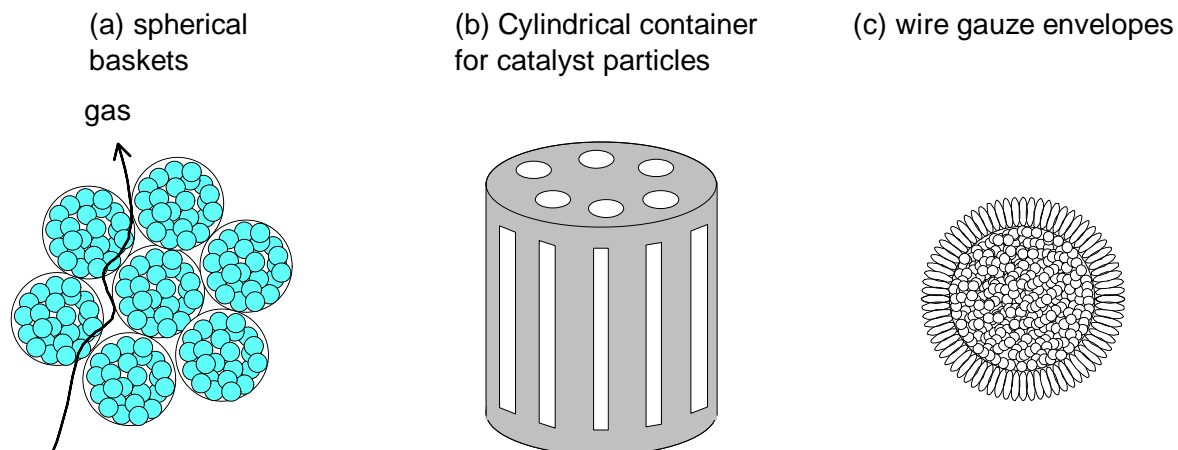
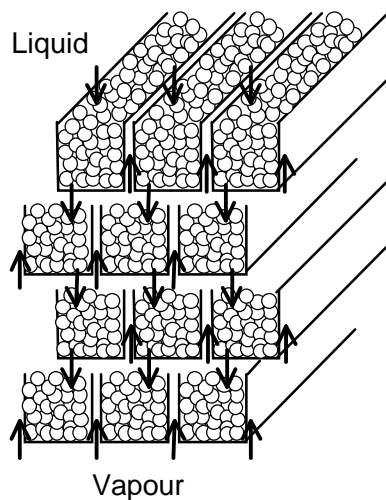


Figure 8. Various “tea-bag” configurations. Catalyst particles need to be enveloped in wire gauze packings and placed inside RD columns.

Scores of these bales are installed in the reactive zone of a typical commercial RD column. Bales are piled on top of each other to give the required height necessary to achieve the desired extent of reaction. When the catalyst is spent the column is shut down and the bales are manually removed and replaced with bales containing fresh catalyst. Improvements to the catalyst bale concept have been made over the years (Johnson, 1993; Crossland et al., 1995). The hydrodynamics, kinetics, and mass transfer characteristics of bale-type packings have recently been published in the open literature (Subawalla et al., 1997; Xu et al., 1995, 1997, 1999).

7. Catalyst particles sandwiched between corrugated sheets of wire gauze (Stringaro, 1991, 1995; Gelbein and Buchholz, 1991; Johnson and Dallas, 1994); see Fig. 11. Such structures are being licensed by Sulzer (called KATAPAK-S) and Koch-Glitsch (called KATAMAX). They consist of two pieces of rectangular crimped wire gauze sealed around the edge, thereby forming a pocket of the order of 1-5 cm wide between the two screens. These catalyst “sandwiches” or “wafers” are bound together in cubes. The resulting cubes are transported to the distillation column and installed as a monolith inside the column to the required height. When the catalyst is spent, the column is shut down and the packing is manually removed and replaced with packing containing fresh catalyst. Information on the fluid dynamics, mixing and mass transfer in such structures are available in the open literature (Bart and Landschützer, 1996; Ellenberger and Krishna, 1999; DeGarmo et al., 1992; Higler et al., 1999c; Moritz and Hasse, 1999). The important advantage of the structured catalyst sandwich structures over the catalyst bales is with respect to radial distribution of liquid. Within the catalyst sandwiches, the liquid follows a criss-crossing flow path. The radial dispersion is about an order of magnitude higher than in conventional packed beds (van Gulijk, 1998). Furthermore, frequent criss-crossing leads to a significant improvement in mass transfer within the sandwich structures (Higler et al., 1999c).

(b) horizontally disposed gutters



(b) horizontally disposed wire gauze tubes

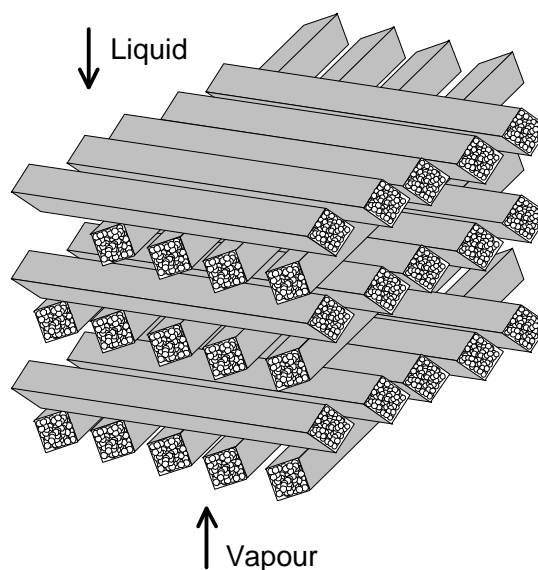


Figure 9. Horizontally disposed (a) wire gauze gutters and (b) wire gauze tubes containing catalyst.

Another alternative is to make the packing itself catalytically active. This is the strategy adopted by Flato and Hoffmann (1992) and Sundmacher and Hoffmann (1994) wherein the Raschig ring shaped packings are made catalytically active; see Fig. 12. The catalyst rings can be prepared by block polymerisation in the annular space. Their activity is quite high, however osmotic swelling processes can cause breakage by producing large mechanical stresses inside the resin. An alternative configuration is the glass supported precipitated polymer prepared by precipitation of styrene-divinylbenzene copolymer, which is subsequently activated by chlorosulphonic acid.

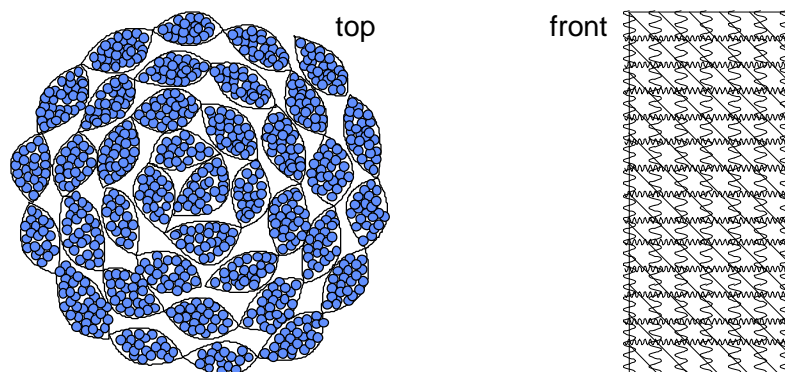


Figure 10. Catalyst bales licensed by Chemical Research and Licensing.

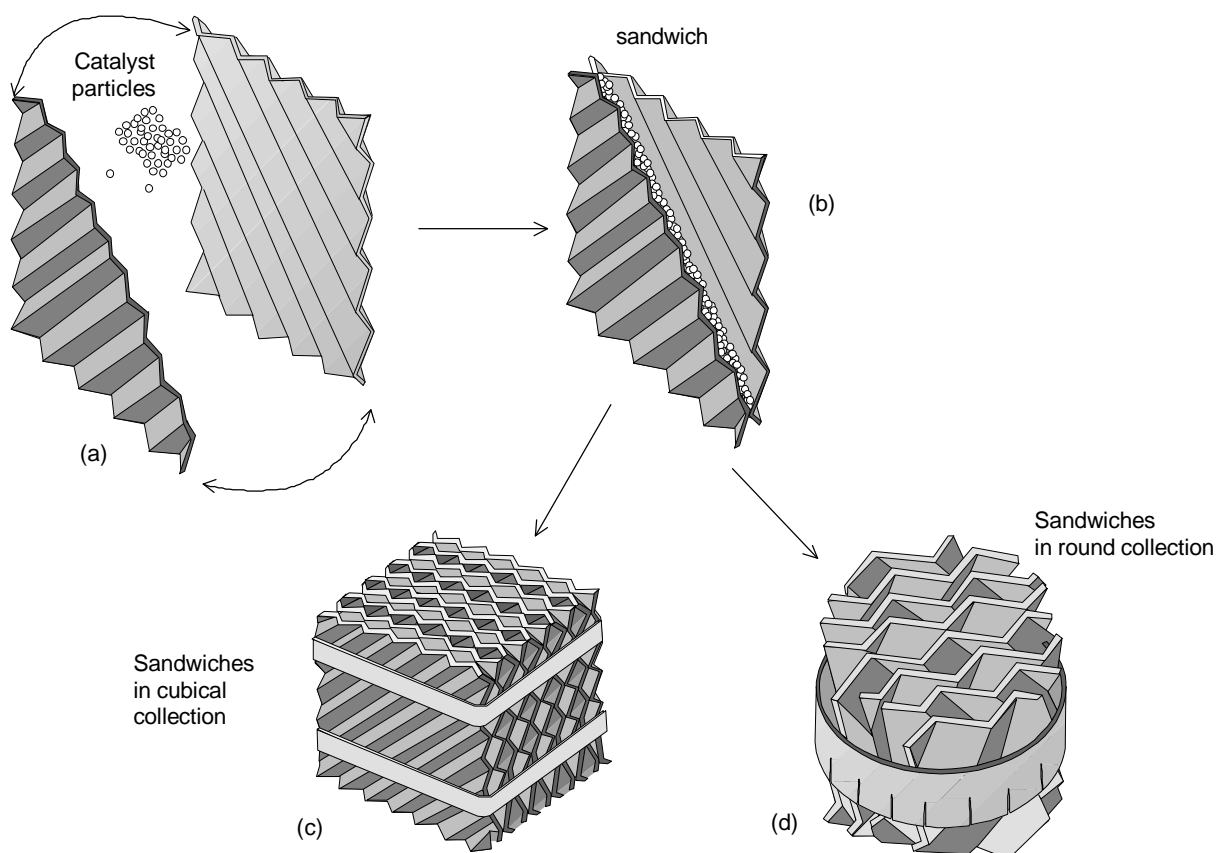


Figure 11. Structured catalyst-sandwiches. (a) Catalyst sandwiched between two corrugated wire gauze sheets. (b) The wire gauze sheets are joined together and sewn on all four sides. (c) The sandwich elements arranged into a cubical collection. (d) The sandwich elements arranged in a round collection.

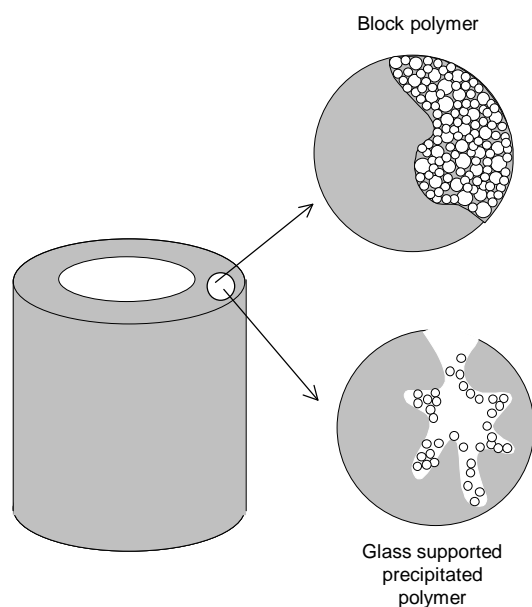


Figure 12. Catalytically active Raschig ring. Adapted from Sundmacher (1995).

Trays or downcomers to hold catalyst particles

The catalyst envelopes can be placed in a trayed RD column and many configurations have been proposed.

1. Vertically disposed catalyst containing envelopes can be placed along the direction of the liquid flow path across a tray (Jones, 1985); see Fig. 13. These envelopes are almost completely immersed in the froth on the tray, ensuring good contact between liquid and catalyst. Furthermore, since the vapour and liquid phase pass along the packed catalyst in the envelopes, and not through them, the pressure drop is not excessive.
2. Catalyst envelopes can be placed within the downcomers (Carland, 1994); see Fig. 14 (a). The primary drawback with installing the catalyst within downcomers is the limited volume available for catalyst inventory. Each “stage” can be regarded as a reaction device (downcomer) followed by a separation section (froth on the tray).
3. Catalyst envelopes can be placed near the exit of the downcomer (Asselineau et al., 1994); see Fig.14 (b). Catalyst inventory is necessarily limited. The vapour does not pass through the catalyst envelopes.
4. Trays and packed catalyst sections can also be used on alternate stages (Quang et al., 1989; Nocca et al., 1989); see Fig. 14 (c). The vapour flows through the packed section through a central chimney without contacting the catalyst. The liquid from the separation trays is distributed evenly into the packed reactive section below by a distribution device.
5. Other designs have been proposed for tray columns with catalyst containing pockets or regions which are fluidised by the upflowing liquid (Nocca et al., 1991; Marion et al., 1998; Jones, 1992). Catalyst attrition is a concern in a fluidized environment, but this can be taken care of by filtration of the liquid and by make-up of the catalyst.

In the tray configurations discussed above, the packed (or fluidised) catalyst containing envelopes are essentially vapour free. Furthermore, the vapour-liquid contacting efficiency can be considered to be practically unimpaired by the presence of the catalyst envelopes. Therefore, the standard tray design procedures (Fair et al., 1997; Lockett, 1986; Stichlmair and Fair, 1998) can be applied without major modification. Care must be exercised, however, in making a proper estimation of the liquid-catalyst contact time, which determines the extent of reaction on the stages.

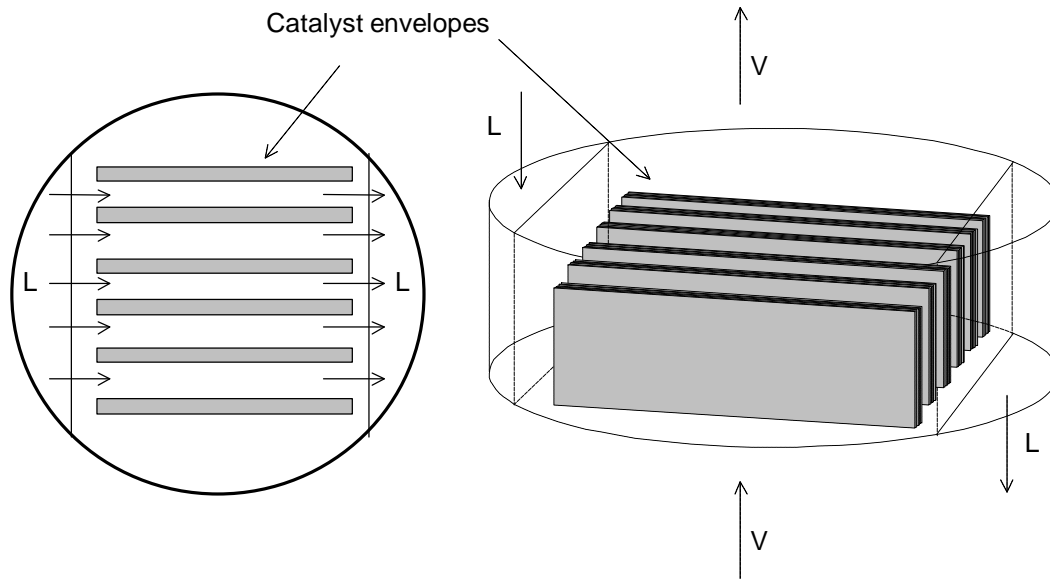


Figure 13. Catalyst envelopes placed along the liquid flow path.

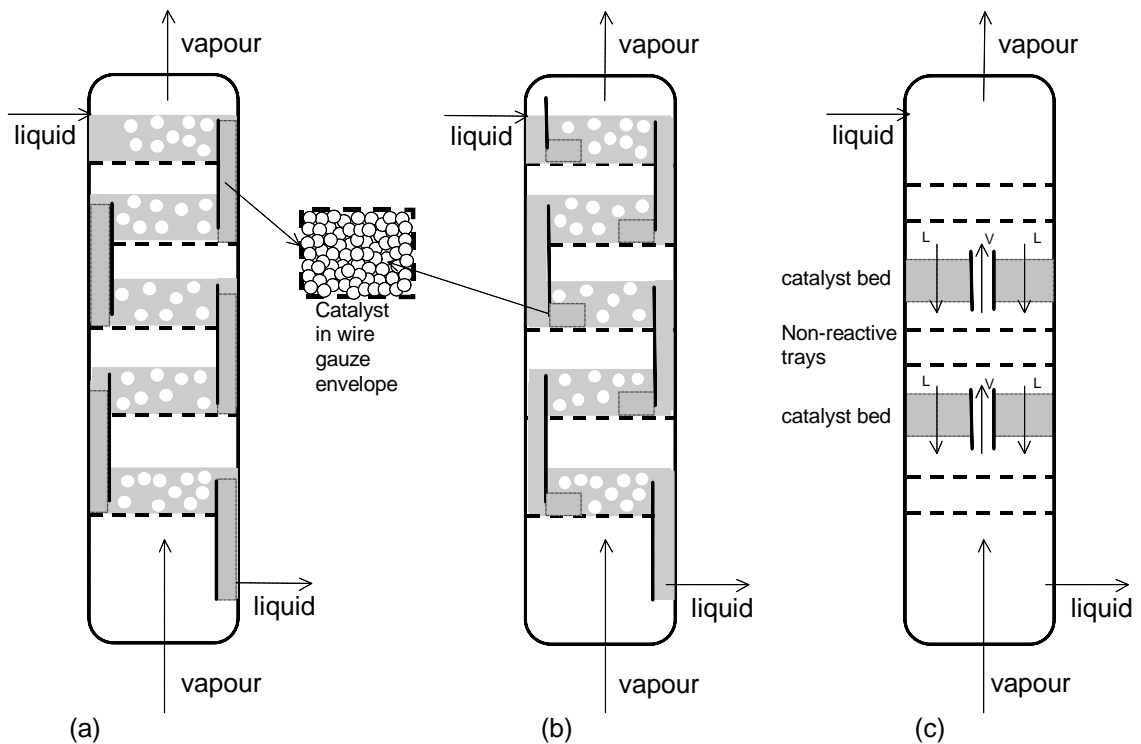


Figure 14. Counter-current vapour-liquid-catalyst contacting in trayed columns. (a) catalyst in envelopes inside downcomers (b) tray contacting with catalyst placed in wire gauze envelopes near the liquid exit from the downcomers. (c) Alternating packed layers of catalyst and trays.

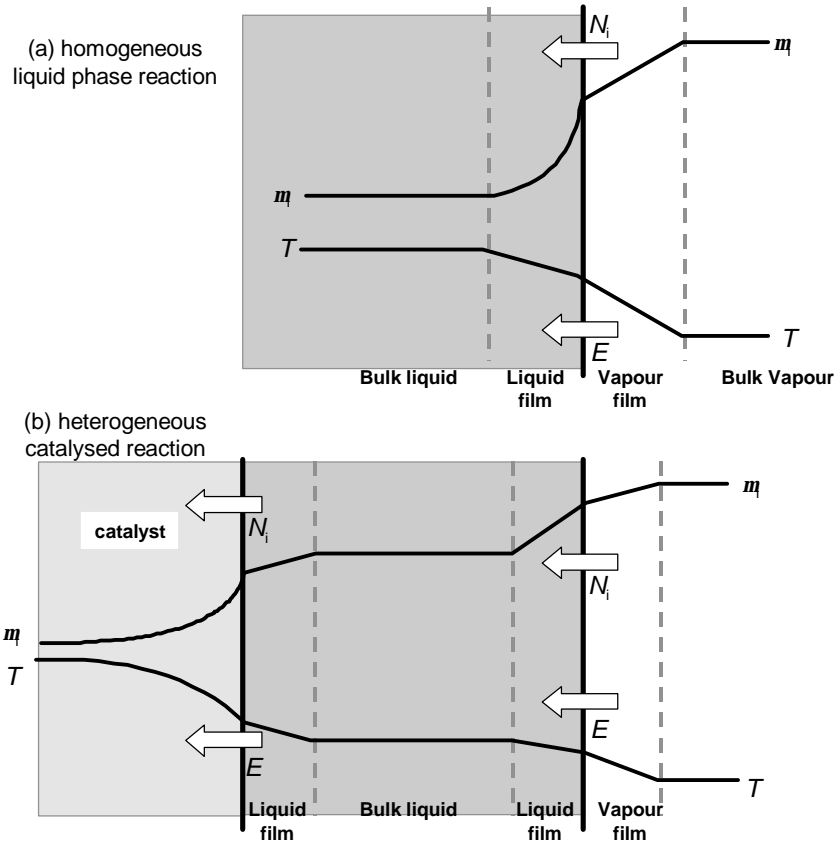


Figure 15. Transport processes in RD. (a) homogeneous liquid phase reaction, and (b) heterogeneous catalysed reactions. Adapted from Sundmacher (1995).

The complexity of RD

The design and operation issues for RD systems are considerably more complex than those involved for either conventional reactors or conventional distillation columns. The introduction of an in-situ separation function within the reaction zone leads to complex interactions between vapour-liquid equilibrium, vapour-liquid mass transfer, intra-catalyst diffusion (for heterogeneously catalysed processes) and chemical kinetics. Figure 15 shows the various transfer processes in homogeneous and heterogeneous RD. In heterogeneous RD the problem is exacerbated by the fact that these transfer processes occur at length scales varying from 1 nm (pore diameter in gels, say) to say a few meters (column dimensions); see Fig. 16. The time scales vary from 1 ms (diffusion within gels) to say a few hours (column dynamics). The phenomena at different scales interact with each other. Such interactions, along with the strong non-linearities introduced by the coupling between diffusion and chemical kinetics in counter-current contacting, have been shown to lead to the phenomenon of multiple steady states and complex dynamics, which

have been verified in experimental laboratory and pilot plant units (Bravo et al, 1993; Mohl et al., 1999; Rapmund et al., 1998). Successful commercialisation of RD technology requires careful attention to the modelling aspects, including column dynamics, even at the conceptual design stage (Doherty and Buzad, 1992; Roat et al., 1986). As will be shown later in this review many of the reactor and distillation paradigms do not translate easily to RD. The potential advantages of RD could be nullified by improper choice of feed stage, reflux, amount of catalyst, boilup rate, etc. Thus, it is possible to decrease conversion by increasing the amount of catalyst under certain circumstances (Higler et al., 1999b). Increased separation capability could decrease process performance (Sneesby et al., 1998a).

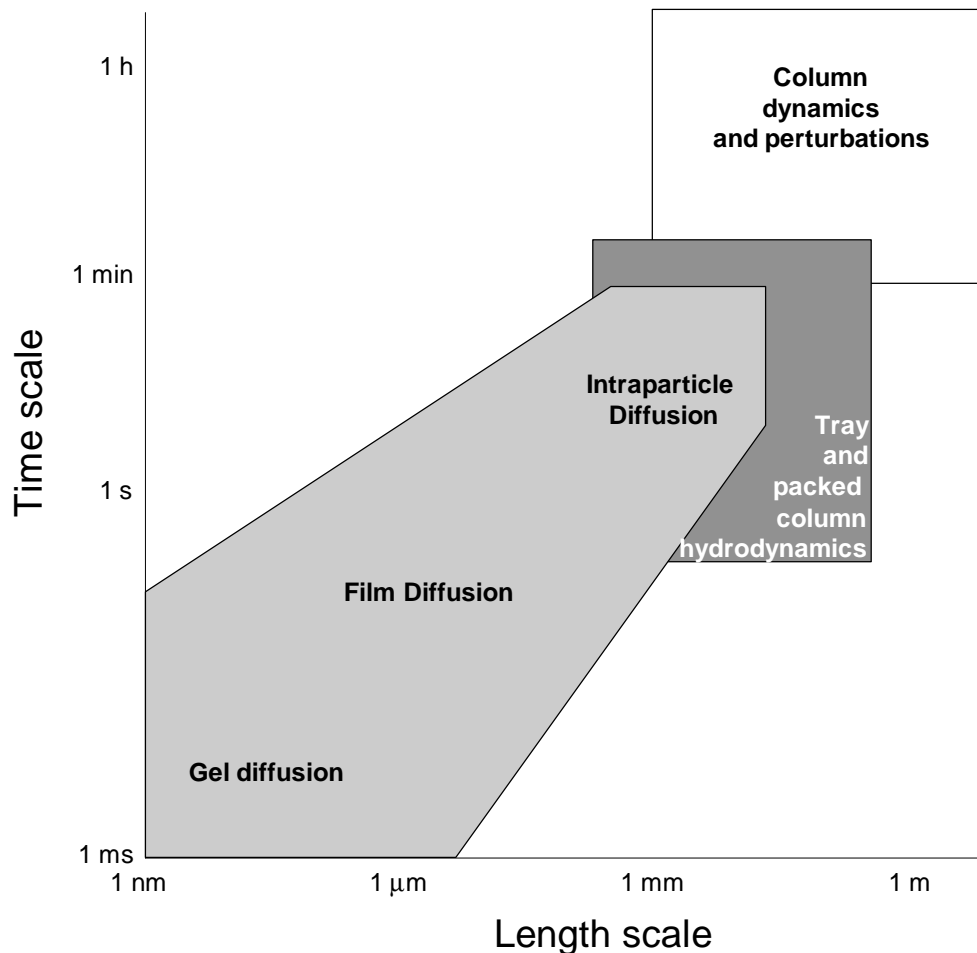


Figure 16. Length and time scales in RD. Adapted from Sundmacher (1995).

Models available for design of RD columns

A variety of models exist in the literature for design of RD columns. They can be classified in the following manner.

1. Steady-state equilibrium (EQ) stage model
2. Dynamic EQ stage model
3. Steady-state EQ stage model with stage efficiencies
4. Dynamic EQ stage model with stage efficiencies
5. Steady-state nonequilibrium (NEQ) stage model, where the interphase mass transfer is described by rigorous Maxwell-Stefan diffusion equations
6. Dynamic NEQ stage model
7. Steady-state NEQ cell model, developed by Higler (1999), in order to account for staging of the vapour and liquid phases during cross-current contacting on a distillation tray

The major objective of this thesis is to develop a dynamic NEQ cell model. The major incentive for doing this is because RD columns often exhibit multiple steady states and exhibit complex dynamics. The thesis is divided into two parts. Part I considers a steady-state analysis of RD columns. This is an essential prelude to Part II, which develops the dynamic NEQ models. The steady-state development in Part I essentially follows the work of Higler (1999), but additionally focuses on several "new" aspects: (a) influence of column hardware, (b) influence of operational aspects on steady-state multiplicity, (c) mass transfer efficiencies in RD. Part II represents the "main menu" of this thesis.

Each chapter has been written in a more-or-less self-contained fashion. Some degree of overlap between the various chapters is unavoidable. But for improved readability there is forward and backward referencing.

Chapter 2

Comparison of Equilibrium Stage and Nonequilibrium Stage Models

Abstract

For modelling reactive distillation columns, two distinctly different approaches are available in the literature: (1) the Equilibrium (EQ) stage model, in which the vapour and liquid phases are assumed to be in thermodynamic equilibrium, and (2) the Nonequilibrium (NEQ) stage model in which the finite mass transfer rates across the vapour-liquid interface are accounted for. In this chapter, these two approaches are compared using two case studies: (a) synthesis of MTBE and (b) hydration of ethylene oxide to ethylene glycol. It is shown that while the phenomena of multiple steady states is exhibited by both modelling approaches, the “window” in which these multiplicities occur is significantly reduced in the NEQ model. It is also shown that in actual column design, some of the steady states calculated by the EQ model cannot be realised due to e.g. flooding or weeping limitations on distillation trays. Another important conclusion that can be drawn from this work is that the hardware design can have a significant influence on the conversion and selectivity. It is concluded that for design of reactive distillation columns we must adopt the NEQ modelling approach.

Introduction

Currently there is considerable academic and industrial interest in multi-functional reactors, involving in-situ separation of products from the reactants (Krishna and Sie, 1994). Reactive distillation is one of the most common means of in-situ product removal and has been receiving increasing attention in recent years as an alternative to the conventional reaction-followed-by-distillation processes (Agreda *et al.*, 1990; DeGarmo *et al.*, 1992; Doherty and Buzad, 1992; Fair, 1998; Sundmacher and Hoffmann, 1994). Doherty and Buzad (1992) have placed this subject in historical perspective and list references to show that the advantages of reactive distillation were recognised as early as in 1921. Reactive distillation is potentially attractive whenever a liquid phase reaction must be carried out with a large excess of one reactant. Under such circumstances, conventional processes incur large recycle costs for excess reactant. Reactive distillation, on the other hand can be carried out closer to stoichiometric feed conditions, thereby eliminating recycle costs. Both homogeneous and heterogeneous catalysed chemical reactions can be carried out in a reactive distillation column.

There are four potential benefits of reactive distillation operation.

1. Higher conversions are obtained for equilibrium-limited reactions due to shifting of the equilibrium to the right. This is exemplified by the production of methyl acetate (Agreda *et al.*, 1990; Siirola, 1995), methyl-tertiary butyl ether, MTBE (Sundmacher, 1995), tert-amyl ether (Bravo *et al.*, 1993) and production of condensation polymers (Grosser *et al.*, 1987).
2. In some applications, chemical reaction has the beneficial effect of “reacting away” some of the azeotropes in the mixture and greatly simplifying the phase equilibrium behaviour. This happens in the process for synthesis of MTBE.
3. Improved selectivity is obtained because of removal of products from the reaction zone and preventing these from undergoing further reaction to by-products. Such benefits are obtained for example in the production of propylene oxide from propylene chlorohydrins (Carra *et al.*, 1979a, 1979b), for the alkylation of benzene to produce cumene (Shoemaker and Jones, 1987) and alkylation of butane to isooctane.
4. Benefits of heat integration are obtained because the heat generated in the chemical reactions is used for vaporisation. This is particularly advantageous for situations involving high heats of reaction such the hydration of ethylene oxide to ethylene glycol (Ciric and Gu, 1994). Hot spot formation is therefore prevented.

A typical set-up used for reactive distillation is shown in Fig. 1. A column usually is split up in three sections: A reactive section, in which the reactants are converted into products and where, by means of distillation, the products are separated out of the reactive zone. The tasks of the rectifying and stripping sections depend on the boiling points of reactants and products. If the product is the lowest boiling component in the process, the rectifying section is used for product purification and reactant recycle, and the stripping section mainly for inert and by-product removal as well as reactant recycle. In case the product is the highest boiling component, the tasks of the rectifying and stripping sections are switched. With the set-up as shown in Fig. 1, it is possible to virtually eliminate an entire

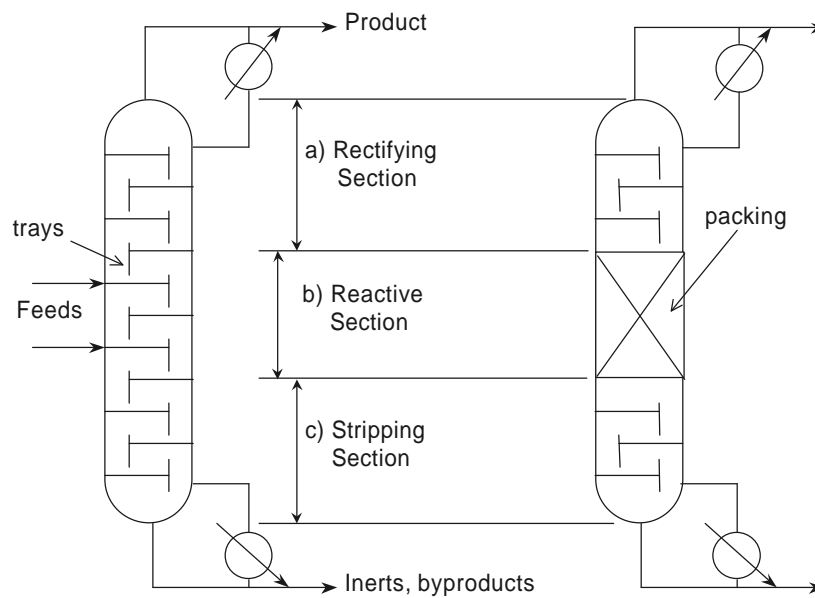


Figure 1. Typical configuration of a reactive distillation tray column consisting of three sections: (a) rectifying section, (b) reactive section and (c) stripping section.

post processing train in a process. One of the most spectacular examples of this kind is the Eastman process for production of methyl acetate (Sirola, 1995).

The design and operation issues for reactive distillation systems are considerably more complex than those involved for either conventional reactors or conventional distillation columns. The introduction of an in-situ separation function within the reaction zone leads to complex interactions between vapour-liquid equilibrium, vapour-liquid mass transfer, intra-catalyst diffusion (for heterogeneously catalysed processes) and chemical kinetics. Such interactions have been shown to lead to the phenomenon of multiple steady states and complex dynamics, which have been verified in experimental laboratory and pilot plant units (Bravo et al, 1993; Mohl et al., 1999; Rapmund et al., 1998).

For carrying out homogeneous reactions in reactive distillation columns, either trays or structured packings can be used. The hardware design is dictated by considerations other than that for conventional distillation. This is because when we carry out a reaction in the liquid phase the liquid phase residence time distribution has a significant impact on the conversion and selectivity. The liquid phase residence time distribution is much less important for conventional distillation. For heterogeneously catalysed processes, hardware design poses considerable challenges. The catalyst particle sizes used in such operations are usually in the 1 - 3 mm range. Counter-current operation in fixed beds packed with such particles is difficult because of flooding limitations. To overcome the limitations of flooding the catalyst particles have either to be enveloped in wire gauze (Bart and Landschützer, 1996; Ellenberger and Krishna, 1999; Higler et al., 1999c; Xu *et al.*, 1997) or the packing itself made catalytically active (Sundmacher and Hoffmann, 1996).

For design of reactive distillation columns, we require a model. Broadly speaking, two types of modelling approaches have been developed in the literature: the Equilibrium (EQ) stage model and the Nonequilibrium (NEQ) stage model. In the EQ stage model the vapour and liquid phase are assumed to be in equilibrium and allowance is made for finite reaction rates (Abufares and Douglas, 1995; Alejski *et al.*, 1988; Carra *et al.*, 1979a, 1979b; Ciric and Gu, 1994; Eldarsi and Douglas, 1998; Espinoza *et al.*, 1994; Hauan *et al.*, 1995; Jacobs and Krishna, 1993; Nijhuis *et al.*, 1993; Pilavachi *et al.*, 1997; Ruiz *et al.*, 1995; Scenna *et al.* 1998; Schrans *et al.*, 1996; Simandl and Svrcek, 1991). Such models stem from conventional equilibrium-stage modelling of distillation columns (Seader and Henley, 1998).

The NEQ stage model for reactive distillation follows the philosophy of rate based models for conventional distillation (Krishnamurthy and Taylor, 1985; Seader and Henley, 1998; Taylor and Krishna, 1993). The description of the interphase mass transfer, in either fluid phase, is almost invariably based on the rigorous Maxwell-Stefan theory for calculation of the interphase heat and mass transfer rates (Bravo *et al.*, 1993; Higler *et al.*, 1998; 1999a, 1999b; Kreul *et al.*, 1998; Lee and Dudukovic, 1998; Sawistowski and Pilavakis, 1979; Sundmacher, 1995; Sundmacher and Hoffmann, 1996; Zheng and Xu, 1992a).

In the literature, there has also been considerable attention to the phenomenon of multiple steady states. Using the EQ stage model, steady-state multiplicities have been reported for applications such as synthesis of MTBE (Güttinger and Morari, 1999; Jacobs and Krishna, 1993; Mohl *et al.*, 1999; Nijhuis *et al.*, 1993; Hauan *et al.*, 1995), synthesis of ETBE (Sundmacher, Uhde and Hoffmann, 1999), synthesis of TAME (Mohl *et al.*, 1999; Rapmund *et al.*, 1998) and for production of ethylene glycol (Ciric and Miao, 1994; Kumar and Daoutidis, 1999). Schrans *et al.* (1996) and Kumar and Daoutidis (1999) have performed dynamic simulations using the EQ stage approach to show the rich dynamic features of reactive distillation columns. For example, it has been shown by Schrans *et al.* (1996) for MTBE synthesis, that a small perturbation of reactant feed to the column could trigger oscillations and could shift the column operation from one steady state with high conversion to another steady state, with a significantly reduced conversion.

The objective of this chapter is compare the EQ and NEQ modelling of reactive distillation columns, focusing on the phenomena of multiple steady states. The column hardware design (column diameter, tray configuration, size and configuration of packing, etc) will have a significant influence on the interphase heat and mass transfer rates which are not taken account of in the EQ stage model. We examine the extent to which column hardware design influences the “window” within which multiple steady states are experienced. Two different case studies are undertaken, MTBE synthesis and production of ethylene glycol.

Nonequilibrium Model Development

A schematic representation of the NEQ model is shown in Fig. 2. This NEQ stage may represent a tray or section of packing. The development of the material balances, component balances, interphase transport equations and reaction rate equations is the same as developed in the earlier work of Higler *et al* (1999a, b). Our model formulation can deal with any number of reactions and the component molar balances for the vapour and liquid phases are

$$V_j y_{i,j} - V_{j+1} y_{i,j+1} - f_{i,j}^V + N_{i,j}^V = 0 \quad (1)$$

$$L_j x_{i,j} - L_{j-1} x_{i,j-1} - f_{i,j}^L - N_{i,j}^L - \sum_{m=1}^r n_{i,m} R_{m,j} e_j = 0 \quad (2)$$

where $N_{i,j}$ is the interfacial mass transfer rate and $R_{m,j}$ is the rate of reaction m on stage j . $n_{i,m}$ represents the stoichiometric coefficient of component i in reaction m and e_j represents the reaction volume.

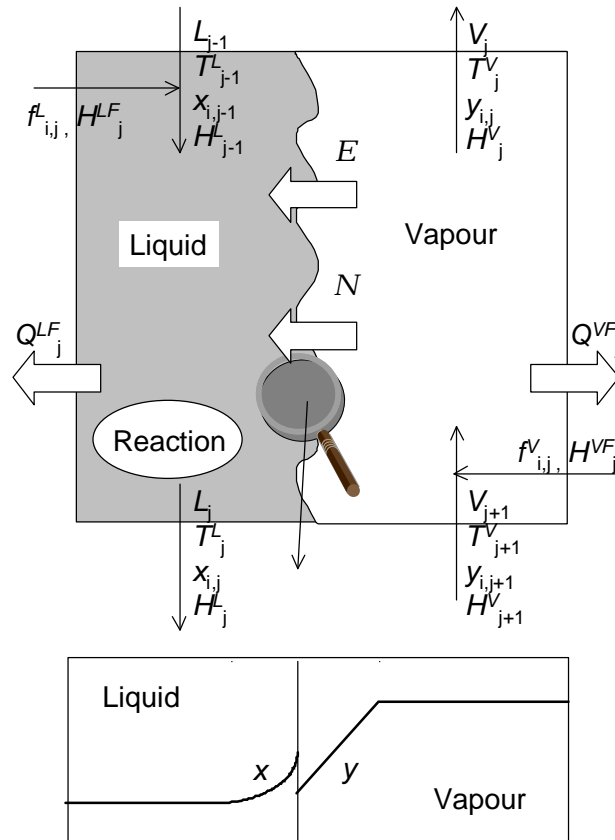


Figure 2. Schematic representation of the nonequilibrium model describing interphase mass transfer, with liquid phase chemical reaction at a position in a tray or packed column. The NEQ model takes account of the enhancement of the mass transfer due to chemical reaction within the diffusion film in the liquid close to the interface (see inset).

For homogeneous reactions this is given by the total liquid holdup on stage j . For heterogeneous reactions, employing the pseudo-homogeneous description, this is given by the total amount of catalyst present on the stage under consideration. The overall molar balances are obtained by summing eqs. (1) and (2) over the total number (c) of components in the mixture. The $N_{i,j}$ are related to the chemical potential gradients in either phase by the generalised Maxwell-Stefan equations (Krishna and Wesselingh, 1997; Taylor and Krishna, 1993)

$$\frac{x_{i,j}}{RT_j} \frac{\mathcal{J}m_{i,j}^L}{\mathcal{J}h} = \sum_{k=1}^c \frac{x_{i,j}N_{k,j}^L - x_{k,j}N_{i,j}^L}{c_{i,j}^L (\mathbf{k}_{i,k}^L A)_j} \quad (3)$$

with a similar relation for the vapour phase. The $\mathbf{k}_{i,k}^L$ represents the mass transfer coefficient of the i - k pair in the liquid phase; this coefficient is estimated from information on the corresponding Maxwell-Stefan diffusivity $\mathcal{D}_{i,k}^L$ using the standard procedures discussed in Taylor and Krishna (1993). Only $c - 1$ of the eqs (3) are independent. The mole fraction of the c -th component is obtained by the summation equations for both phases. The enthalpy balances for both vapour and liquid phase are

$$V_j H_j^V - V_{j+1} H_{j+1}^V - F_j^V H_j^{VF} + E_j^V + Q_j^V = 0 \quad (4)$$

$$L_j H_j^L - L_{j-1} H_{j-1}^L - F_j^L H_j^{LF} - E_j^L + Q_j^L = 0 \quad (5)$$

where the interphase energy transfer rates E_j (equal in both phases) have conductive and convective contributions

$$E_j^L = -h_j^L A \frac{\mathcal{J}T^L}{\mathcal{J}h} + \sum_{i=1}^c N_{i,j}^L H_{i,j}^L \quad (6)$$

with a similar relation for the vapour phase. h_j^L is the heat transfer coefficient in the liquid phase.

At the vapour liquid interface we assume phase equilibrium

$$y_{i,j}^I - K_{i,j} x_{i,j}^I = 0 \quad (7)$$

where the superscript I denotes the equilibrium compositions and $K_{i,j}$ is the vapour - liquid equilibrium ratio for component i on stage j .

In addition to eqs (1) – (7), we have the summation equations for the mole fractions in the vapour and liquid phase and equations expressing the continuity of fluxes of mass and energy across the interface. Furthermore, in the NEQ model we take account of the pressure drop across a stage

$$(\Delta p_{j-1}) = p_j - p_{j-1} \quad (8)$$

where p_j and p_{j-1} are the stage pressures and $\mathbf{D}p_{j-1}$ is the pressure drop per tray from stage $(j - 1)$ to stage j . The pressure drop over the stage is considered to be a function of the stage flows, the physical properties and the hardware design.

Table 1. *Thermodynamic, physical property and mass transfer models.*

K-value models	Enthalpy
Raoult's law Equation of State Gamma-Phi Chao-Seader Polynomial	None Ideal Ideal + Excess (from EOS or Activity model)
Equations of State	Activity Coefficients
Ideal Gas Virial Redlich-Kwong Soave-Redlich-Kwong API-SRK Peng-Robinson	Ideal Scatchard-Hildebrand Margules Van Laar Wilson NRTL UNIQUAC UNIFAC ASOG
Molar Volume	Vapour Pressure
EOS based methods Rackett equation Yen-Woods Thompson-Probst-Hankinson Amagat's law	Antoine Extended Antoine DIPPR polynomial Riedel Lee-Kesler Cubic EOS
Viscosity	Thermal Conductivity
DIPPR polynomial (gases and liquids) Chapman-Enskog-Brokaw (gases) Brokaw (gas mixtures) Yoon-Thodos (gases) Letsou-Stiel (liquid mixtures) DIPPR procedure 8H	DIPPR polynomial (gases and liquids) Mistic-Thodos (gases) Stiel-Thodos (gases) API procedure 12A1 (liquids) DIPPR procedure 9I (liquid mixtures) DIPPR procedure 9B (gases) Wassiljewa-Mason-Saxena (gas mixtures) DIPPR procedure 9E (liquids) DIPPR procedure 9H (liquid mixtures)
Surface Tension	Binary Diffusion Coefficients
DIPPR polynomial Lielmezs-Herrick API method Brock-Bird Digulio-Teja McLeod-Sugden Winterfield-Scriven-Davis	Kinetic theory (gases) Fuller-Schettler-Giddings (gases) Wilke-Change (dilute liquids) Hayduk-Laudie (dilute liquids) Hayduk-Minhas (dilute liquids) Siddiqi-Lucas (dilute liquids) Generalized Vignes (liquid mixtures) Leffler-Cullinan (liquid mixtures) Rathbun-Babb (liquid mixtures)
Mass Transfer Coefficients – Packings	Mass Transfer Coefficients – Trays
Onda et al Bravo-Fair Billet Schultes Sherwood number correlation Bravo-Rocha-Fair (1985) Bravo-Rocha-Fair (1992) Brunazzi Ronge; Zogg; Zogg-Toor-Marchello	AICHe method Hughmark Chan-Fair Zuiderweg Harris Chen-Chuang

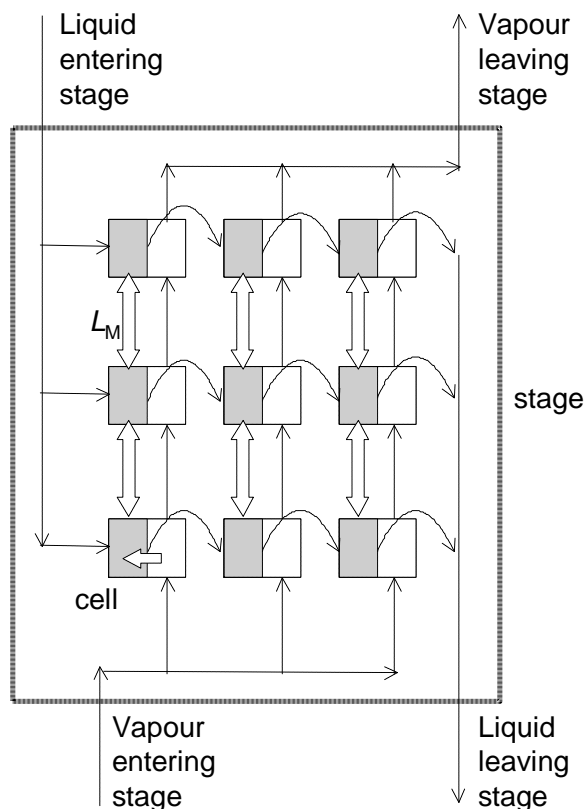


Figure 3. Schematic of the nonequilibrium cell model. For details of the NEQ cell model see Higler et al. (1999b).

In the NEQ model, hardware design information must be specified so that mass transfer coefficients, interfacial areas, liquid hold-ups can be calculated. The NEQ model requires thermodynamic properties, not only for calculation of phase equilibrium but also for calculation of driving forces for mass transfer and, in reactive distillation, for taking into account the effect of nonideal component behaviour in the calculation of reaction rates and chemical equilibrium constants. In addition, physical properties such as surface tension, diffusion coefficients, viscosities, etc. for calculation of mass (and heat) transfer coefficients and interfacial areas are required. A list of property models and mass transfer correlations available in our program is provided in Table 1. For the most part the property models are those recommended by Reid et al. (1988) and by Danner and Daubert (1983). The details of the models used for estimation of diffusivities and mass transfer coefficients are discussed in standard texts (Lockett, 1986; Seader and Henley, 1998; Taylor and Krishna, 1993). The tray design procedure is discussed in detail in Kooijman (1995) and Taylor et al. (1994). Interested readers can download the technical manual from <http://www.clarkson.edu/~chengweb/faculty/taylor/chemsep/chemsep.html>, which contains details of all thermodynamics, hydrodynamics and mass transfer models for tray and packed columns which have already been implemented into our reactive distillation software. The code for these models represents a large fraction of the overall program size.

For each reaction, we need to know the stoichiometric coefficients, reaction orders, and kinetic constants and whether the reaction is heterogeneous or homogeneous. A homogeneous reaction can also take place in the mass transfer film, the modelling of which requires additional equations for taking into account the effect of the reaction on the interphase mass transfer rate. Finally, we need to know the reaction volume. In EQ model simulations, the reaction volume often is specified. In the NEQ model, the reaction volume is equal to the total liquid hold-up on a stage; this is obtained directly from the packing specifications and hydrodynamic correlations. For a heterogeneous reaction, there are two options for the description of the reaction term. The simplest way is to treat the reaction pseudo-homogeneously, whereby catalyst diffusion and reaction is lumped into an overall reaction term. In this case, one only needs to specify catalyst weight and activity. This approach is adopted here. A more rigorous approach would involve a more

detailed description of diffusion and reaction inside the catalyst particles; see for example, Sundmacher (1995). In this case one also needs information about the catalyst geometry (surface area, mean pore diameter, etc). The steady-state model equations are solved using Newton's method as outlined in Taylor *et al.* (1994). In addition, we have equipped the program with a continuation method for analysis of multiple steady state behaviour. For more details about this method, the reader is referred to Wayburn and Seader (1987) and Kubicek (1976).

A further aspect that needs to be considered concerns the modelling of the residence time distribution of the vapour and liquid phases on any "stage". In a column with random dumped or structured packings, it is reasonable to assume that the vapour and liquid phases at any horizontal slice are in true *counter-current* (plug) flow. The situation with respect to vapour-liquid contacting on trays is significantly different. The contacting pattern on any tray, i.e. stage, is *cross-flow* of the vapour and liquid phases. Depending on the flow regime (froth or spray), dispersion height and liquid flow path length each phase (vapour or liquid) could be considered to be in plug flow, well mixed or have a mixing characteristics in between these extremes. Since the residence times and residence time distributions of the liquid and vapour phase can severely affect the performance of a reactor, it is important to develop a proper model to handle these extremes. For this purpose we have adopted the multiple-cells-per-stage approach; see Fig. 3. In this more recent development each stage is considered to be made up of multiple cells in either fluid phase; see Fig. 3 (Higler et al., 1999b). The vapour-liquid dispersion on a tray is split up in several cells within which interphase mass transfer and subsequent chemical reactions occur. For each of these cells we can write a set of equations as presented above for a single stage. Various forms of mixing behaviour can now be modelled by specifying a number of cells in the direction of flow of the vapour and liquid phases. Literature correlations are available to determine these mixing characteristics (Bennett and Grimm, 1991; Fair et al., 1997). By varying the number of cells in a flow path we can go from a perfectly mixed phase on a stage (1 cell per flow path), to an approximation of plug flow (large number of cells, typically more than 4). To make the multi-cell model complete we need to specify the interchange of liquid (with a molar flow rate of L_M) between horizontal rows of cells; this interchange is denoted by double headed arrows in Fig.3. In

setting up the proper component and enthalpy balances for the multi-cell model we need to take the following considerations into account.

- The amount of liquid entering a cell from the cell above (below) is exactly the same as the amount of liquid leaving the cell to the cell below (above).
- The liquid mixing flow L_M is large as compared to the flow of the liquid entering and leaving each cell.

In practice the vapour jet issuing from the holes on a tray will create a "fountain" effect; this will tend to mix the liquid phase more or less completely in the vertical direction (Lockett, 1986; Zuiderweg, 1982). In order to model this situation in which the liquid compositions in any vertical column of cells have the same composition, we choose a value of L_M which is considerably larger, say 10 times, than the liquid flow on that stage. In all the calculations presented in this chapter involving tray internals, the liquid phase in a vertical column of cells is assumed to be well mixed.

Two special versions of the NEQ model formulation were derived as special cases. In the EQ version, the vapour and liquid phases were assumed to be in thermodynamic equilibrium. Another special version of the NEQ model was prepared, called the equal diffusivities NEQ model, in which the Maxwell-Stefan diffusivities in either fluid phase, $D_{i,k}$, equal one another.

MTBE Case Study

The column configuration chosen for the simulations is shown in Figure 4; this is the configuration described by Jacobs and Krishna (1993) in their simulation study using the EQ stage model. The total number of stages is 17, including a total condenser and a partial reboiler; the column pressure is 11 atm. Reactive stages are located in the middle of the column, stage 4 down to and including stage 11. The column has two feed streams: a methanol feed and a mixed butenes feed. A small stoichiometric excess of methanol is used. The methanol feed stage location is varied in the simulations between stage 2 and stage 16. The mixed butenes feed, to stage 11, contains a mixture of *iso*-butene, which is reactive, and *n*-butene, which is non-reactive or inert. The reflux-ratio is set to 7 and the bottom flow rate is either set to 203 mol/s or varied (as a continuation parameter). The product removed from the top of the column is predominantly the inert *n*-butene. The bottoms product consists predominantly of MTBE. For a properly designed and operated column it is possible to achieve close to 100% conversion of *iso*-butene.

On each of the eight stages in the reactive zone, 1000 kg of catalyst is introduced. The total amount of catalyst in the reactive zone is 8000 kg. For NEQ model calculations, it is necessary to further specify the hardware configurations. In this study the reactive section is taken to be packed with catalytically active packing material in the form of Raschig rings. Specifically, we use ¼ inch Raschig ring shaped ion-exchange (Amberlyst 15) catalyst packing as described by Sundmacher and Hoffmann (1994). The specifications of the reactive section are: column diameter = 6 m, reactive packed zone height = 0.7 m, specific packing surface = 600 m²/m³, void fraction in the column = 0.72, packing density

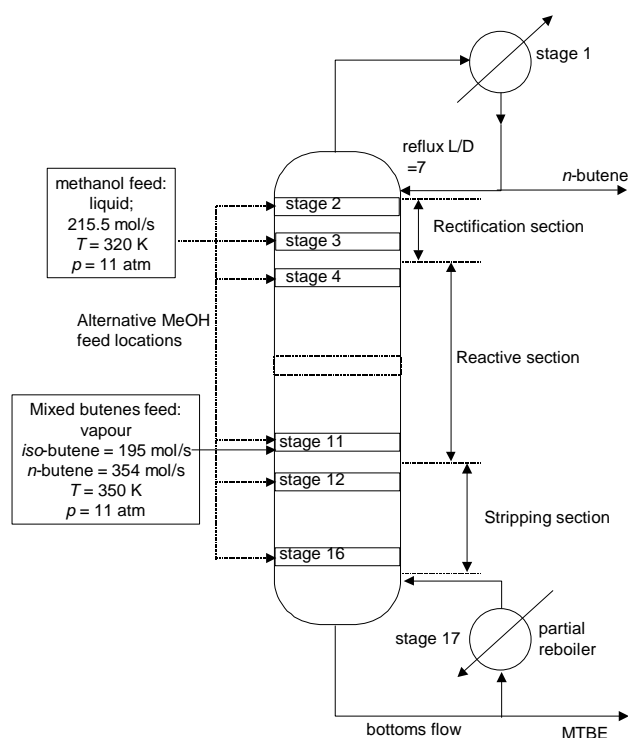


Figure 4. Configuration of the MTBE synthesis column, following Jacobs and Krishna (1993). The column consists of 17 stages.

$= 410 \text{ kg/m}^3$, catalyst pore voidage = 0.45, ion-exchange capacity of catalyst = 4.54 (meq H^+ /gram). The non-reactive rectifying and stripping sections are configured as sieve trays. The design specifications are given in Table 2. The UNIQUAC model was used for description of liquid phase nonideality, while the Soave-Redlich-Kwong equation of state was used for the vapour phase. The extended Antoine equation was used for calculation of the vapour pressure. Thermodynamic and kinetic data are taken from Rehfinger and Hoffmann (1990a, 1990b).

The basic objective of this chapter is to compare the results of EQ and NEQ models. The separation capability of the non-reactive stripping and rectifying sections will also affect the overall column performance. Subsequently, we focus on the differences of the EQ and NEQ modelling of the reactive section only and, therefore, assumed the non-reactive stages to have equal separation capability in both implementations. Towards this end, a tray efficiency of 60% is assumed in the EQ model implementation for the non-reactive stages; this value corresponded closely to the calculations of the NEQ model for the non-reactive stripping and rectifying sections using the *A.I.Ch.E.* calculation method for sieve tray mass transfer (for details of this model see Lockett, 1986). Of course, in the NEQ model implementation of the non-reactive stages, stage efficiencies are not used in the calculations but can be calculated from the simulation results; these stage efficiencies

Table 2. *Tray Specifications for the rectifying and stripping sections in the MTBE column*

	Rectifying Section	Stripping Section
Type of tray	Sieve	Sieve
Column diameter/[m]	5.595	5.019
Total tray area/[m ²]	24.58	19.78
Number of liquid flow passes	5	5
Tray spacing/[m]	0.61	0.61
Liquid flow path length/[m]	0.92	0.82
Active area/[m ²]	19.21	15.32
Total hole area/[m ²]	2.12	1.52
Downcomer area/[m ²]	2.68	2.23
Hole diameter/[m]	0.0047625	0.0047625
Weir length/[m]	22.95	20.62
Weir height/[m]	0.0508	0.0508
Weir type	Segmental	Segmental
Downcomer clearance/[m]	0.0381	0.0381
Deck thickness/[m]	0.00254	0.00254

vary for individual components. For the reactive section, the EQ model assumes vapour and liquid phases to be in equilibrium. In the NEQ model for the reactive section the mass transfer coefficients are calculated using the Onda et al. (1968) correlation. The 0.7 m high packed reactive section needs to be divided into a sufficient number of “slices” for accurate calculations. Our study shows that at least 90 slices are required for acceptable accuracy. Increasing the number of slices beyond 90 does not alter the results.

A series of simulation runs were carried out with varying methanol feed stage location; the methanol feed is moved sequentially down the column from stage 2 to stage 16 and up again. Once a run is completed successfully, different cases are generated by slightly altering the specifications and initiating the calculations using the previously obtained, converged, results. Figure 5 (a) compares the *iso*-butene conversions for the EQ and NEQ models with varying methanol feed stage locations. Consider the simulations of the EQ model first. Moving the methanol feed down the column from stage 2 to stage 11 gives a series of solutions that correspond to high (90% +) conversion. When the feed is moved one stage further, i.e. to stage 12, a sharp decrease in conversion is observed. A series of low conversion solutions is found moving the methanol feed from stage 12 to stage 16. Starting at stage 16 the methanol feed is moved upward. Until stage 12, the solutions for the up- and down- going sequences are identical. Continuing the up- going sequence beyond stage 12, does not give the expected jump back to the high conversion level but a different set of solutions is found. Thus, a set of low conversion solutions is found when methanol is fed to trays 11 or 10. The above results are largely in agreement with the simulations of Jacobs and Krishna (1993) which were performed with the commercial software RADFRAC of Aspen Technology, USA.

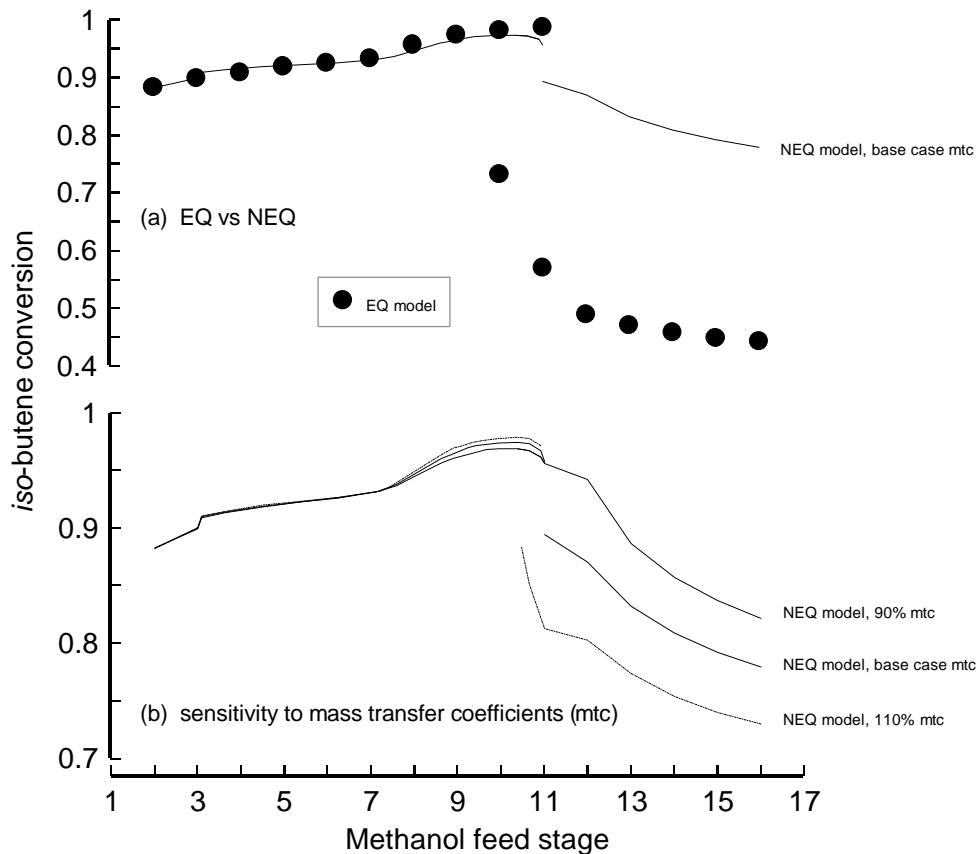


Figure 5. (a) High and low conversion branches obtained by EQ and NEQ simulations for the configuration shown in Fig. 4. The bottoms flow in these simulations were fixed at 203 mol/s. (b) NEQ simulations to study the sensitivity to mass transfer coefficients. The three curves represent (1) base case, (2) mass transfer coefficients increased to 110% of base case and (c) mass transfer coefficients reduced to 90% of base case.

The calculations using the NEQ model are also shown in Fig. 5 (a) as continuous curves. The differences in conversion between the high conversion branches of the EQ and NEQ models are small. Moving the methanol feed from stage 11 to stage 12 results in a jump to a lower conversion level, but this jump is much smaller than for the EQ model. A further difference between the EQ and NEQ models is that we did not observe any hysteresis effect for the NEQ model and moving the methanol feed from stage 12 to stage 11 results in a high conversion steady state.

The results of Fig. 5 (a) are counter-intuitive in that introduction of mass transfer resistance (in the NEQ model) results in a higher conversion for methanol feed introduction between stages 11 to 16. We also carried out NEQ model simulations to study the sensitivity of the NEQ model to variations in the interphase mass transfer coefficients, 110% and 90% of the base case; these simulations are shown in Fig. 5 (b). It is interesting to note that when the mass transfer coefficient is increased to 110%, the *iso*-butene conversion decreases for the low-conversion branch. When the mass transfer

coefficient is decreased to 90% of the base case value, the conversion of the low-conversion branch increases. Increase or decrease in the mass transfer coefficients does not affect the high-conversion branch to any significant extent (in fact the conversion values correspond closely to that of the EQ model). For the 90% mass transfer coefficient simulation, the NEQ model calculations show no conversion jump and yield a continuous smooth line over the whole range of stages on which methanol is injected.

In order to understand this counter-intuitive effect, let us consider the specific simulation in which the methanol is fed to stage 11. For this simulation, the *iso*-butene consumption rates are plotted along the height of the packed reactive section in Fig. 6. Figures 6 (a) and (b) show the calculations for the high conversion and low conversion branches respectively. Also plotted in Fig. 6 are the interphase mass transfer rates calculated from the NEQ model (for the EQ model the mass transfer coefficients are infinitely large, leading to phase equilibrium). Examination of Fig. 6 (b) shows that in the EQ model the reaction is proceeding in the reverse direction (reaction of MTBE to *iso*-butene and methanol) in the bottom half of the reactive section; this is evidenced by the fact that the *iso*-butene consumption rate is negative. This is clearly an undesirable situation. Introduction of mass transfer resistance (as is done in the NEQ model) hinders this. The counter-intuitive effect observed in Fig. 5 (a) is because in the low conversion branch the reaction is proceeding in the “wrong” direction and decreasing the interphase transfer facility helps by mitigating a bad situation.

Furthermore when we compare the mass transfer rates with the *iso*-butene consumption rates, we see from Figs 6 (a) and (b) that for the high-conversion branch the mass transfer rates are considerably higher than the consumption rates and mass transfer is not a limiting factor. This explains why increase or decrease in the mass transfer coefficient in this high conversion-branch does not affect the conversion level, as observed in Fig. 5 (b). For the low-conversion branch, on the other hand, the *iso*-butene consumption rates are very close to the mass transfer rates. For this case, therefore, the mass transfer coefficient has a significant influence on the conversion. Furthermore, at the bottom of the reactive section the reaction is proceeding in the “wrong” direction; introduction of more mass transfer resistance is helpful. This also explains why increase in the mass transfer coefficient decreases the conversion of *iso*-butene for the low conversion branch (cf. Fig. 5 (b)).

In the dynamic simulation study of Schrans et al. (1996), using the EQ model, it was shown that a small perturbation in the concentration of either methanol or *iso*-butene feed to the column could trigger oscillations and, perhaps, a shift in operation from the high conversion branch to the lower conversion branch. It should be clear from the results of Fig. 5 that in practice, where we do have interphase mass and heat transfer resistances, the oscillations would be much smaller in magnitude and the conversion jumps would be much less severe than anticipated by the EQ model. In order to stress the point we have carried out simulations using the EQ and NEQ model with the bottoms flow rate as continuation parameter. For methanol feed to stage 11, Fig. 7 shows the bifurcation diagrams for the EQ and NEQ models. It is clear that the “window” within which steady-

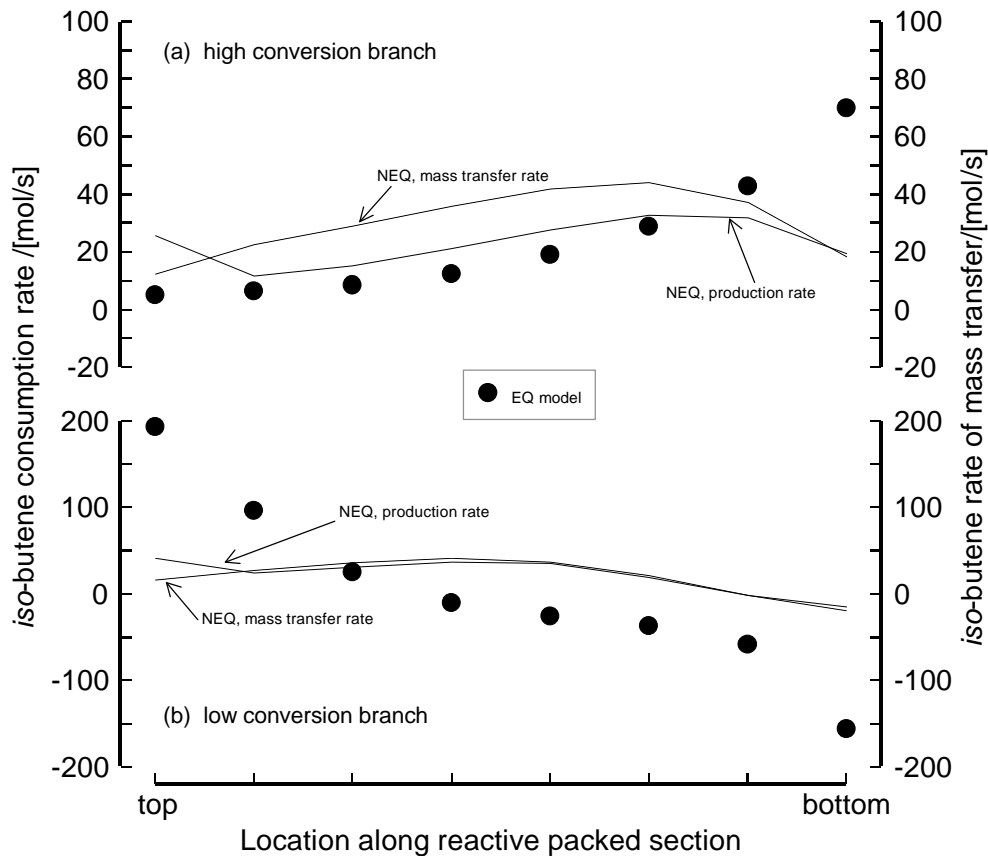


Figure 6. The *iso-butene* consumption rates for the (a) high and (b) low conversion branches obtained by EQ and NEQ simulations for the configuration shown in Fig. 4. The bottoms flow in these simulations were fixed at 203 mol/s. For the NEQ simulations, the interphase mass transfer rates are also plotted for the high and low conversion steady states.

state multiplicity is observed is much narrower with the NEQ model. Furthermore, the “downside” scenario (i.e. lower conversion branch operation) is much less bleak. This would suggest that the phenomena of multiple-steady states gets exaggerated attention if we use the EQ model. Also drawn in Fig. 7 are the results of the NEQ model calculations in which the diffusivities of the species are forced to equal one another in either fluid phase. We see that for a bottom flow rate of 203 mol/s, the equal diffusivities model exhibits only the low conversion steady-state whereas both the EQ and NEQ model (with the complete Maxwell-Stefan formulation), each predict three steady-states.

For the low-conversion branch the *iso-butene* conversion with the equal diffusivities model is lower than that of the NEQ Maxwell-Stefan model because the latter model takes proper account of the fact that the facility for transfer of MTBE should be lower

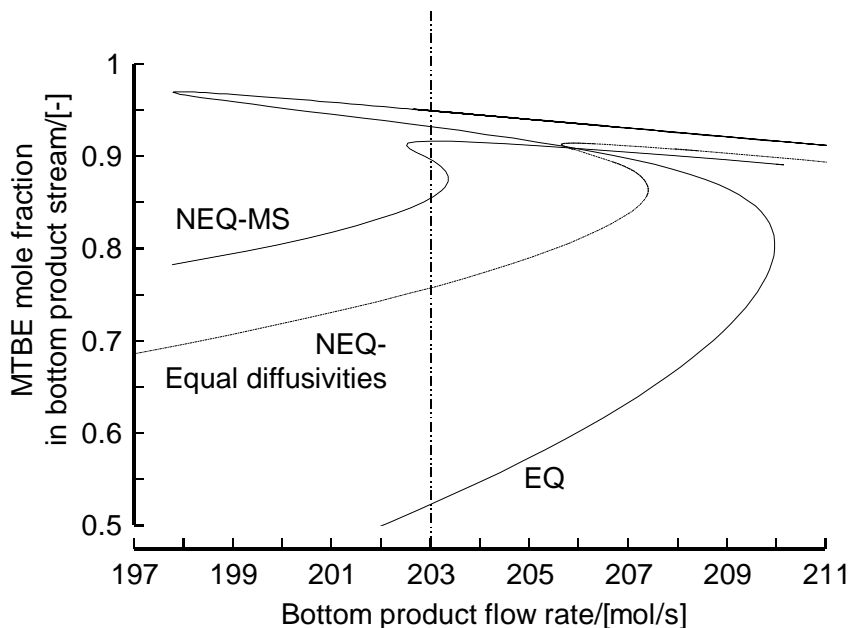


Figure 7. Bifurcation diagram for the EQ and models NEQ (both Maxwell-Stefan and equal diffusivities) with the bottoms product flow rate as continuation parameter. In these simulations the methanol feed is to stage 11 of the column configuration shown in Fig. 4.

than that of the other species. This reduced facility of MTBE transfer helps to prevent the backward reaction of MTBE to the reactants. Clearly, a proper modelling of mass transfer phenomena is essential in describing multiple steady-states and column dynamics.

Ethylene Glycol Case Study

We now consider the reaction of ethylene oxide (EO) with water to produce ethylene glycol (EG) in a reactive distillation column. The reaction is irreversible and proceeds in the presence of a catalyst



In addition we have an unwanted side reaction in which ethylene glycol reacts with ethylene oxide to di-ethylene-glycol (DEG)



The reaction rate constant of the second reaction is, under reaction conditions, about threetimes as large as the rate constant of the first reaction. Therefore, in a conventional reactor with equimolar feed, a considerable amount of DEG is produced. Furthermore, the reactions are both highly exothermic requiring good temperature control. A reactive

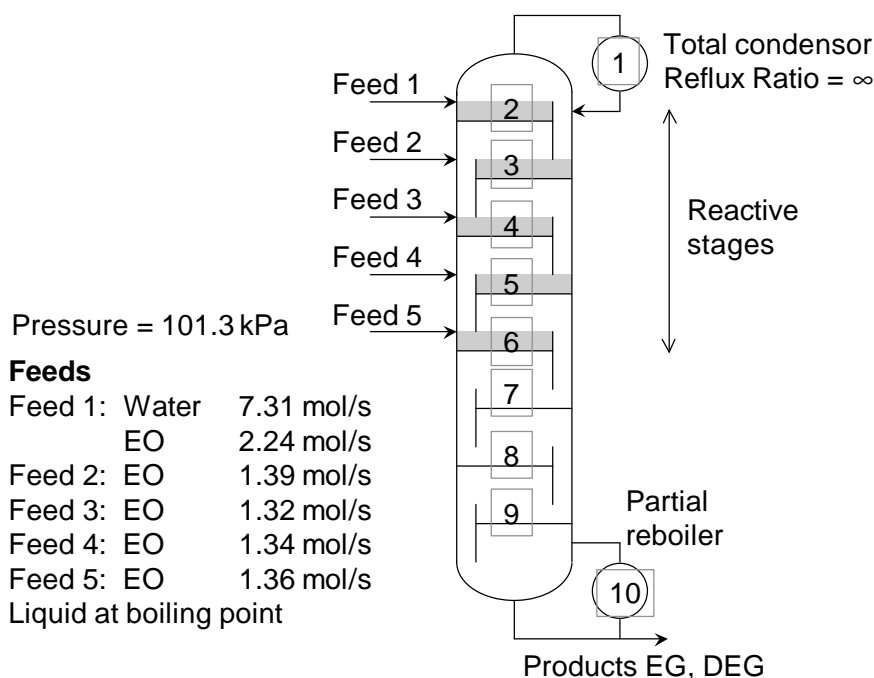


Figure 8. Configuration of reactive distillation column for hydration of ethylene oxide to ethylene glycol. Further details to be found in Ciric and Miao (1994).

distillation column offers both the advantages of heat integration and in-situ separation of the desired product, EG, preventing further reaction to DEG. By choosing total reflux operation, one can ensure that water mole fraction in the liquid phase on all the trays in the reactive section is close to unity (EO is considerably more volatile than water). The ethylene oxide that is supplied to the column reacts with water to form EG and because of the high surplus of water in the liquid, the concentrations of ethylene oxide and ethylene glycol will be very low. This results in a low production rate of DEG. Furthermore, the distillation process provides direct temperature control, since the liquid phases will always be at their boiling points. Hot spot formation and the danger of runaway reactions are non-existent in reactive distillation.

The column configuration chosen for the EG production is similar to the set up of Ciric and co-workers (Ciric and Gu, 1994; Ciric and Miao, 1994), details of which are given in Figure 8. This is a 10-stage sieve tray column (including total condenser and partial reboiler). Water is supplied to the top of the column, while the EO feed is distributed along the top section of the column. The column is operated at total reflux, while in the bottom a boilup ratio of 24 is maintained. The reaction kinetics and thermodynamics data are the same as those reported in the papers by Ciric et al. Ciric and Miao (1994) used an EQ model with homotopy continuation method to prove the existence of multiple steady states in the proposed setup. We have carried out simulations with both the EQ and NEQ models. In both the EQ and NEQ model calculations, the condenser (stage 1) and the reboiler (stage 10) are modelled as equilibrium stages. Since the NEQ model calculations

Table 3. Sieve tray specification for ethylene glycol reactive distillation column

	Config- uration 1	Config- uration 2	Config- uration 3	Config- uration 4	Config- uration 5
Type of tray	Sieve	Sieve	Sieve	Sieve	Sieve
Column diameter /[m]	1.7	3.0	1.7	1.7	1.7
Total tray area /[m ²]	2.27	7.07	0.67	2.27	2.27
Number of liquid flow passes	1	1	2	1	1
Tray spacing /[m]	0.7	0.7	0.7	0.7	0.7
Liquid flow path length /[m]	1.28	2.26	0.67	1.28	1.28
Active area /total tray area	0.86	0.86	0.86	0.86	0.86
Hole diameter /[m]	0.0045	0.0045	0.0045	0.0045	0.0045
Total hole area /total tray area	0.0858	0.0858	0.0858	0.0858	0.0858
Downcomer area /total tray area	0.07	0.07	0.07	0.07	0.07
Weir length /[m]	1.52	2.68	2.9	1.52	1.52
Weir length /column diameter	0.895	0.895	0.895	0.895	0.895
Weir height /[m]	0.08	0.08	0.08	0.05	0.10
Downcomer clearance /[m]	0.01	0.01	0.01	0.01	0.01

require the estimation of heat and mass transfer coefficients, we need to specify the tray configuration and layout. Four different sieve tray column configurations, with column diameters of 1.7 and 3.0 m, were chosen for stages 2 to 9; these are specified in Table 3. Reactions are assumed to take place only on stages 2 to 6 because catalyst is considered to be present only on these stages. In the NEQ model calculations, the vapour and liquid phases were both assumed to be well-mixed on the given stage; this assumption was later relaxed to account for plug flow of both phases. To compare our results with those of Ciric and Miao (1994) we also performed calculations with the EQ model.

Let us first consider the simulation results with the EQ model. These simulations, which are necessarily identical for all sieve tray configurations (cf. Table 3), are shown in Fig. 9. Three steady states SS-1 (high conversion), SS-2 (intermediate conversion) and SS-3 (low conversion) were found. The desired high conversion steady state solution (SS-1) corresponds to high column temperatures (cf. Fig. 9 (b)) and lowest molar flow rate of the vapour up the column (cf. Fig. 9 (c)). At first sight, it may appear counter-intuitive that the high conversion steady-state corresponds to the solution which yields the smallest molar flows in the column. In order to understand what is happening we have listed the important variables for the three steady-states in Table 4. We note that even though the molar flows in the three cases are widely different, the mass flow rate of the product leaving the column is identical for the three cases, as it should be in order to satisfy the overall column material balance. The reboiler duties in the three cases are nearly the same but not identical because of the difference is the molar heats of vaporisation of ethylene glycol and water.

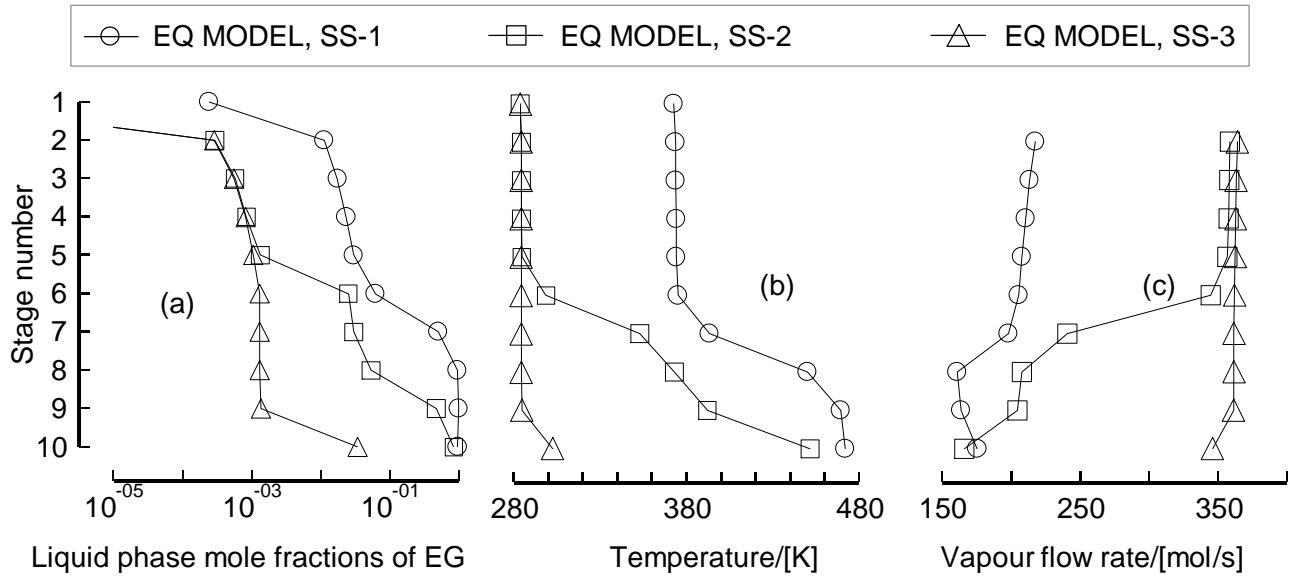


Figure 9. Equilibrium model calculations for the ethylene glycol process. Column profiles for (a) liquid phase mole fraction, (b) temperature and (c) vapour phase molar flow.

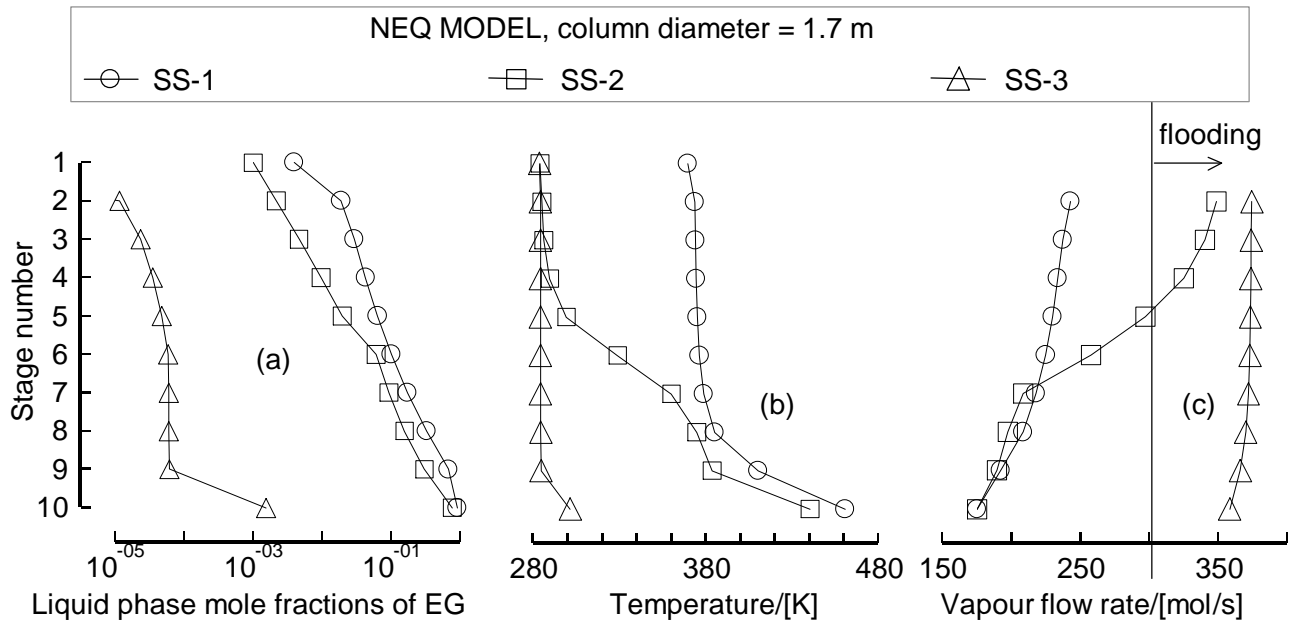


Figure 10. Nonequilibrium model calculations for the ethylene glycol process for a column of diameter 1.7 m. Column profiles for (a) liquid phase mole fraction, (b) temperature and (c) vapour phase molar flow.

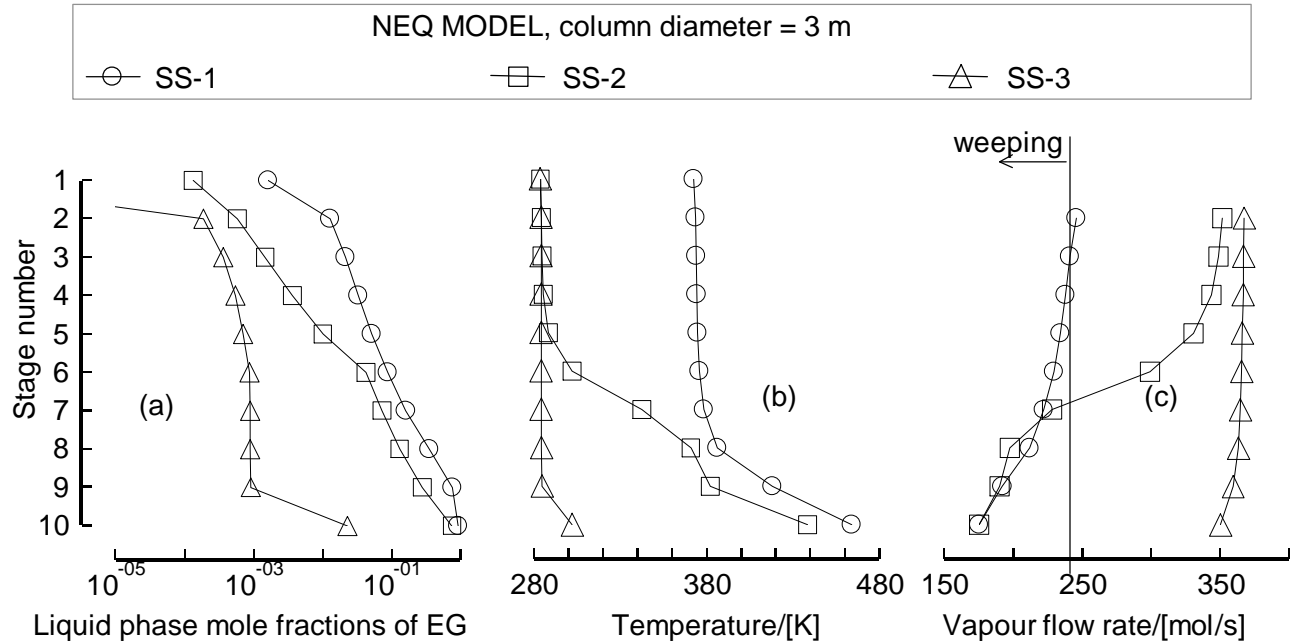


Figure 11. Nonequilibrium model calculations for the ethylene glycol process for a column of diameter 3.0 m. Column profiles for (a) liquid phase mole fraction, (b) temperature and (c) vapour phase molar flow.

Let us now consider the NEQ model simulations for the 1.7 m diameter column configuration. Again, three steady states were detected, high (SS-1), intermediate (SS-2) and low conversion (SS-3) of EO. For this chosen column diameter, only one solution, SS-1, can be realised in the column. The other solutions SS-2 and SS-3 could not be realised in the NEQ because for the higher vapour flows, the column floods in some (SS-2) or all (SS-3) of the stages; the flooding boundaries are drawn in Fig. 10 (c).

For NEQ model simulations in the 3.0 m diameter column (configuration 2 of Table 3) we found the expected three steady states; see Fig. 11. The column diameter is however too large to accommodate the lower flows corresponding to SS-1 and SS-2. These lower vapour flows result in weeping on some (in case of SS-2) or all (in case of SS-1) of the trays; see Fig. 11 (c). We therefore conclude that in the 3 m diameter column only the low conversion steady state can be realised.

The simulations presented in Figures 9, 10 and 11 were carried out assuming that on any tray the liquid and vapour phases are both well mixed. For modelling purposes the number of cells (cf. Fig. 3) used for each phase was equal to unity. For the 1.7 m diameter column calculations reported above, we had assumed that the liquid and vapour phases are both well mixed. With the NEQ cell model implementation (Fig. 3), we can study the influence of staging of the liquid and vapour phases by increasing the number of cells in either flowing phases. For five mixing cells in both vapour and liquid phases (which corresponds closely to plug flow conditions for either phase), the formation

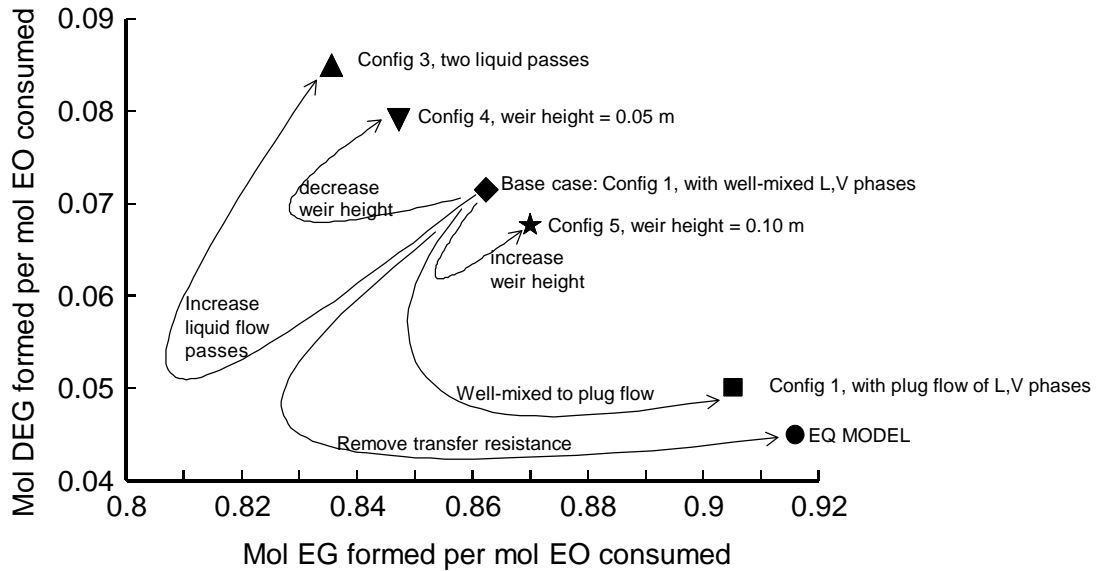


Figure 12. Formation of by-product DEG versus formation of EG for various tray configurations, specified in Table 3 and for various mixing model assumptions.

of by-product DEG is reduced while the conversion to EG is increased; see Fig. 12. Removing the mass transfer resistances, i.e. assuming the EQ model, gives the best performance with respect to conversion and selectivity; see the point towards the bottom right of Fig. 12.

We also carried out simulations to study the influence of tray hardware on conversion and selectivity and three variations of the base case configuration 1 were studied; these configurations (3,4 and 5) are specified in Table 3. For these simulations the number of mixing cells in the liquid and vapour phase were assumed to be equal to 1. The conversion to EG and to DEG are shown in Fig. 12. To understand the simulated values we need to have an understanding of the change in hydrodynamics with changing tray

Table 4. Steady-states for ethylene glycol column, using EQ model

	SS-1	SS-2	SS-3
Ethylene glycol mole fraction at bottom of column	0.9500	0.8446	0.0403
Heat Duty of condenser/ [J]	-8.8×10^6	-9.6×10^6	-9.2×10^6
Heat Duty of reboiler/ [J]	8.4×10^6	9.1×10^6	9.1×10^6
Temperature of reboiler [K]	471	451	302
Molar product flow at bottom of column/ [mol/s]	7.3	7.3	14.2
Mass product flow at bottom of column/ [kg/s]	0.47	0.47	0.47

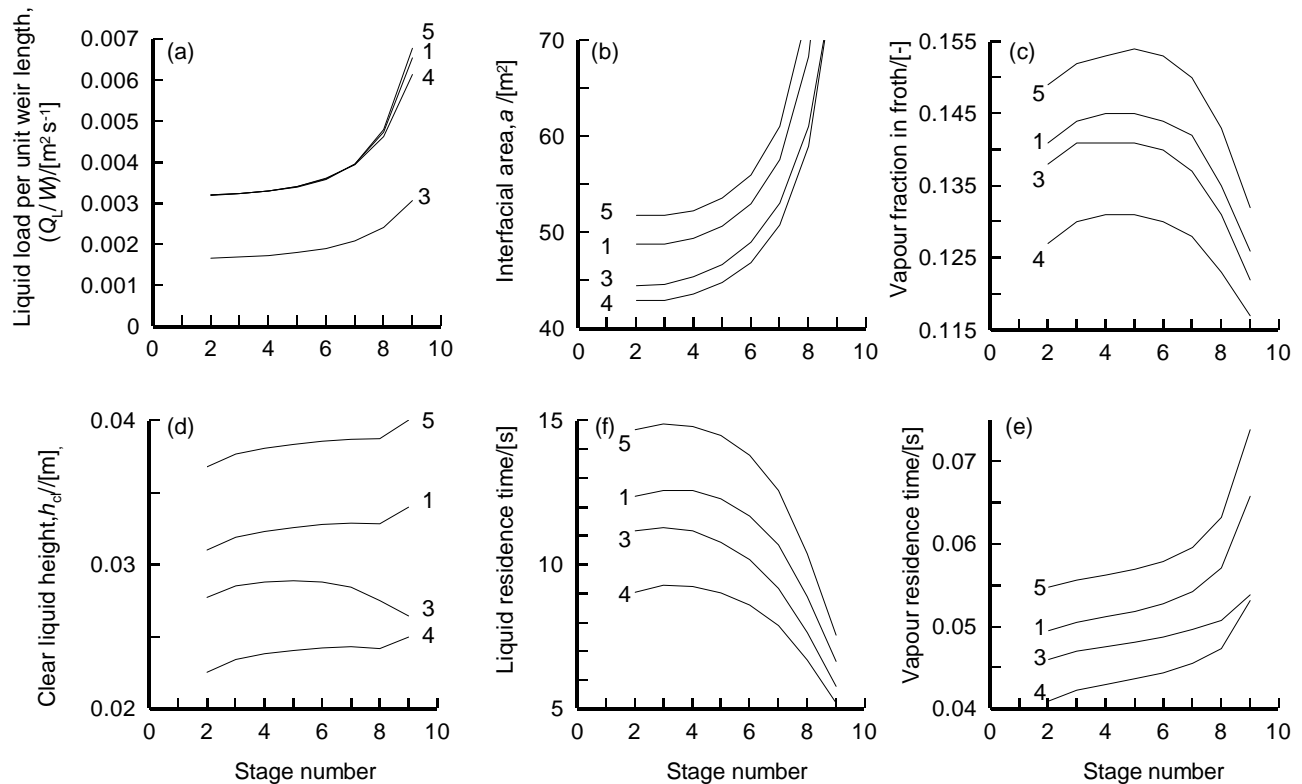


Figure 13. Hydrodynamic and mass transfer parameters for various tray configurations 1,3,4 and 5 specified in Table 3.

hardware. The important hydrodynamic and mass transfer parameters, plotted in Fig. 13 as a function of stage number, are (a) liquid load per unit weir length, Q_L/W , (b) total interfacial area on the tray, a , (c) vapour fraction in the froth on the tray (d) clear liquid height on the tray, h_{cl} , (e) liquid phase residence time on the tray and (f) vapour phase residence time on the tray.

Decreasing the weir height from 80 mm to 50 mm (changing from configuration 1 to 4 of Table 3) decreases formation of EG and increases by-product DEG formation; cf. Fig. 12. This reduction in performance is because the clear liquid height in configuration 4 is considerably lower than in the base case configuration 1 and the total interfacial area on the tray is reduced. The residence time of the vapour and liquid phases are also reduced. Mass transfer limitations are therefore increased in configuration 4, leading to lower conversion and selectivity. Increasing the weir height from 80 mm to 100 mm (changing from configuration 1 to configuration 5) leads to improved conversion and improved selectivity because of the exactly opposite effects as noted above in the change to configuration 4. High weir heights, and operation in the froth regime, are generally to be preferred in reactive distillation operations.

Consider the change in the performance when switching from Configuration 1 to 3 of Table 3 in which we have two liquid flow passes on the trays (for an explanation of single pass and multipass liquid flow configurations the reader is referred to the text of Lockett, 1986). In this case the liquid load per weir length is reduced by 50%. This reduction in the liquid load leads to a reduction in the clear liquid height and lowering in the total interfacial area; see Fig 13. Furthermore the liquid and vapour residence times are lower in the 2-pass configuration 3 when compared to the 1-pass configuration 1. All of this results in a lowering in the mass transfer rate, which has a detrimental influence on both the conversion and selectivity. It appears that the usual rules for conventional distillation column design cannot be carried over to reactive distillation columns because, for a column of 1.7 m diameter the conventional design philosophy would be to use 2 passes for the liquid flow.

Concluding Remarks

Comparison of the EQ and NEQ models for the MTBE and EG processes shows that the phenomena of multiple steady states has a much smaller realisable “window” if interphase mass and heat transfer resistances are taken into account. Some of the steady states found in the EQ model cannot be realised in the chosen column configuration because of flooding or weeping limitations.

The ethylene glycol case study was used to highlight the importance of hardware design on the performance of reactive distillation columns. While the EQ model anticipates three steady states, flooding and weeping considerations will ensure that only one steady state can be realised. Overdimensioning of the column will guarantee that only the low conversion steady state is realisable. The choice of weir height and number of passes has a significant influence on the conversion and selectivity.

It is concluded that for steady-state design of reactive distillation columns we must routinely resort to nonequilibrium stage modelling.

In Chapters 6, and 7 we will consider the dynamics of RD columns and the influence of column hardware thereof.



Chapter 3

Influence of Column Hardware on the Performance of Reactive Distillation Columns

Abstract

We compare the performance of an MTBE synthesis column using two different hardware configurations: (1) a sieve tray column in which the catalyst particles, encased inside wire gauze envelopes, are placed along the liquid flow path, and (2) a column filled with catalytically active packing of Raschig ring shape. The columns simulations are performed using the rigorous nonequilibrium model introduced in Chapter 2. Using the bottoms flow rate of MTBE as continuation parameter it is shown that the two different hardware configurations exhibit significantly different bifurcation diagrams. The sensitivity of this bifurcation diagram has been studied with varying (a) methanol feed, (b) iso-butene feed, (c) inert feed and (d) reflux ratio. We show that the cross-flow contacting on the sieve tray configuration is beneficial to conversion.

Introduction

Both homogeneous and heterogeneous catalysed chemical reactions can be carried out in a reactive distillation (RD) column. For heterogeneously catalyzed reactive distillation processes packed columns (random packed or structured) or tray columns could be used. In this chapter we compare the influence of column hardware choice on the performance of a reactive distillation column for MTBE synthesis. The major objective is to demonstrate the importance of hardware selection on column performance.

In the NEQ model, hardware design information must be specified so that mass transfer coefficients, interfacial areas, and liquid hold-ups can be calculated. The NEQ model requires thermodynamic properties, not only for calculation of phase equilibrium but also for calculation of driving forces for mass transfer and, in reactive distillation, for taking into account the effect of nonideal component behaviour in the calculation of reaction rates and chemical equilibrium constants. In addition, physical properties such as surface tension, diffusion coefficients, viscosities, etc. for calculation of mass (and heat) transfer coefficients and interfacial areas are required. For the most part the property models are those recommended by Reid et al. (1988) and by Danner and Daubert (1983). The details of the models used for estimation of diffusivities and mass transfer coefficients are discussed in standard texts (Lockett, 1986; Taylor and Krishna, 1993). The tray design procedure is discussed in detail in Kooijman (1995) and Taylor et al. (1994).

A further aspect that needs to be considered concerns the modelling of the residence time distribution of the vapour and liquid phases on any "stage". In a column with random dumped or structured packings, it is reasonable to assume that the vapour and liquid phases at any horizontal slice are in true *counter-current* (plug) flow. The situation with respect to vapour-liquid contacting on trays is significantly different. The contacting pattern on any tray, i.e. stage, is *cross-flow* of the vapour and liquid phases. Depending on the flow regime (froth or spray), dispersion height and liquid flow path length each phase (vapour or liquid) could be considered to be in plug flow, well mixed or have a mixing characteristics in between these extremes. Since the residence times and residence time distributions of the liquid and vapour phase can severely affect the performance of a reactor, it is important to develop a proper model to handle these extremes. For this purpose we have adopted the multiple-cells-per-stage approach. In this more recent development each stage is considered to be made up of multiple cells in either fluid phase (Higler et al., 1999d). The vapour-liquid dispersion on a tray is split up in several cells within which interphase mass transfer and subsequent chemical reactions occur. For each of these cells we can write a set of equations as presented in Chapter 2. Various forms of mixing behaviour can now be modelled by specifying a number of cells in the direction of flow of the vapour and liquid phases. By varying the number of cells in a flow path we can go from a perfectly mixed phase on a stage (1 cell per flow path), to an approximation of plug flow (large number of cells, typically more than 4). In practice the vapour jet issuing from the holes on a tray will create a "fountain" effect; this will tend to mix the liquid phase more or less completely in the vertical direction (Lockett, 1986). In all the calculations presented in this chapter involving tray internals, the liquid phase in a vertical column of cells is assumed to be well mixed.

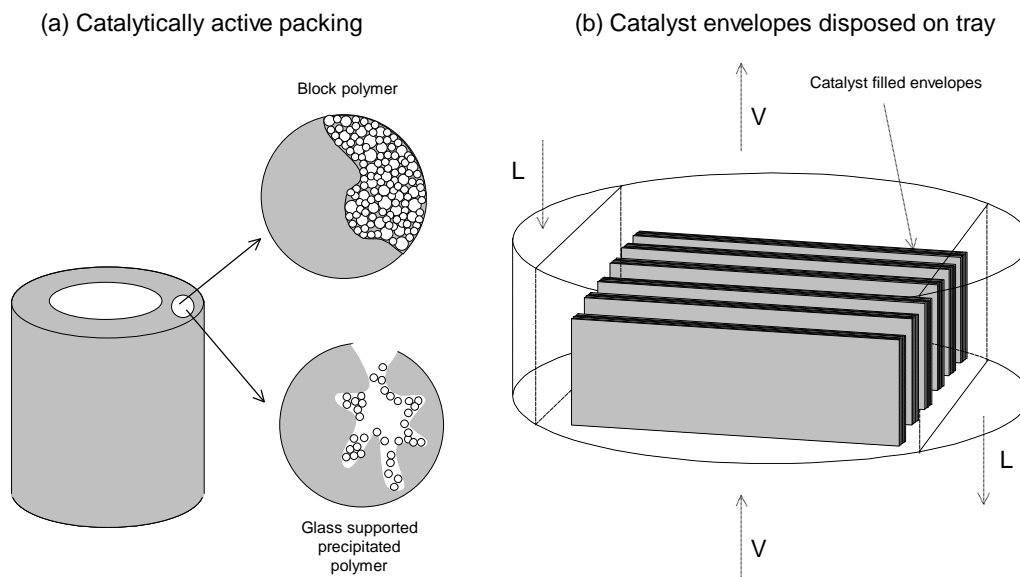


Figure 1. Catalyst configurations in (a) packed column and (b) tray column.

Simulation Study and Results

The MTBE synthesis column configuration chosen was essentially that of Jacobs and Krishna (1993) and shown in Fig. 4, Chapter 2. The column diameter was chosen to be 6 m. The stripping and rectifying sections consist of sieve trays. The configuration of the sieve trays are: total tray area = 28.27 m²; number of liquid flow passes = 5; tray spacing = 0.7m; liquid flow path length = 0.97 m; fractional active area = 0.76; fractional hole area = 0.1; fractional downcomer area = 0.12; hole diameter = 4.5 mm; weir height = 50 mm; total weir length = 22 m; weir type = segmental; downcomer clearance = 0.0381 m; tray deck thickness = 25 mm. Two types of configurations have been chosen for the reactive section. First, we choose ¼ inch random packed Raschig ring shaped catalysts used by Sundmacher and Hoffmann (1994) and shown in Fig. 1 (a)). The second choice is that of sieve trays with catalyst envelopes maintained on the trays (see Fig. 1 (b)).

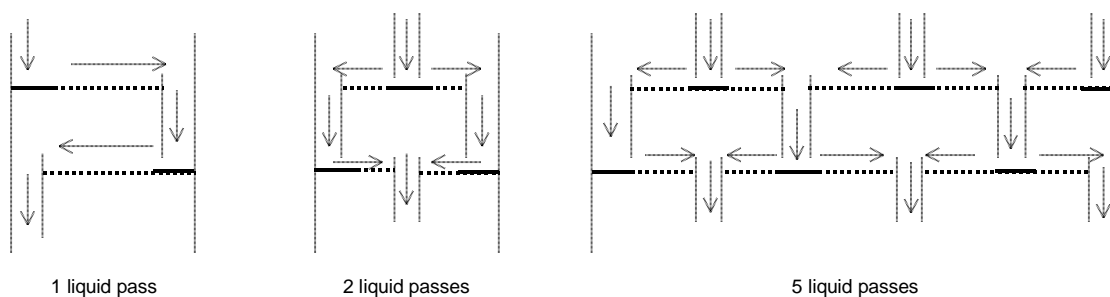


Figure 2. Tray configurations

Details of this second configuration are available in Jones (1985). The catalyst inventory in the reactive zone is 8000 kg for both hardware configurations. In the base case tray configuration we have chosen the five-liquid flow pass configuration (see Fig. 2). We also study the influence of the choice of the number of liquid flow passes on the conversion level.

Figure 3 (a) shows the bifurcation diagram for the packed and tray column configurations for the base case operating conditions. For the reactive tray configuration we assumed that both the liquid and vapour phases on the trays are well mixed. If the bottom flow rate were to be set at 202 mol/s, say, we see that the packed column shows steady-state multiplicity whereas there is only one steady-state for the tray column. For maximizing the conversion one must try to operate in the high conversion “branch” of the bifurcation diagram. For this case there is a small conversion advantage for the packed column configuration with respect to the tray configuration. The same trend holds when the MeOH feed is increased by 7%; see Fig. 3 (b). We now note that at a bottoms flow of 205 mol/s, say, all both the tray and packed column configurations show steady-state multiplicity. There is a range of bottoms flows where the tray configuration yields a lower conversion level than the packed column configuration. Figure 3 (c) shows the bifurcation diagram for the case in which the iso-butene feed to the column is increased by 10%. No steady-state multiplicity is observed for either the packed or tray configurations. The tray configuration is superior to the packed column configuration over the whole range of bottoms flow rates. Figure 3 (d) shows the bifurcation diagram for the case in which the n-butene feed to the column is increased by 10%. No steady-state multiplicity is observed for either the packed or tray configurations. When comparing Fig. 3 (d) with 3 (a) it is interesting to note that both the tray and packed columns show a slight improvement in the conversion. The reason is that the inerts tend to facilitate the separation of the lighter reactants (MeOH and iso-butene) from the product (MTBE). When the reflux ratio is decreased from 7 to 6.5 (see Fig. 3 (e)), we see that the multiplicity vanishes for both tray and packings. Increasing the reflux ratio to 8, on the other hand (see Fig. 3 (f)), introduces multiplicity for both tray and packed configurations. This means increasing the reflux ratio makes the system more susceptible to disturbances in the operating conditions.

In the calculations shown in Figure 3, we have assumed five-liquid flow passes in the reactive section. Figure 4 (a) shows the effect of reducing the number of liquid flow passes from 5 to 2. When operating at the high conversion branch, the conversion level increases. Decreasing the number of liquid flow passes increases the liquid load per weir length. This in turn has the effect of increasing the clear liquid height on the tray and the total interfacial area is also increased. A further influence of reducing the number of liquid flow passes is that the vapour and liquid residence times are increased. All of the foregoing serves to improve the conversion, provided one strives to remain on the “high conversion branch”. It is interesting to note that for a column of 6 m diameter, chosen in this study, the conventional wisdom for distillation tray design would be to use multiple flow passes. This does not hold for reactive distillation in which we carry out a liquid phase chemical reaction.

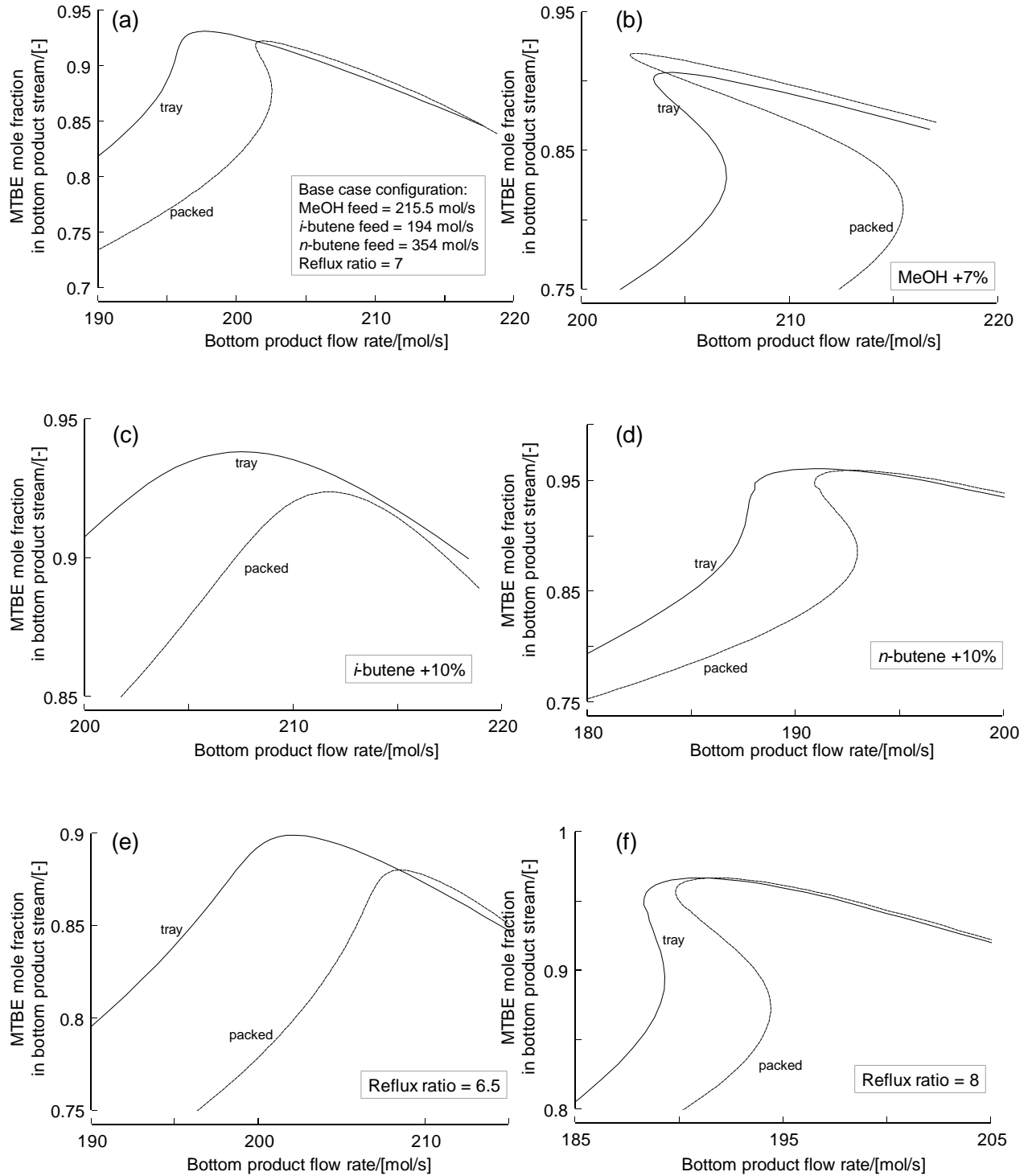


Figure 3. Bifurcation diagrams for tray and packed columns for various operating conditions.

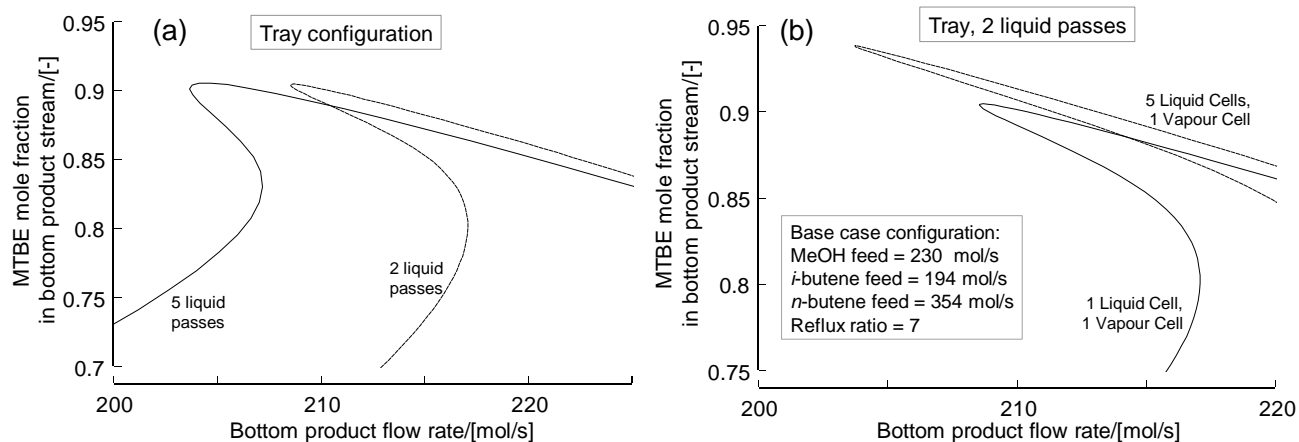


Figure 4. Bifurcation diagrams for tray column (a) influence of liquid flow passes. (b) influence of staging of the liquid phase. The operating conditions for both (a) and (b) are specified in the inset to Fig. 5 (b).

In all the foregoing calculations each tray was considered to be one well-mixed stage. We have investigated the influence of introducing staging in the liquid phase. Figure 4 (b) shows calculations for the 2-liquid pass tray configuration in which the each liquid flow path is considered to be made up of 5 well-mixed cells. This will ensure near plug flow of the liquid phase. As might be expected the conversion level is significantly improved.

Concluding Remarks

The tray and packed column configurations show different bifurcation behaviours. When operating on the high conversion branch, the conversions obtained with the tray and packed column configurations are virtually the same. However, performance obtained in the tray column configuration can be improved by decreasing the number of liquid flow passes and thereby increasing the liquid load per weir height and the liquid phase residence time. This results in improved conversion. The NEQ cell model implementation was used to show that if the liquid flow across the tray can be considered to be in plug flow, then this results in a significant improvement in the conversion level.

The NEQ model described in this work can be used for hardware choice and optimization.

In Chapter 6 we will compare the dynamics of tray and packed column configurations for the MTBE RD column. The material presented in Chapter 3 is a necessary prelude to understanding the respective column dynamics.

Chapter 4

Mass Transfer Efficiencies in Reactive Distillation

Abstract

It is shown that component Murphree efficiencies in reactive distillation defy simple correlation in terms of phase hydrodynamics, equilibria, thermodynamic and transport properties. These efficiencies show a complex dependence on reaction rates and stoichiometry.

Introduction

Several commercial software packages such as RADFRAC of ASPEN TECH allow for interphase mass transfer processes in reactive distillation (RD) processes by means of user-supplied component efficiencies. The objective of the present chapter is to show that component efficiencies in RD defy easy prediction and correlation. In order to underline our arguments we perform three case studies: (1) hydration of ethylene oxide to ethylene glycol in a 10-stage tray column, and (2) MTBE synthesis in a 17-stage tray column and (3) metathesis of 2-pentene to 2-butene and 3-hexene

For calculation of the component efficiencies we have used the rigorous nonequilibrium (NEQ) model for RD columns which utilises the Maxwell-Stefan diffusion equations in either fluid phase (Krishna and Wesselingh, 1997; Taylor and Krishna, 1993). The NEQ model is described in detail in Chapter 2.

Ethylene Glycol Case Study

We consider the reaction of ethylene oxide (EO) with water to produce ethylene glycol (EG) in a reactive distillation column. The reaction is irreversible and proceeds in the presence of a catalyst



In addition we have an unwanted side reaction in which ethylene glycol reacts with ethylene oxide to di-ethylene-glycol (DEG)



The column configuration chosen for the EG production is similar to the set up of Ciric and co-workers (Ciric and Gu, 1994; Ciric and Miao, 1994), details of which are given in Figure 1 (a). This is a 10-stage sieve tray column (including total condenser and partial reboiler). The column configuration is specified in Table 1. Water is supplied to the top of the column, while the EO feed is distributed along the top section of the column. The column is operated at total reflux, while in the bottom a boilup ratio of 24 is maintained. The reaction kinetics and thermodynamics data are the same as those reported in the papers by Ciric et al. (1994). We use a nonequilibrium (NEQ) model for simulating the column and for calculation of the component efficiencies. Reactions are assumed to take place only on stages 2 to 6 because catalyst is considered to be present only on these stages. In the NEQ model calculations, the vapour and liquid phases were both assumed

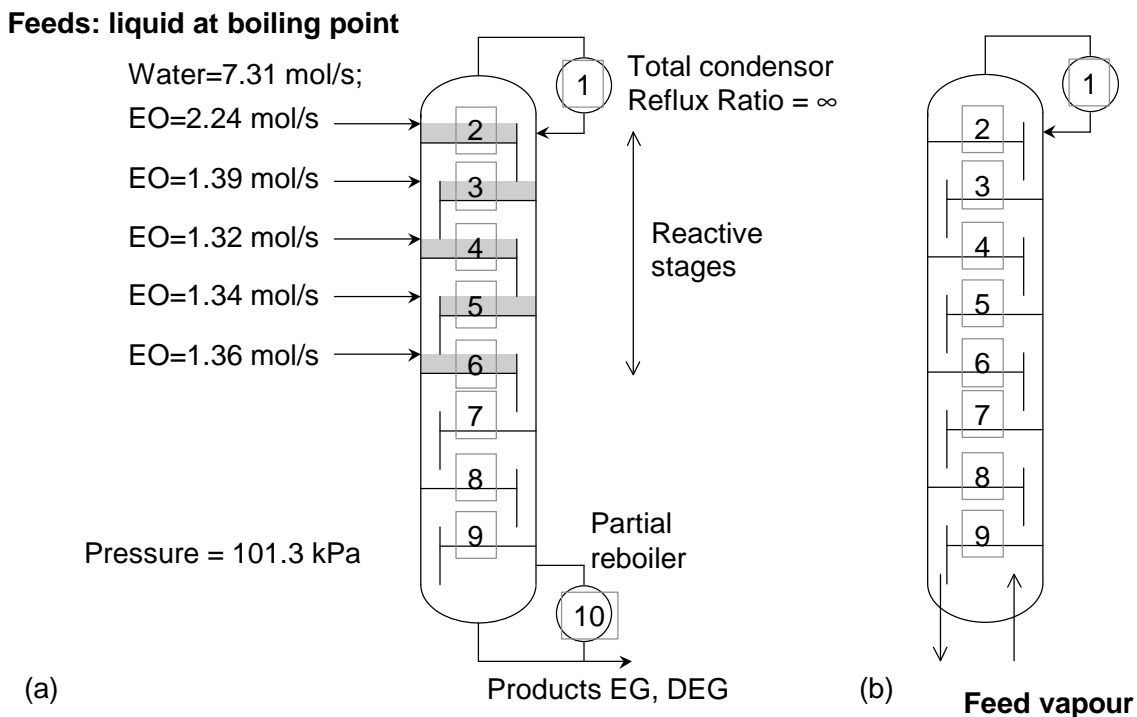


Figure 1. (a) Configuration of reactive distillation column for hydration of ethylene oxide to ethylene glycol. Further details to be found in Ciric and Miao (1994). (b) Equivalent configuration of a non-reactive column consisting only of the rectifying section and with vapour feed to the bottom stage.

to be well-mixed on a given stage. We also carried out a simulation of the rectifying section in which the reactions were "turned-off" and consisting only of the rectifying section as shown in Fig. 1 (b). The composition of the vapour feed to the column is chosen as EO (0.3325), Water (0.3325), EG (0.3225) and DEG (0.0125). The molar flow rate of the vapour feed to the column is adjusted so as to obtain similar vapour and liquid loads on the trays.

The component efficiencies for EO, Water, EG and DEG, calculated from the NEQ model are shown in Fig. 2 with filled symbols for the reactive distillation case (Fig. 1 (a)) and with open symbols for the non-reactive case (Fig. 1 (b)). For the non-reactive column the component efficiencies are close to one another and in the range 0.5 - 0.65. The smallest molecule, water, has the highest component efficiency. The largest molecule DEG has the smallest component efficiency. The component efficiencies of EO and EG lie in between those of water and DEG. For RD operation, the component efficiencies show great variation between the different components. Clearly, chemical reactions influence the values of the component efficiencies in a complex and unpredictable way.

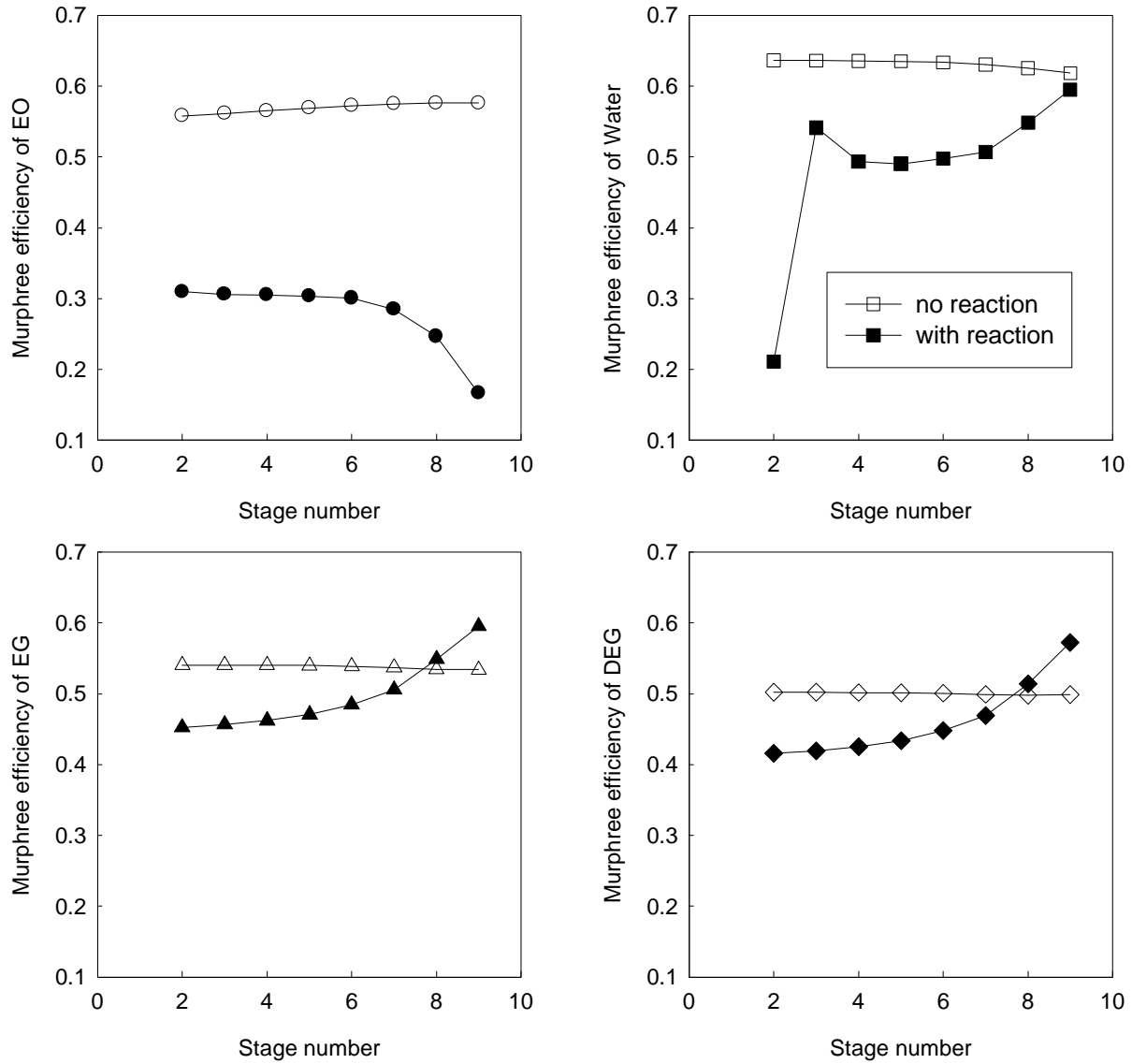


Figure 2. Component efficiencies for EO, water, EG and DEG for reactive and non-reactive operation.

Table 1. Sieve tray specification for ethylene glycol reactive distillation column

	Configuration
Type of tray	Sieve
Column diameter /[m]	1.7
Total tray area /[m ²]	2.27
Number of liquid flow passes	1
Tray spacing /[m]	0.7
Liquid flow path length /[m]	1.28
Active area /total tray area	0.86
Hole diameter /[m]	0.0045
Total hole area /total tray area	0.0858
Downcomer area /total tray area	0.07
Weir length /[m]	1.52
Weir length /column diameter	0.895
Weir height /[m]	0.08
Downcomer clearance /[m]	0.01

MTBE Case Study

We now consider the case study involving the synthesis of MTBE. The column configuration chosen for the simulations is shown in Figure 3; this is essentially the configuration described by Jacobs and Krishna (1993) in their simulation study using the EQ stage model. The total number of stages is 17, including a total condenser and a partial reboiler; the column pressure is 11 atm. Reactive stages are located in the middle of the column, stage 4 down to and including stage 11. The column has two feed streams: a methanol feed and a mixed butenes feed. A small stoichiometric excess of methanol is used. The mixed butenes feed, to stage 11, contains a mixture of *iso*-butene, which is reactive, and *n*-butene, which is non-reactive or inert. The reflux-ratio is set to 7 and the bottom flow rate is either set to 205 mol/s or varied (as a continuation parameter). The product removed from the top of the column is predominantly the inert *n*-butene. The bottoms product consists predominantly of MTBE. For a properly designed and operated column it is possible to achieve close to 100% conversion of *iso*-butene.

The column diameter was chosen to be 6 m. The stripping, rectifying and reactive sections consist of sieve trays. The configuration of the sieve trays are: total tray area = 28.27 m²; number of liquid flow passes = 5; tray spacing = 0.7 m; liquid flow path length = 0.97 m; fractional active area = 0.76; fractional hole area = 0.1; fractional downcomer area = 0.12; hole diameter = 4.5 mm; weir height = 50 mm; total weir length = 22 m; weir type = segmental; downcomer clearance = 0.0381 m; tray deck thickness = 25 mm. The

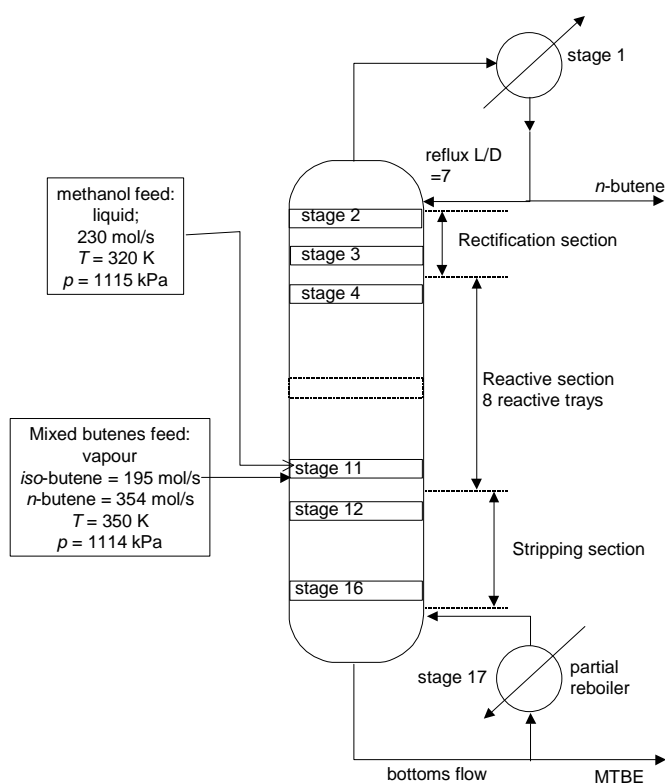


Figure 3. Configuration of the MTBE synthesis column, following Jacobs and Krishna (1993). The column consists of 17 stages.

five-liquid-pass tray configuration is shown in Fig. 4 (a). On each of the eight stages in the reactive zone, 1000 kg of catalyst is introduced in the form of “envelopes” placed along the flow path length; see Fig. 4. The details of such a construction are available in the patent literature (Jones, 1985). The total amount of catalyst in the reactive zone is 8000 kg. The ion exchange capacity of the catalyst is 4.54 (meq H^+ /gram).

The UNIQUAC model was used for description of liquid phase nonideality, while the Soave-Redlich-Kwong equation of state was used for the vapour phase. The extended Antoine equation was used for calculation of the vapour pressure. Thermodynamic and kinetic data are taken from Rehfinger and Hoffmann (1990a, 1990b).

With the molar bottoms flow rate as continuation parameter we obtain the bifurcation diagram as shown in Fig. 5. For the simulations to be discussed below the bottoms flow rate was fixed at 205 mol/s. For this condition we have two stable steady-states, a high conversion state (HSS) and a low-conversion state (LSS). There is an unstable state which lies in between HSS and LSS. The vapour and liquid loads on the trays for the two stable steady-states, HSS and LSS are similar.

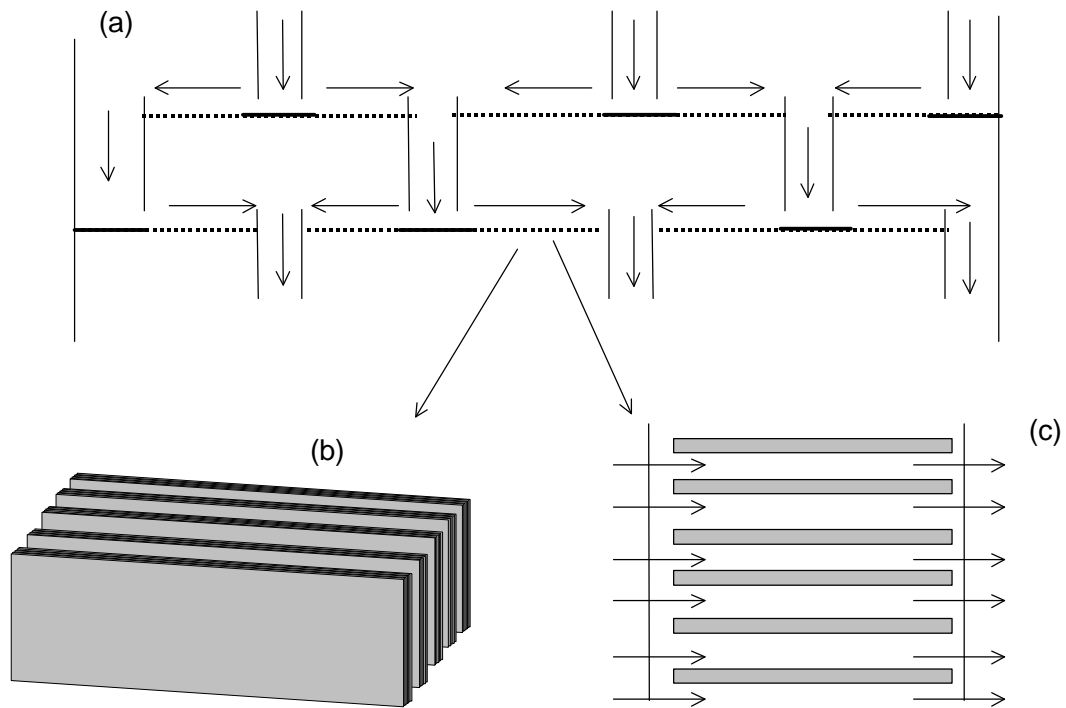


Figure 4. (a) Five-liquid-pass sieve tray configuration. (b) and (c) The reactive section consists of catalyst envelopes placed along the liquid flow path.

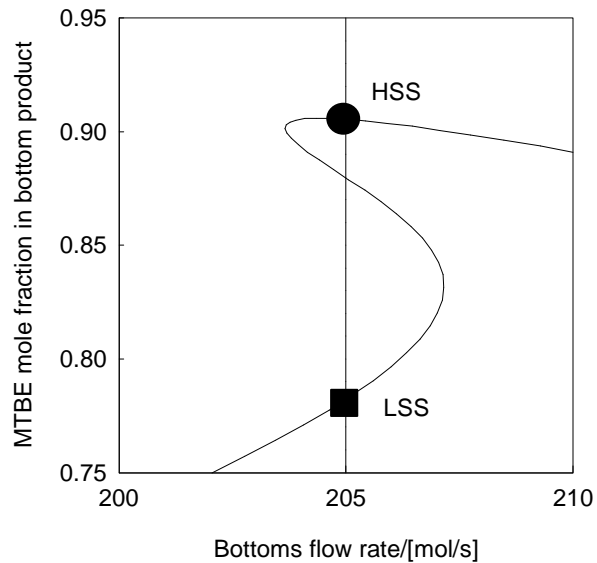


Figure 5. Bifurcation diagram for sieve tray MTBE RD column calculated with NEQ model.

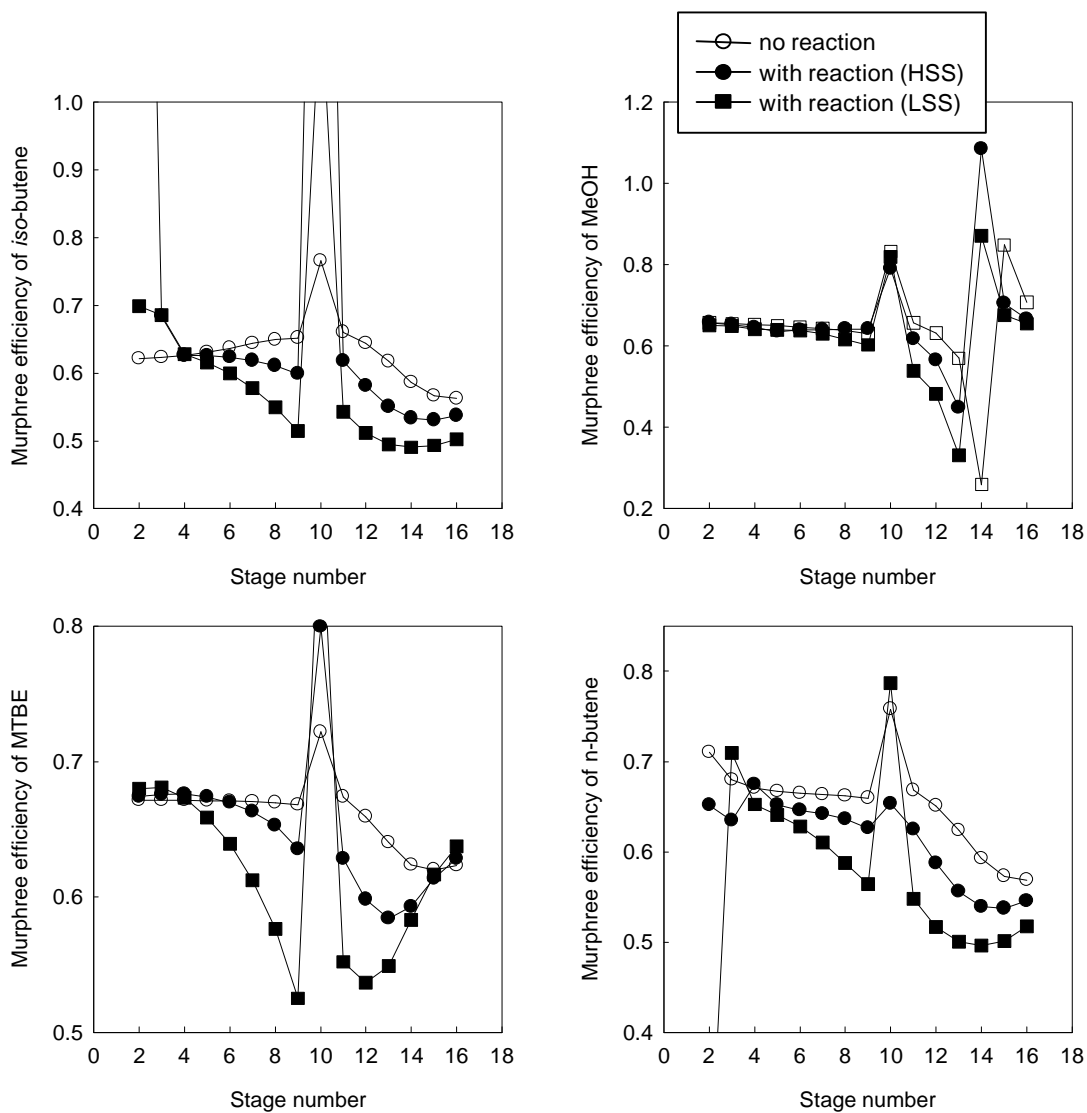


Figure 6. Component efficiencies for iso-butene, MeOH, MTBE and n-butene for reactive and non-reactive operations.

The component efficiencies calculated from the NEQ model calculations for HSS and LSS are shown in Fig. 6 along with the component efficiencies calculated for a non-reacting column whose feed (on stage 11) consists of the products from the column for the reacting case.

We note that at the feed stage 11, all component efficiencies show a sharp spike. This is due to the fact that the feed is partially vaporised at the column conditions and this distorts the efficiency calculations for the feed stage. For all other stages in the non-reacting column the component efficiencies are reasonably well behaved. With chemical reaction the component efficiencies vary strongly from component to component and from one stage to another. Furthermore, for operation at LSS the component efficiencies are significantly lower than for operation at HSS. Bearing in mind that the molar flow rates are almost the same in these two cases, we expect the hydrodynamics to be the same. Yet the component efficiencies are significantly different. This underlines the non-usability of component efficiencies for RD operations.

Metathesis of 2-pentene

We now consider the example of metathesis of 2-pentene to 2-butene and 3-hexene. This reaction can be effectively carried out in a RD column, as discussed by Okasinski and Doherty (1998). The reaction is reversible:

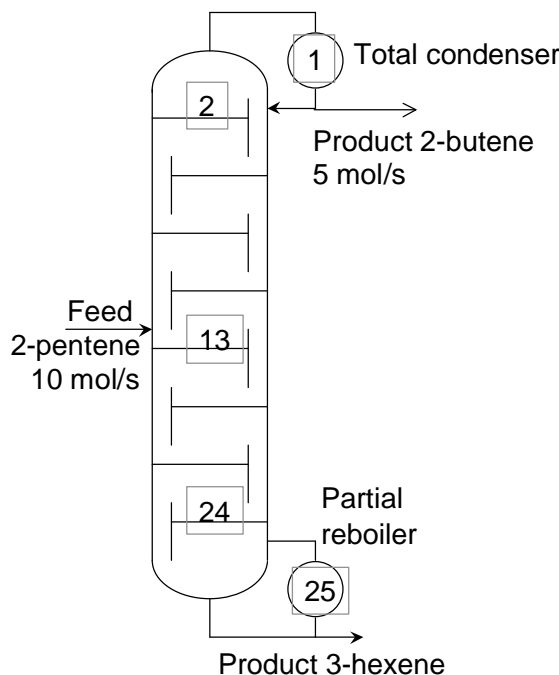
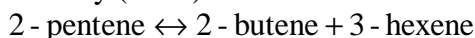


Figure 7. Configuration of the RD column for metathesis of 2-pentene.

Table 2. Sieve tray specification for metathesis RD column

	Configuration
Type of tray	Sieve
Column diameter /[m]	1.8
Total tray area /[m ²]	2.545
Number of liquid flow passes	2
Tray spacing /[m]	0.61
Liquid flow path length /[m]	0.62
Active area /total tray area	0.76
Hole diameter /[m]	0.0045
Total hole area /total tray area	0.10
Downcomer area /total tray area	0.12
Weir length /[m]	3.13
Weir height /[m]	0.08
Downcomer clearance /[m]	0.038

The overall rate of reaction of 2-pentene is given by

$$R = 0.5c_{c5}k_f(x_{c5}^2 - x_{c4}x_{c6}/K_{eq})$$

The forward reaction rate constant is

$$k_f = 78.2 \exp\left(-\frac{27600}{RT}\right) \quad [\text{s}^{-1}]$$

and the equilibrium reaction rate constant

$$K_{eq} = 0.25$$

The RD column configuration chosen consists of a 25-stage column with liquid feed of pure 2-pentene on stage 13; see Fig. 7. The feed flow rate is 10 mol/s. The condenser and top column pressures are fixed at 101.3 kPa. The RD column is constructed of sieve plates and the configuration details are given in Table 2. The pressure drop on each tray is calculated using the Bennett et al. (1983) correlation. The top product flow rate is fixed at 5 mol/s. The boilup ratio is fixed at 8. For calculation of the thermodynamic properties the Peng-Robinson equation of state was used. The AIChE method was used for estimation of the mass transfer coefficients in the vapour and liquid phases.

Two different NEQ model implementations were used to determine the component efficiencies: the NEQ 1 × 1 cell and NEQ 3 × 3 cell models. The component efficiencies are shown in Fig. 8. It can be observed that the introduction of staging in the vapour and liquid phases has a pronounced influence on the component efficiencies. The NEQ 3 × 3 cell yields significantly higher component efficiencies, as might be expected because of the beneficial influence of staging in RD columns. Clearly component efficiencies in RD columns also depend on the degree of staging in the vapour and liquid phases on the tray.

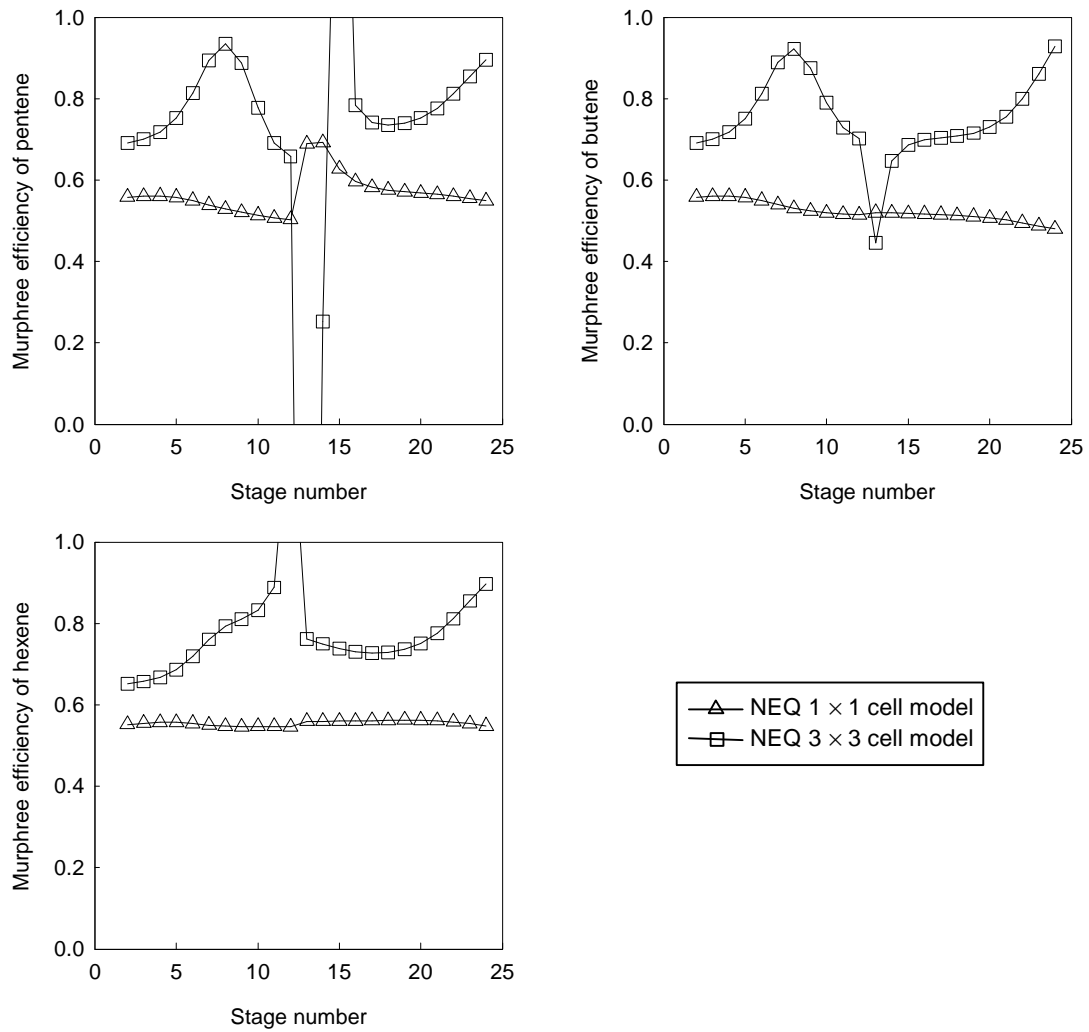


Figure 8. Component efficiencies for 2-pentene, 2-butene and 3-hexene in RD column calculated with NEQ 1 × 1 cell and 3 × 3 cell models.

Concluding Remarks

Using the three case studies we have underlined the shortcomings of the use of component efficiencies for RD.

1. Component efficiencies are strongly influenced by chemical reaction. Whether a component is a reactant or product influences the component efficiency
2. When the RD column exhibits steady-state multiplicity, each of these steady-states yields significantly different component efficiency values.
3. Component efficiencies in RD are also influenced significantly by the degree of staging in the vapour and liquid phases.

We conclude by saying that *a priori* estimation efficiencies in RD columns is well nigh impossible.

Though we have tried to underline the difficulty of predicting component efficiencies in RD columns, many existing software design packages use this approach. In Chapter 6 we will demonstrate that the use of an EQ model with (constant) component efficiencies might also give an improper representation of column dynamics.

Chapter 5

Influence of Mass Transfer on Distillation Trajectories

Abstract

In contrast to the previous chapters in this thesis, the present chapter focusses on *non*-reactive distillation. The idea is to examine the influence of mass transfer on the composition trajectories during distillation of mixtures that exhibit distillation boundaries. Simulations for total reflux distillation of the systems methanol- *iso*-propanol - water and benzene - *iso*-propanol- *n*-propanol show that composition trajectories originating along the distillation boundary could end up in completely different corners of the composition triangle depending on whether or not diffusional interactions are taken into account. Using published experimental data it is concluded that for reliable design and simulation it is necessary to use a rigorous model for mass transfer based on the Maxwell-Stefan diffusion equations.

Introduction

Most commercially available simulation programs for distillation columns (Seader and Henley, 1998) cater to “real” or non-equilibrium trays. The departure of these real trays from equilibrium behaviour is allowed for in either of two ways. In the first procedure, the user is allowed to specify the individual component Murphree efficiencies for each stage. These component efficiencies can be estimated “off-line” by using the various mass transfer correlations (AIChE method 1958; Chan and Fair 1983; Zuiderweg 1982) as discussed in the book of Lockett (1986). The second approach, which is gaining currency, is to use a fully rate-based approach. In this approach, the interphase mass and heat transfer equations are solved simultaneously along with the interphase equilibrium relations for each stage (Krishnamurthy and Taylor 1985; Taylor and Krishna 1993). In the rate-based approaches, the interphase mass transfer relations are invariably based on the Maxwell-Stefan diffusion equations in either fluid phase (Taylor and Krishna 1993; Krishna and Wesselingh 1997). This is the approach used in Chapter 2 to describe reactive distillation.

There is some evidence in the published literature that experimentally measured composition profiles in distillation columns are better simulated with models based on the rigorous Maxwell-Stefan diffusion equations than with simpler models that assume equal component efficiencies (Taylor and Krishna 1993; Krishna and Wesselingh 1997; Gorak 1995; Ronge 1995).

Castillo and Towler (1998) computed nonequilibrium distillation lines for a sieve tray column and demonstrated that modest differences between the efficiencies of different components in a ternary mixture could lead to significant differences in curvature between equilibrium and nonequilibrium distillation lines. They go on to show that, in some cases, differences in curvature could be exploited by the engineer in order to obtain process designs that could not be contemplated if mass transfer effects were ignored, and that some designs based solely on equilibrium models can become infeasible when mass transfer is considered.

It is the purpose of this chapter to contribute further to this emerging discussion of nonequilibrium distillation lines. In particular, we show that these lines can be extremely sensitive to the choice of model, particularly near to distillation boundaries. Specifically, we shall show that methods that ignore differences between binary pair (Maxwell-Stefan) diffusion coefficients (for example, the method of Zuiderweg 1982) can lead to erroneous predictions of column performance.

Distillation boundaries are also encountered in reactive distillation and we expect that some of the insights gained in the present study could also be significant for RD operations.

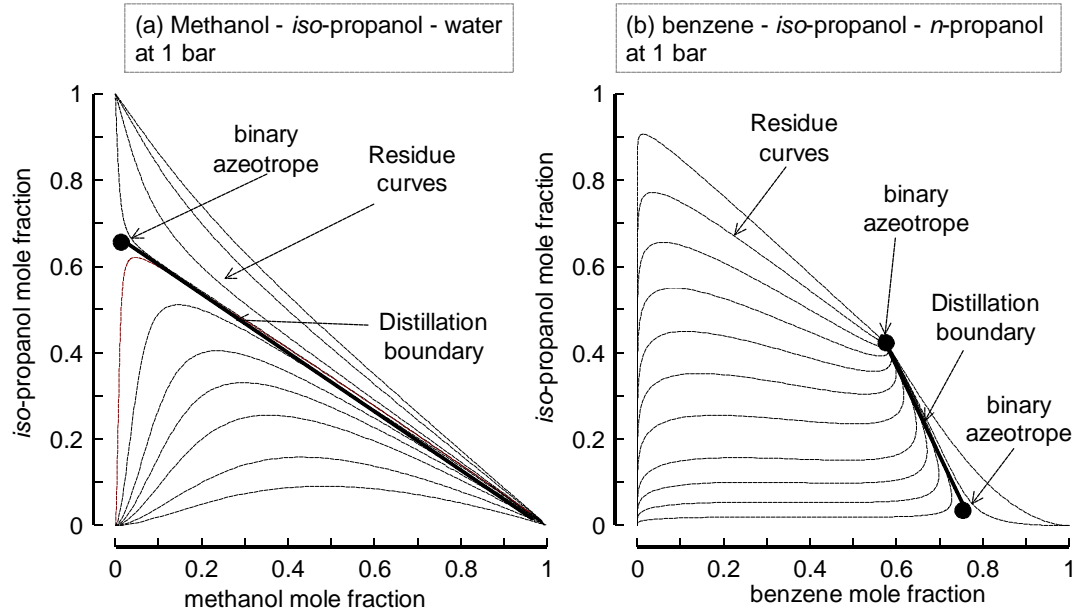


Figure 1. Residue curve maps for the systems (a) methanol- iso-propanol-water and (b) benzene - iso-propanol- n-propanol.

Simulations of Total Reflux Operations in Sieve Tray Columns

We examine the influence of mass transfer on column composition profiles, focussing our attention on two non-ideal mixtures which exhibit a distillation boundary: methanol- *iso*-propanol-water and benzene - *iso*-propanol- *n*-propanol. Shown in Fig. 1 are the residue curve maps (described for example in Seader and Henley 1998) for these systems, calculated using the NRTL model (parameters listed in Table 1). The calculations of the residue curves were performed using Maple V Release 4 with BESIRK, a differential-algebraic equation solver. The distillation boundaries for the two systems are indicated by

Table 1. NRTL parameters for the mixtures methanol- *iso*-propanol-water and benzene - *iso*-propanol- *n*-propanol

Component i	Component j	$A_{i,j}/[\text{J/mol}]$	$A_{j,i}/[\text{J/mol}]$	$\mathbf{a}_{i,j}$
methanol	<i>iso</i> -propanol	546.323	-746.121	0.3040
methanol	water	-1518.18	4943.753	0.2970
<i>iso</i> -propanol	methanol	587.483	6062.742	0.2880
<i>iso</i> -propanol	benzene	1386.688	3260.067	0.2913
<i>iso</i> -propanol	<i>n</i> -propanol	-2819.03	4150.621	0.2978
benzene	<i>n</i> -propanol	4236.07	659.124	0.2888

Table 2. *Specification of sieve tray column used in the simulations.*

Column internals	Sieve tray
Number of stages	40
Column diameter /[m]	0.8
Tray spacing /[m]	0.6
Number of flow passes	1
Weir length /[m]	0.74
Weir height /[m]	0.05
Hole diameter /[m]	0.005

thick lines. The mixture methanol- *iso*-propanol-water has a binary minimum boiling azeotrope for *iso*-propanol-water. The distillation boundary splits the residue curve map into two regions. For the system benzene - *iso*-propanol- *n*-propanol we have two minimum boiling azeotropes: benzene - *iso*-propanol and benzene - *n*-propanol. The distillation boundary connects these two azeotropes and again distinguishes two regions. It can be seen that the residue curves, which originate along the distillation boundary, can choose two different paths ending up in different corners of the composition triangle. The residue curves coincide with the liquid composition trajectories during distillation at total reflux in a differential-contact column, such as a packed column, in which the liquid and vapour phases are in thermodynamic equilibrium.

Column simulations were carried out for the two systems methanol- *iso*-propanol-water and benzene - *iso*-propanol- *n*-propanol at total reflux in a 40-stage sieve tray column

with the hardware specifications in Table 2. The simulations were carried out using ChemSep, a steady-state equilibrium stage and non-equilibrium stage simulator described in earlier work (Taylor and Krishna, 1993; Taylor *et al.*, 1994).

Figure 2 (a) shows the liquid composition trajectories in the column, calculated using four different models for interphase mass transfer: (1) AIChE correlation, (2) Chan and Fair correlation, (3) Zuiderweg correlation and (4) a model in which all component efficiencies are assumed to be equal to one another. The detailed description of the mass transfer correlations are available elsewhere (Lockett 1986; Taylor and Krishna 1993). In addition, both vapour and liquid phases are assumed to be completely mixed on any tray. In all cases, excepting the fourth one, the generalized Maxwell-Stefan diffusion equations are used to predict the ternary mass transfer behaviour based on the information of the constituent binary pairs. For the fourth, equal efficiency model, the values of the

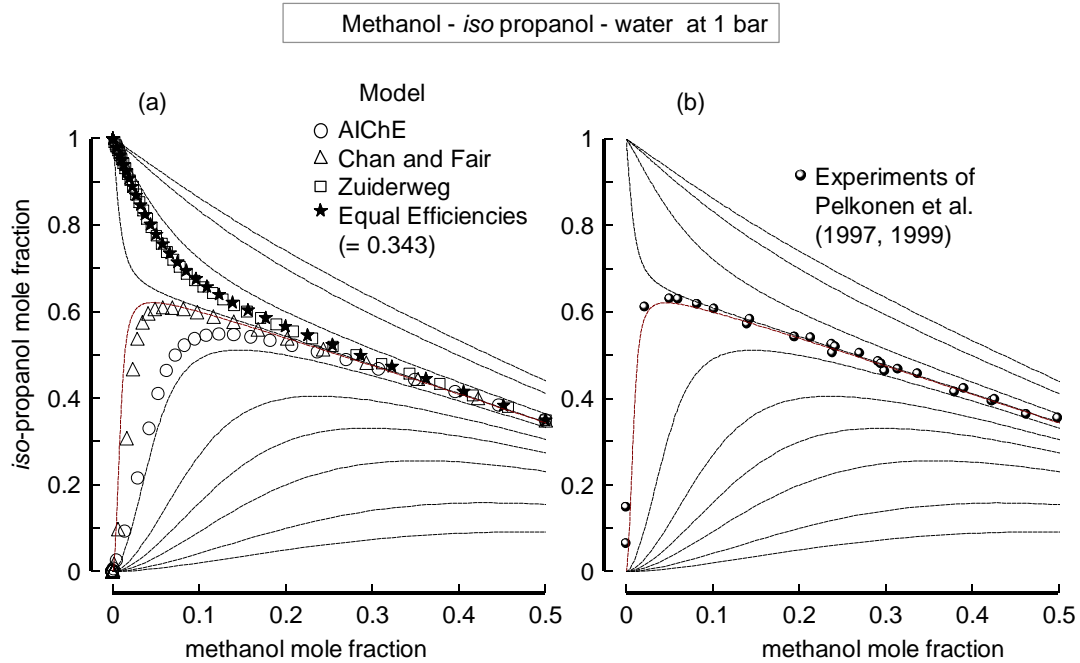


Figure 2. Composition trajectories for the system methanol- iso-propanol-water. (a) Liquid composition trajectories in a sieve tray column predicted with four different mass transfer models. In all calculations shown here the liquid and vapour phases were assumed to be well mixed on a tray. For the equal efficiency model all the component efficiencies were set equal to 0.343, which represents the average of the component efficiencies shown in Fig. 3. (b) Liquid composition trajectories measured by Pelkonen et al.^{13,14} in a 0.1 m diameter column packed with Sulzer BX packing and operating at total reflux. The broken lines in the figure represent the residue curves.

component efficiencies of each of the components were forced to be equal to the average of the component efficiencies calculated using the Maxwell-Stefan formulation and the AIChE correlation. A detailed step-by-step calculation procedure for the estimation of the mass transfer fluxes, and component efficiencies in multicomponent systems is to be found in Chapter 13 of the book by Taylor and Krishna (1993). Also shown with broken lines in Fig. 2 (a) are the residue curves for this system. All four mass transfer models predict composition trajectories, which tend to follow the residue curves, albeit ending up in different corners of the composition triangle. The Zuiderweg and Equal-component-efficiency models predict almost identical column composition trajectories. More interestingly, we note that the AIChE and Chan-Fair correlations predict that the reboiler composition corresponds to pure water whereas the Zuiderweg and Equal-component-efficiency model predicts the reboiler to consist of pure *iso*-propanol. Put another way, the choice of the mass transfer model dictates which residue curve path is followed if the column compositions originate from a distillation boundary.

Though the rate based approach does not use Murphree component efficiencies in the material and energy balances, these can be calculated on each stage:

$$E_i^{MV} = \frac{\overline{y_{iL}} - y_{iE}}{y_i^* - y_{iE}}; \quad i = 1, 2, \dots, c \quad (1)$$

where $\overline{y_{iL}}$ is the average composition of the vapour leaving the tray, y_{iE} is the composition of the vapour entering the tray and y_i^* is the composition of the vapour in equilibrium

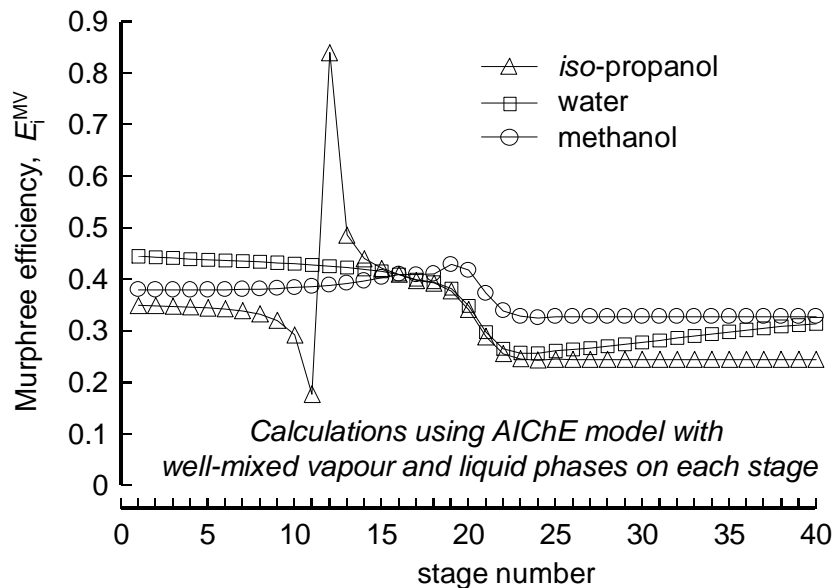


Figure 3. Component vapour phase Murphree tray efficiencies for the system methanol-*iso*-propanol-water. Calculations using the AIChE model and assuming liquid and vapour phases to be well mixed.

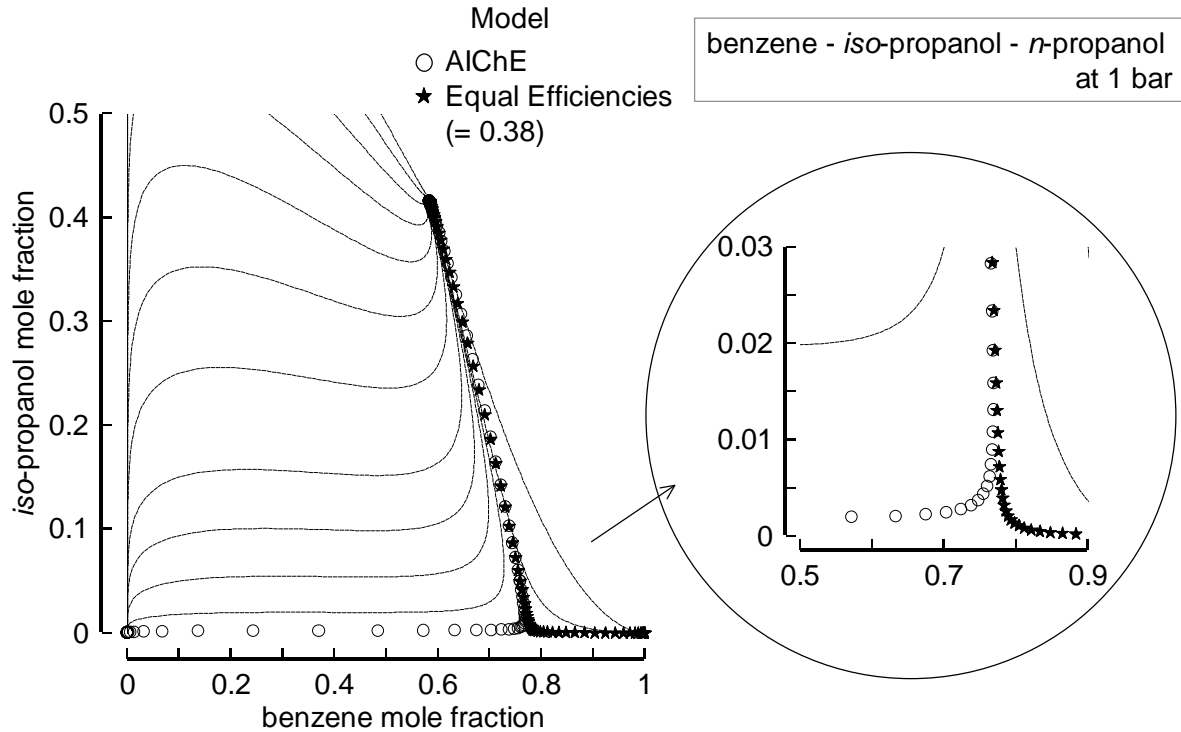


Figure 4. Composition trajectories for the system benzene- iso-propanol - n-propanol in a 40-stage sieve tray column. For the equal efficiency model all the component efficiencies were set equal to 0.38, which represents the average of the component efficiencies shown in Fig. 5.

with the liquid leaving the tray. Since the mole fractions add to unity, only $(n-1)$ of the Murphree component efficiencies are independent. For distillation of systems with three or more species, the component efficiencies are almost always unequal to one another and these can routinely assume values greater than unity or less than zero (Taylor and Krishna, 1993; Krishna and Wesselingh, 1997). The component efficiencies, calculated with the AIChE model for the sieve tray, are shown in Figure 3. The component efficiency of *iso*-propanol is significantly lower than that of the other two components; this is the major reason why the trajectory followed by the AIChE model ends up with a reboiler with pure water (lower left corner). When all component efficiencies are forced to equal one another (as in model (4)), the column trajectory ends up in the upper left corner with pure *iso*-propanol in the reboiler.

The correlations developed by Zuiderweg (1982) for the vapour and liquid phase mass transfer coefficients on sieve trays are summarized below

$$k_G = 0.13/r_G - 0.065/r_G^2 \quad (1 < r_G < 80) \quad (2)$$

$$k_L = 0.024D_L^{0.25} \quad (3)$$

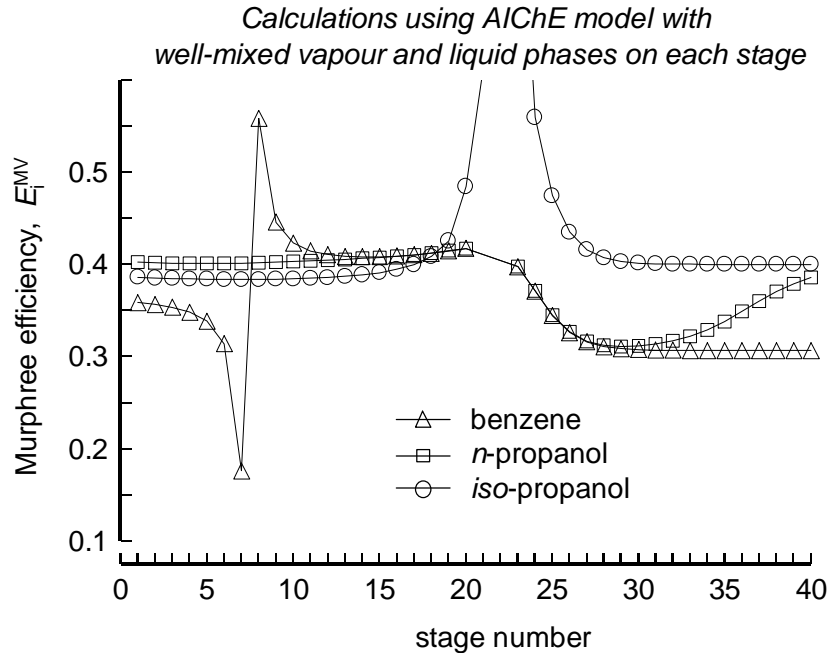


Figure 5. Component vapour phase Murphree tray efficiencies for the system benzene-*iso*-propanol - *n*-propanol. Calculations using the AIChE model and assuming liquid and vapour phases to be well mixed.

It is important to note that the gas phase diffusivity does not appear in the correlation for the gas phase mass transfer coefficient. Therefore, the component efficiencies, for systems dominated by vapour phase mass transfer, will be equal for all components. This explains why the Zuiderweg and Equal-component-efficiency model predict almost identical composition trajectories.

Lockett (1986) has also underlined the special feature of the Zuiderweg correlation (2) for the gas phase mass transfer coefficient and its independence on the gas phase diffusivity. He has suggested a hybrid approach in which the gas phase mass transfer coefficient is calculated using the AIChE method while the liquid phase mass transfer coefficient is estimated from the Zuiderweg correlation.

We have carried out analogous calculations for columns with other types of internals (bubble cap trays, dumped and structured packings), and with other assumptions regarding the mixing characteristics of the vapour and liquid phases (plug flow in either or both phase) with essentially the same results as discussed above.

Experiment data points reported by Pelkonen *et al.* (1995, 1999) for total reflux operation of methanol - *iso*-propanol - water in a 0.1 m diameter column packed with Sulzer BX packing are plotted in Figure 2 (b) as black circles. Also shown with broken lines in Fig. 2 (b) are the residue curves for this system. The experimental composition trajectories, which lie along a residue curve, start at a composition $x_{\text{methanol}} = 0.5$, $x_{\text{isopropanol}} = 0.35$ at the

top of the column and end up with virtually pure water in the reboiler. Model calculations carried out by Pelkonen *et al.* (1997), also using ChemSep, assuming equal HETPs for each individual component predicted that the reboiler would consist of pure *iso*-propanol, i.e. follow the residue curve emanating from $x_{\text{methanol}} = 0.5$, $x_{\text{isopropanol}} = 0.35$ but going in the opposite direction to the experiments towards the pure *iso*-propanol vertex. The experiments and simulation results of Pelkonen *et al.* (1995, 1999) could be used to conclude that the Zuiderweg and Equal Component Efficiency (=0.343) model calculations in Fig. 2 (a) follow the *wrong* residue curve originating from the distillation boundary.

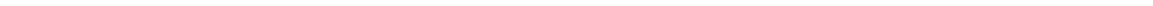
Results analogous to the foregoing are obtained for the system benzene - *iso*-propanol - *n*-propanol. Simulation results for the AIChE and equal-component-efficiency models are shown in Figure 4. Again, we note that the two composition trajectories end up in two different composition corners, pure *n*-propanol and pure benzene, respectively. The component efficiency for benzene is significantly lower than that of the other two components (see Figure 5). This is the reason that the composition trajectory predicted by the rigorous Maxwell-Stefan model (taking differences in component efficiencies into consideration) predicts a reboiler composition which consists of pure *n*-propanol. Forcing the component efficiencies to equal one another results in a trajectory with pure benzene in the reboiler. Using the evidence of the Pelkonen experiments for the system methanol - *iso*-propanol – water we anticipate the reboiler to consist of pure *n*-propanol. It would be interesting to obtain experimental verification of this.

Concluding Remarks

We have demonstrated that the column composition trajectories in sieve tray operations can follow different residue curve paths originating from a distillation boundary. A model, in which the component efficiencies are all forced to equal one another, predicts a column composition profile ending up in the “wrong” corner. In the context of sieve tray design for non-ideal mixtures, the Zuiderweg correlation is not to be recommended. This correlation is perhaps adequate for thermodynamically ideal hydrocarbon mixtures.

The need for rigorous modelling of mass transfer has been demonstrated for non-reactive distillation. This conclusion is even more emphatically true for *reactive* distillation.

In Chapter 7 we will be examining the dynamic behaviour of a distillation column for separating the mixture methanol – *iso*-propanol – water. To understand the dynamics it is important to appreciate the steady-state behaviour, as discussed in the current chapter.



Chapter 6

Development of Dynamic Nonequilibrium Stage Model

Abstract

In this chapter we develop a generic, dynamic, nonequilibrium (NEQ) *stage* model for reactive distillation (RD). The features of our model are: (1) use of the Maxwell-Stefan equations for describing mass transfer between fluid phases, (2) the reaction is assumed to take place in the liquid phase, both within the diffusion layer and in the bulk, (3) coupling between mass transfer and chemical reactions within the diffusion layer is accounted for, (4) solid catalysed reactions are treated using a pseudo-homogeneous liquid phase model with the appropriate pseudo-homogeneous kinetic expressions, and (5) a comprehensive set of design correlations, for both trays (sieve, bubble caps) and packings (random dumped, structured), for hold-up and mass transfer have been incorporated into the software package following earlier work (Taylor et al. 1994). We report some unusual, hitherto unrecognised dynamic features of RD columns by examining the response of a column for MTBE synthesis to perturbations in the feed of methanol, iso-butene or n-butene. When operating at a high-conversion branch of the bifurcation diagram, small perturbations are shown to lead to a transition to a low conversion branch. The NEQ model is shown to be more susceptible to feed perturbations than a conventional equilibrium (EQ) model with constant component efficiencies. More interestingly, when starting at the low conversion branch of the bifurcation diagram, small perturbations in the feed flows could lead to transition to a higher conversion steady state.

Introduction

In the literature both equilibrium (EQ) stage and nonequilibrium (NEQ) stage models have been used for studying the dynamic behaviour of reactive distillation (RD) columns and we review the key publications below.

Savkovic-Stevanovic (1982) put forth an unsteady-state EQ stage model of a distillation process in which one component takes part in an association reaction in both phases. Euler's method was used to integrate the differential equations. A comparison with data for the acetic acid – benzene system shows good agreement with the model, but no actual data are provided.

Roat et al. (1986) integrate the control system equations with the column model equations. They show, using the Eastman methyl acetate process, that control schemes with good steady-state characteristics may fail under unsteady-state conditions.

Ruiz *et al.* (1995) describe a software package called READYS (REActive Distillation dYnamic Simulator) for which an EQ stage model is used which adopts the assumption of physical equilibrium, ideal mixing, thermal equilibrium with a chemical reaction confined to the liquid phase. Column hydraulics is accounted for through a pressure drop equation and departures from equilibrium can be modeled using a Murphree-type efficiency factor. Extensive numerical results are provided. The authors state that their program can be used to study unsteady and unstable column operations such as start-up, shutdown and abnormal hydraulic column behaviour. The package allows for a number of standard thermodynamic property packs as well as user-supplied models. Scenna et al. (1998) employ READYS to study the start-up of reactive distillation columns. They show that the start-up policy can have a strong influence on the ultimate steady state behaviour by sending the column to an undesirable operating point.

READYS and Aspen Plus were used by Perez-Cisneros et al. (1996, 1997b) who also discussed their own somewhat different approach to the EQ model. Their model uses chemical 'elements' rather than the actual components. The chemical elements are the molecule parts that remain invariant during the reaction. The actual molecules are formed from different combinations of elements. A benefit of this approach is that the chemical and physical equilibrium problem in the reactive mixture is identical to a strictly physical equilibrium model. A comparison with the RD data of Suzuki et al. (1971) is provided and it is noted that these data are difficult to match unless the "fitted" activity coefficient model proposed by Suzuki et al. is used.

Gani et al. (1998) described a generalized reactive separation unit model. Theirs is an unsteady-state EQ stage model that can handle systems both with and without reactions and with more than two fluid phases. The methodology is quite unique in that it is based on the element approach of Perez-Cisneros et al. (1997a). Several numerical examples cover a range of simulation problems. Pilavachi et al. (1997) use the same approach, but their paper does not dwell on the computational methods; rather its focus is on some of

the parameters that are important in RD modelling. For example, they discuss the effect of thermodynamic models and their parameters on RD simulation.

Abufares *et al.* (1995) use an EQ stage model for steady state and dynamic modelling of a reactive distillation column for production of MTBE. The steady state model is RADFRAC from Aspen Plus. The unsteady state model equations are solved using SpeedUp, a commercial dynamic process simulation program. The focus of their paper is the transient response of the system.

Alejski and Duprat (1996) described a dynamic model for modelling kinetically controlled RD processes. The model is based on the conventional assumptions of negligible vapour phase hold-up and perfect mixing of the two phases. Departures from phase equilibrium could be handled by specification of a vaporisation efficiency, and corrections of the conversion due to imperfect mixing are accounted for using a “conversion efficiency”, the latter being calculated from an eddy diffusion model in terms of the Peclet number. The model is compared to data obtained in a pilot scale column for the esterification of ethanol with acetic acid and sulphuric acid as homogeneous catalyst. Column start-up and disturbances of continuous operation were investigated. The dynamic temperature profiles are in reasonable agreement with the data, but the predicted dynamic concentration profiles are very different from the observed profiles. Alejski and Duprat (1996) also recommend that tray hydraulics be accounted for in any dynamic model of reactive distillation.

Schrans *et al.* (1996) carried out dynamic simulations, using SPEEDUP, of the MTBE synthesis process using the Jacobs-Krishna (1993) RD column configuration. Their simulations showed that increase in the iso-butene feed by 4 % leads to oscillatory behaviour. A further increase of iso-butene feed by 5% causes a jump from the high-conversion steady-state to the lower one. They offer no explanation for the observed oscillatory behaviour.

Sneesby *et al.* (1997a) model the synthesis of ETBE using an EQ stage model that they solve with SpeedUp. Simulation results are compared to results obtained with the commercial simulation program Pro/II. Homotopy methods are used to investigate the effects of important design variables (feed composition, ethanol excess, pressure, number of equilibrium stages – reactive or non-reactive, reboiler duty and so on). A process design methodology is suggested. In a companion paper Sneesby *et al.* (1997b) develop a dynamic model of the same process using SpeedUp. Their dynamic model assumes reaction equilibrium is attained on all stages, neglecting reaction kinetics. The authors recommend including control issues early in the design process. Subsequent papers from this group look at multiple steady states in RD (Sneesby *et al.*, 1998a-c). Sneesby *et al.* (1998b) (as well as Bartlett and Wahnschafft (1998) using RADFRAC) report that the transition from one steady state to another can be prevented using appropriate control strategies.

Espinosa *et al.* (1994) presented a simplified dynamic model for a reactive distillation column. Vapour hold-ups, heat losses to the environment and the heat of reaction were

neglected. In addition, equimolar overflow and physical and chemical equilibrium was assumed. The resulting equations were rewritten in terms of the transformed variables presented by Barbosa and Doherty (1987). In order to save calculation time, the order of the model was reduced using an orthogonal collocation method. Some calculations were done for an ideal quaternary system. The reduced order model was verified against a “rigorous” model and a reasonably good match was found. No extensive numerical dynamic data are presented.

Grosser et al. (1987) use a dynamic model based on the following assumptions:

- the mixture reaches reaction and phase equilibrium instantaneously on each tray
- the solutions are dilute (thus the temperature change can be ignored)
- the liquid hold-up is constant on each tray (the vapour hold-up is ignored)
- constant molar overflow (modified somewhat) relates the flows from stage to stage.

They study the separation by RD of close-boiling mixtures such as mixtures of xylenes, C4 hydrocarbons, and chlorobenzenes. They report that RD is an attractive alternative to conventional distillation when the relative volatility is less than 1.06.

Kumar and Daoutides (1999) presented a comprehensive dynamic EQ stage model of an ethylene glycol RD column. They compare a model that includes vapour phase balances to a more conventional model that ignores the vapour hold-up and suggest that it is important to include the vapour phase in order to more accurately model the process dynamics. The major thrust of this work is the design of a control system that performs well with stability in the high purity region.

Moe et al. (1995) discuss possible numerical problems when developing dynamic models of reactive distillation based on phase and chemical equilibrium principles.

Kreul et al. (1998) described a NEQ model for reactive distillation in packed columns. Theirs is a dynamic model that, as is usual in such models, neglects the hold-up in the vapour phase. Their paper addresses the problems of modelling mass transfer and reaction in a vapour-liquid-porous catalyst system. In addition, they describe a two-phase model in which diffusion and reaction to and within the solid catalyst is not accounted for by additional equations (and parameters), but their effects are lumped into a kinetic term that appears in the liquid phase material balances. The choice of which of these two approaches was adopted for their simulations is not completely clear. The material balances (partial differential equations) are discretised in the spatial dimension (the column height) using the method of lines. The model equations were solved using the equation-based modelling environment ABACUS (Allgor et al., 1996). The 1998 paper includes a limited comparison with some unsteady state data for a methyl acetate column. The results shown in the paper suggest that their dynamic model is well able to describe the product composition transients. The actual experimental data are not provided in the paper.

Kreul et al. (1999) described a NEQ model to study batch distillation. In essence, the model is an extension and generalisation of the dynamic NEQ models of Kooijman and Taylor (1995) for tray columns and Pelkonen et al. (1997) for packed columns. The

Maxwell-Stefan equations were used to model vapour and liquid phase mass transfer. The model system was implemented and solved using the ABACUS system. The paper includes extensive comparisons of true model *predictions* of experiments performed in a pilot plant column involving the system methanol – acetic acid – methyl acetate – water. Under the conditions in the experiments there was essentially no liquid phase chemical reaction; vapour phase dimerisation was, however, taken into account. The agreement between the predicted and measured compositions is exceptionally good.

The primary objective of the current chapter is to first develop a rigorous dynamic NEQ *stage* model for RD columns, for both sieve tray and random packed configurations. With the developed NEQ model we study the differences in the RD column dynamics predicted by the NEQ model with the more widely used EQ model (often with a stage efficiency). We aim to show that the dynamic responses could even be qualitatively different. Furthermore, we study the differences in the dynamics of two typical RD hardware configurations, a sieve tray column and a randomly packed column.

Dynamic Nonequilibrium (NEQ) Model Development

Conservation relations

The dynamics of a stage are determined, *inter alia*, by the storage capacity, or accumulation, of mass and energy in the vapour and liquid phase on any given stage. We develop below the transient balances for a contacting stage portrayed in Fig. 1. Both the vapour and liquid phases on the stage are assumed to be well-mixed. The time rate of change of the number of moles of component i in the vapour (M_i^V) and liquid (M_i^L), phases on stage j are given by the following balance relations

$$\frac{dM_{i,j}^V}{dt} = V_{j+1}y_{i,j+1} - V_j y_{i,j} + z_{i,j}^V F_{i,j}^V - N_{i,j}^V; \quad i = 1, 2, \dots, c \quad (1)$$

$$\frac{dM_{i,j}^L}{dt} = L_{j-1}x_{i,j-1} - L_j x_{i,j} + z_{i,j}^L F_{i,j}^L + N_{i,j}^L + \sum_{k=1}^r \mathbf{n}_{i,k} R_{k,j} \mathbf{e}_j^L; \quad i = 1, 2, \dots, c \quad (2)$$

where $N_{i,j}$ is the interfacial mass transfer rate. A total of r chemical reactions take place in the liquid phase and $R_{k,j}$ is the rate of reaction k on stage j , $\mathbf{n}_{i,m}$ represents the stoichiometric coefficient of component i in reaction k and \mathbf{e}_j^L represents the volumetric liquid hold-up on stage j . Heterogeneous chemical reactions taking place inside catalyst particles are taken account by using a pseudo-homogeneous description of catalyst effectiveness factors and effective reaction rate constants. The feed entering the column at any inlet is treated as follows. The vapour portion of this feed enters the tray above and the liquid portion of the feed enters the tray below. The feed flow rate of component i in the vapour phase to stage j is $z_{i,j}^V F_{i,j}^V$ and the feed flow rate of component i in the liquid phase to stage j is $z_{i,j}^L F_{i,j}^L$ where $z_{i,j}^V$ and $z_{i,j}^L$ are the corresponding mole fractions of the feed streams.

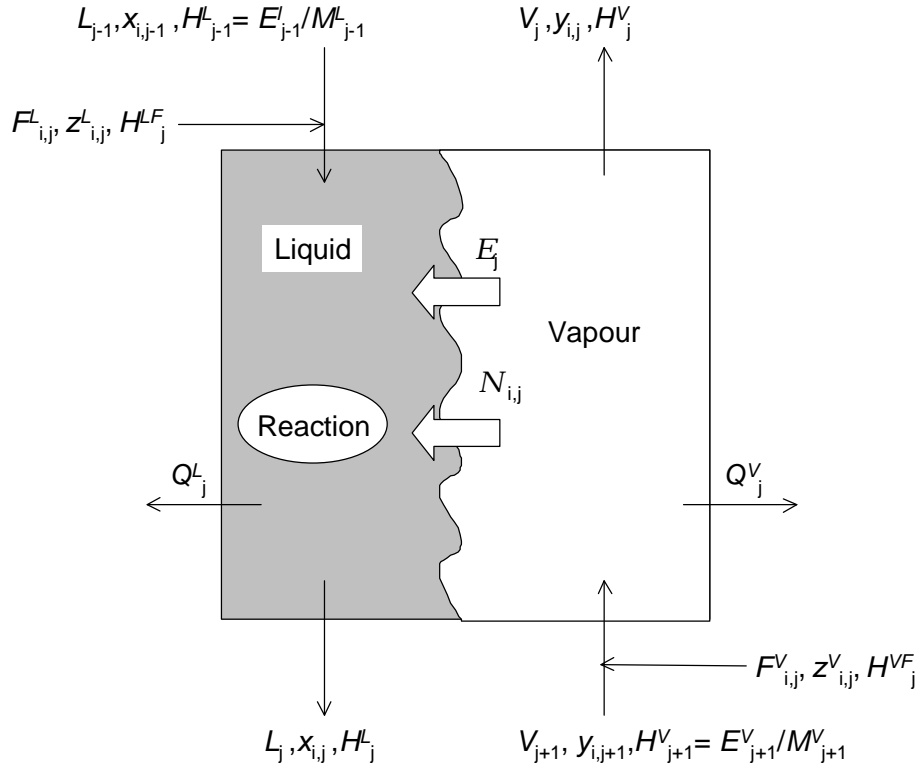


Figure 1. Schematic representation of a NEQ stage

The overall molar balances are obtained by summing eqs. (1) and (2) over the total number of components, c in the mixture.

$$\frac{dM_j^V}{dt} = V_{j+1} - V_j + F_j^V - \sum_{k=1}^c N_{k,j}^V \quad (3)$$

$$\frac{dM_j^L}{dt} = L_{j-1} - L_j + F_j^L + \sum_{k=1}^c N_{i,j}^L + \sum_{i=1}^c \sum_{k=1}^r n_{i,k} R_{k,j} \mathbf{e}_j^L \quad (4)$$

The mole fractions of the vapour and liquid phases are calculated from the respective phase molar hold-ups

$$y_{i,j} = \frac{M_{i,j}^V}{M_j^V}; \quad x_{i,j} = \frac{M_{i,j}^L}{M_j^L}; \quad i = 1, 2, \dots, c-1 \quad (5)$$

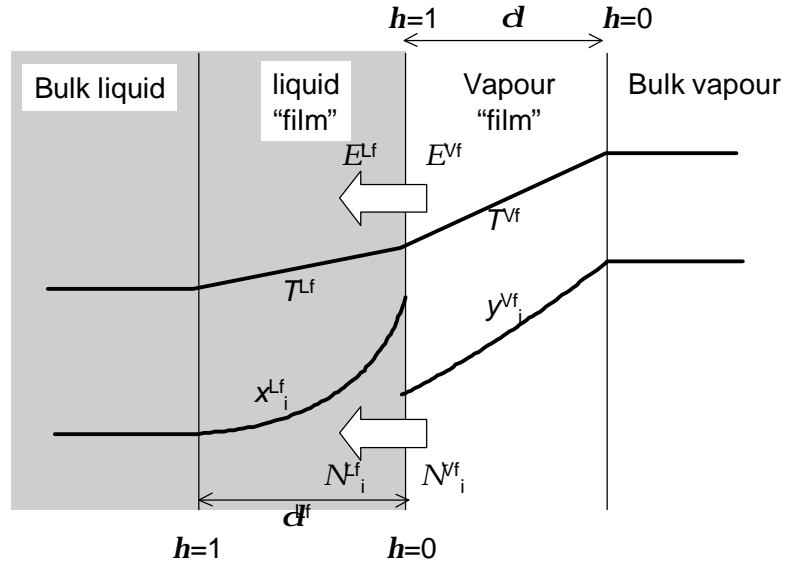


Figure 2. Composition and temperature profiles within the vapour and liquid “films”. The NEQ model takes account of the enhancement of the mass transfer due to chemical reaction within the diffusion film in the liquid close to the interface.

Only $c-1$ of these mole fractions are independent because the phase mole fractions sum to unity

$$\sum_{k=1}^c y_{k,j} = 1; \quad \sum_{k=1}^c x_{k,j} = 1 \quad (6)$$

In our model $c-1$ molar component balances (1) and (2) have been implemented along with eqs (3) – (6).

The energy balances for the vapour and liquid phases are written in terms of the energy “hold-ups” in the vapour and liquid phases on the stage j :

$$\frac{dE_j^V}{dt} = V_{j+1} \frac{E_{j+1}^V}{M_{j+1}^V} - V_j \frac{E_j^V}{M_j^V} + F_j^V H_j^{Vf} - E_j^V - Q_j^V \quad (7)$$

$$\frac{dE_j^L}{dt} = L_{j-1} \frac{E_{j-1}^L}{M_{j-1}^L} - L_j \frac{E_j^L}{M_j^L} + F_j^L H_j^{Lf} + E_j^L - Q_j^L \quad (8)$$

where E_j represent the interphase energy transfer rates and the Q_j represent the heat addition (or removal) via external heat exchange. The energy hold-ups are related to the corresponding molar hold-ups via the stage enthalpies

$$E_j^V = H_j^V M_j^V; \quad E_j^L = H_j^L M_j^L \quad (9)$$

There is no need to take separate account in eq. (8) of the heat generated due to chemical reaction since the computed enthalpies include the heats of formation. The phase temperatures T_j^V and liquid T_j^L are determined from the corresponding phase enthalpies using an ideal or excess enthalpy model.

Interfacial mass and energy transfers

The resistance to mass and energy transfer is located in thin “films” adjacent to the vapour-liquid interface; see Fig. 2. The liquid phase diffusion film thickness \mathbf{d}^f is of the order of 10 μm and the vapour phase diffusion film thickness \mathbf{d}^v is of the order of 100 μm . The storage capacity for mass and energy in these films is negligibly small compared to that in the bulk fluid phases and so the interfacial transfer rates can be calculated from quasi-stationary interfacial transfer relations. For transfer within the vapour phase diffusion film (superscript Vf) we have

$$\frac{\partial N_i^{Vf}(\mathbf{h}^{Vf})}{\partial \mathbf{h}^{Vf}} = 0 \quad (10)$$

$$\frac{\partial E^{Vf}}{\partial \mathbf{h}^{Vf}} = 0 \quad (11)$$

Here \mathbf{h}^{Vf} represents the dimensionless distance along the liquid diffusion path: $\mathbf{h}^{Vf} = 0$ at the edge of the film (of thickness \mathbf{d}^f) and $\mathbf{h}^{Vf} = 1$ at the vapour-liquid interface; see Fig. 2. The interfacial transfer rates are constant across the vapour phase diffusion film. The situation within the liquid phase diffusion film is more complex for we need to take account of the chemical reaction within this film:

$$\frac{\partial N_i^{Lf}(\mathbf{h}^{Lf})}{\partial \mathbf{h}^{Lf}} + \sum_{k=1}^r n_{i,k} R_k(\mathbf{h}^{Lf}) A \mathbf{d}^f = 0 \quad (12)$$

$$\frac{\partial E^{Lf}}{\partial \mathbf{h}^{Lf}} = 0 \quad (13)$$

A represents the interfacial area and $A \mathbf{d}^f$ represents the volume available for liquid phase chemical reaction. The coupling of diffusion and chemical reaction within the liquid film is particularly important for fast chemical reactions (Hatta number exceeding unity).

In order to solve equations (10) – (13) for each stage j in the column we need constitutive relations for the interfacial mass and energy transfer rates. The molar transfer rate N_i^{Lf} in the liquid phase is related to the chemical potential gradients by the Maxwell-Stefan equations (Krishna and Wesselingh, 1997; Taylor and Krishna, 1993)

$$\frac{x_i^{LF}}{RT^{Lf}} \frac{\mathbf{j}m_i^{Lf}}{\mathbf{j}h} = \sum_{k=1}^c \frac{x_i^{LF} N_k^{Lf} - x_k^{LF} N_i^{Lf}}{c_i^{Lf} \mathbf{K}_{i,k}^{Lf} A}; \quad i = 1, 2, \dots, c \quad (14)$$

The $k_{i,k}^{Lf}$ represents the mass transfer coefficient of the i - k pair in the liquid phase; this coefficient is estimated from information on the corresponding Maxwell-Stefan diffusivity $\mathfrak{D}_{i,k}^L$ using the standard procedures discussed in Taylor and Krishna (1993).

Only $c - 1$ of the eqs (14) are independent. The summation equations hold:

$$\sum_{k=1}^c y_{i,j}^{VF} = 1; \quad \sum_{k=1}^c x_{i,j}^{LF} = 1 \quad (15)$$

The interphase energy transfer rates E^{Lf} have conductive and convective contributions

$$E^{Lf} = -h^{Lf} A \frac{\mathfrak{H}^{Lf}}{\mathfrak{h}} + \sum_{i=1}^c N_i^{Lf} H_i^{Lf} \quad (16)$$

h^{Lf} is the heat transfer coefficient in the liquid phase. A relation analogous to eq. (16) holds for the vapour phase.

At the vapour-liquid interface we assume phase equilibrium

$$y_i \Big|_I - K_i x_i \Big|_I = 0; \quad T^{Vf} \Big|_I = T^{Lf} \Big|_I \quad (17)$$

where the subscript I denotes the equilibrium compositions and K_i is the vapour - liquid equilibrium ratio for component i . At the interface we have continuity of mass and energy:

$$N_i^{Vf} \Big|_I = N_i^{Lf} \Big|_I; \quad E^{Vf} \Big|_I = E^{Lf} \Big|_I \quad (18)$$

Properties, hydrodynamics and mass transfer

The NEQ model requires thermodynamic properties, not only for calculation of phase equilibrium but also for calculation of driving forces for mass transfer and, in reactive distillation, for taking into account the effect of nonideal component behaviour in the calculation of reaction rates and chemical equilibrium constants. In addition, physical properties such as surface tension, diffusion coefficients, viscosities, etc. for calculation of mass (and heat) transfer coefficients and interfacial areas are required. For the most part the property models we use are those recommended by Reid et al. (1988) and by Danner and Daubert (1983). The details of the models used for estimation of diffusivities are discussed in standard texts (Reid et al., 1988; Seader and Henley, 1998; Taylor and Krishna, 1993).

In the dynamic NEQ model, hardware design information must be specified so that mass transfer coefficients, interfacial areas, liquid hold-ups and pressure drops can be calculated. A listing of the correlations for tray and packed columns are given in Table 1. The theory behind the tray and packed column design is available in Fair et al. (1997), Kooijman (1995), Lockett (1986) Stichlmair and Fair (1998) and Taylor and Krishna (1993). Interested readers can download the technical manual from the ChemSep website:

Table 1. *Hydrodynamics and mass transfer correlations for sieve trays and packings incorporated in our dynamic NEQ model for RD columns.*

Parameter	Correlation or model
Sieve Trays	
Pressure drop	Stichlmair and Mersmann Lockett Perry
Clear liquid height	Bennett et al. Colwell
Fractional liquid hold-up in froth, froth height	Bennett et al. Colwell Barker and Self
Interfacial area (depending on operation either in the spray or froth regime)	Zuiderweg
Spray-to-froth transition	Zuiderweg
Mass transfer or NTU correlation	AICHe Bubble Tray Design Manual Zuiderweg Chan and Fair Hughmark Harris Chen and Chuang
Packings	
Pressure drop	Generalized correlation from Perry (1998) Stichlmair Billet-Schultes Bravo-Fair
Mass transfer or NTU correlation	Onda et al. Bravo-Fair Billet-Schultes Sherwood number correlation Bravo-Rocha-Fair Zogg Brunazzi Zogg-Toor-Marchello

<http://www.clarkson.edu/~chengweb/faculty/taylor/chemsep/chemsep.html>, which contains details of all thermodynamics, hydrodynamics and mass transfer models for tray and packed columns which have already been implemented into our reactive distillation software. The code for these models represents a large fraction of the overall program size.

For a sieve tray column, for example, the volumetric liquid hold-up on the tray can be calculated from knowledge of the active (or bubbling) tray area, A_{bub} , and estimation of the clear liquid height, h_{cl} :

$$\frac{1}{c_{t,j}^L} M_j^L \equiv \mathbf{e}_j^L = h_{\text{cl},j} A_{\text{bub},j} \quad (19)$$

The clear liquid height can be estimated from correlations of Bennett et al. (1983) or Barker and Self (1962). If the tray spacing is h_t , the volumetric hold-up of the vapour phase can be calculated from

$$\frac{1}{c_{t,j}^V} M_j^V \equiv \mathbf{e}_j^V = (h_t - h_{cl,j}) A_{bub,j} \quad (20)$$

Summary of model equations for a single stage

Table 2 summarises the set of equations describing for the vapour and liquid phases for a single stage. The number of equations and variables on a single stage is $8c + 12$. The differential equations that describe mass transfer through the vapour and liquid films are discretised over the film thickness by application of a finite difference scheme, with fixed grid points.

Table 2. Model equations for single stage nonequilibrium model . The model equations are either ordinary differential equations (ODE), partial differential equations (PDE) or algebraic equations (AE). The number of discrete points in the liquid film is denoted with nL , and in the vapour film with nV , respectively.

		Bulk Liquid phase			Bulk Vapour phase			
Description of equation	Number of eqns	Type	Eq. (xx)	Var.	Number of eqns	Eq. (xx)	Var.	
Total molar balance	1	ODE	Eq. (4)	M_i^L	1	Eq. (3)	M_i^V	
Molar component balance	c-1	ODE	Eq. (2)	$M_{i,j}^L$	c-1	Eq. (1)	$M_{i,j}^V$	
Mole fractions	c	AE	Eq. (5)		$x_{i,j}$	c		Eq. (5)
Summation	1	AE	Eq. (6)			1		Eq. (6)
Energy balance	1	ODE	Eq. (8)	E^L	1	Eq. (7)	E^V	
Energy hold-up	1	AE	Eq. (9)	T_j^L	1	Eq. (9)	T_j^V	
Volumetric hold-up	1	AE	Eq. (19)	L	1	Eq. (20)	V	
		"Film" Liquid phase			"Film" Vapour phase			
Molar component balance	$nL \times c$	PDE	Eq. (12)	$N_{i,j}^{Lf}$	c	Eq. (10)	$N_{i,j}^{Vf}$	
Maxwell-Stefan equations	$nL \times (c-1)$	PDE	Eq. (14)		x_{ij}^{Lf}	$nV \times (c-1)$		Eq. (14)
Summation	$nL \times 1$	AE	Eq. (15)			$nV \times 1$		Eq. (15)
Energy balance	$nL \times 1$	PDE	Eq. (13)	E_j^{Lf}	$nV \times 1$	Eq. (11)	E_j^{Vf}	
Energy transfer rate	$nL \times 1$	PDE	Eq. (16)	T_j^{Lf}	$nV \times 1$	Eq. (16)	T_j^{Vf}	
Total: $(5c + 8 + nL \times (2c + 2) + nV \times (c+2))$ implemented eqs. per stage								

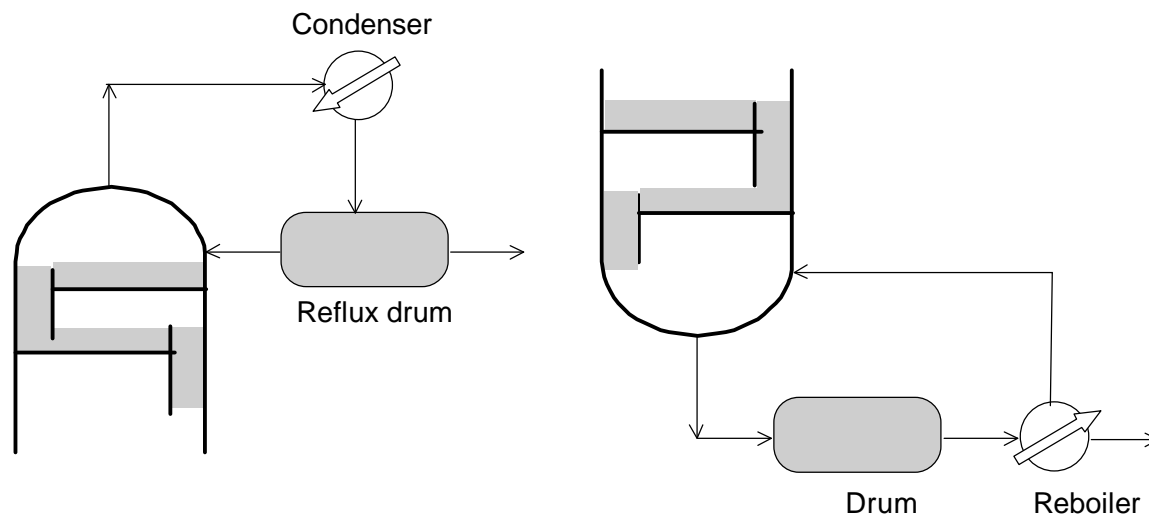


Figure 3. *Condenser and reboiler model configurations.*

Condenser and reboiler configuration

The liquid hold-up in the reboiler and condenser is usually much larger than the hold-up on a particular stage. High liquid hold-ups lead to operational robustness, but also cause the equations to be very stiff. In our dynamic NEQ model implementation, liquid buffers are incorporated at the top and bottom, as indicated in Fig. 3. The partial, or total, condenser is followed by a reflux drum buffering the condensate. A partial condenser is modelled as an equilibrium stage (Seader and Henley, 1998). The reflux drum is considered to be a well-mixed system with a specified volumetric capacity. The mean liquid residence time and dynamic characteristics are therefore fully determined with this specification.

The liquid leaving the bottom of the column is led to a reboiler drum with a specified volumetric capacity (hold-up) and assumed to be well-mixed. The contents are then transferred to a partial, or total reboiler. A partial reboiler is modelled as an equilibrium stage.

Numerical solution

The resulting set of differential-algebraic (DAE) equations is solved using BESIRK (Kooijman, 1995; Kooijman and Taylor, 1995). BESIRK is a semi-implicit Runge-Kutta method originally developed by Michelsen (1976) and extended with an extrapolation scheme (Bulirsch and Stoer, 1966), improving the efficiency in solving the DAE problem. The evaluation of the sparse Jacobian is primarily based on analytical expressions, except for the computation of entries for correlations like enthalpies, mass and heat transfer coefficients, hold-ups and pressure drops.

Our model also supports steady-state computations using Newton's method, as outlined in Taylor et al. (1994). In addition, the program is equipped with a continuation method

for analysis of multiple-steady state behaviour. For more details about this continuation method the reader is referred to Wayburn and Seader (1987) and Kubicek (1976).

Dynamics of Sieve Tray RD column: EQ vs NEQ Models

In order to illustrate the dynamics of RD columns we undertook a case study involving the synthesis of MTBE. The column configuration chosen for the simulations is shown in Figure 4; this is the configuration described by Jacobs and Krishna (1993) in their simulation study using the EQ stage model. The total number of stages is 17, including a total condenser and a partial reboiler; the column pressure is 11 atm. Reactive stages are located in the middle of the column, stage 4 down to and including stage 11. The column has two feed streams: a methanol feed and a mixed butenes feed. A small stoichiometric excess of methanol is used. The mixed butenes feed, to stage 11, contains a mixture of *iso*-butene, which is reactive, and *n*-butene, which is non-reactive or inert. The reflux-ratio is set to 7 and the bottom flow rate is either set to 205 mol/s or varied (as a continuation parameter). The product removed from the top of the column is predominantly the inert *n*-butene. The bottoms product consists predominantly of MTBE.

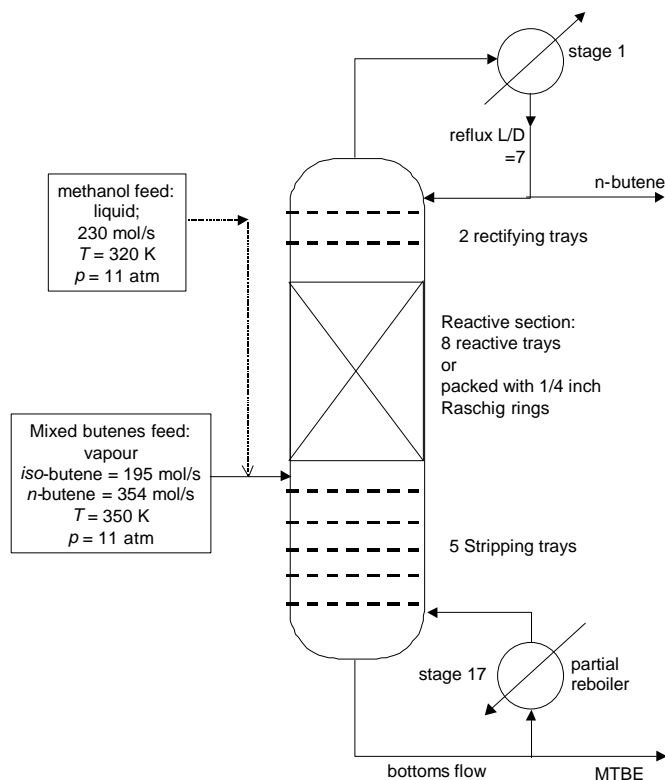


Figure 4. Configuration of the MTBE synthesis column, following Jacobs and Krishna (1993). The column consists of 17 stages. The reactive stages are configured either as sieve trays (see Fig. 5) or packed with catalytically active Raschig rings.

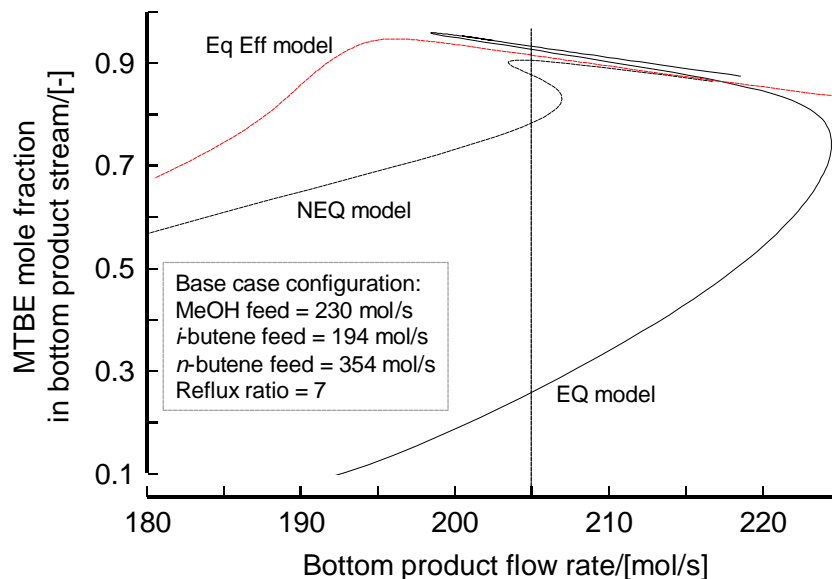


Figure 5. Bifurcation diagram for sieve tray configuration for three different model implementations, EQ, NEQ and Equal Efficiencies.

For a properly designed and operated column it is possible to achieve close to 100% conversion of *iso*-butene.

The column diameter was chosen to be 6 m. The stripping, rectifying and reactive sections consist of sieve trays. The configuration of the sieve trays are: total tray area = 28.27 m²; number of liquid flow passes = 5; tray spacing = 0.7 m; liquid flow path length = 0.97 m; fractional active area = 0.76; fractional hole area = 0.1; fractional downcomer area = 0.12; hole diameter = 4.5 mm; weir height = 50 mm; total weir length = 22 m; weir type = segmental; downcomer clearance = 0.0381 m; tray deck thickness = 25 mm. The five-liquid-pass tray configuration is shown in Fig. 4 in Chapter 4. The total amount of catalyst in the reactive zone is 8000 kg. The ion exchange capacity of the catalyst is 4.54 (meq H⁺/gram). The capacity of the reflux drum is taken to be 1300 L and that of the reboiler drum is 2300 L.

The UNIQUAC model was used for description of liquid phase nonideality, while the Soave-Redlich-Kwong equation of state was used for the vapour phase. The extended Antoine equation was used for calculation of the vapour pressure. Thermodynamic and kinetic data are taken from Rehfinger and Hoffmann (1990a, 1990b).

The first objective of our dynamic RD simulations is to compare the results of EQ and NEQ models. The separation capability of the non-reactive stripping and rectifying sections will also affect the overall column performance. We decided to focus on the differences of the EQ and NEQ modelling of the reactive section only and, therefore, assumed the non-reactive stages to have equal separation capability in both

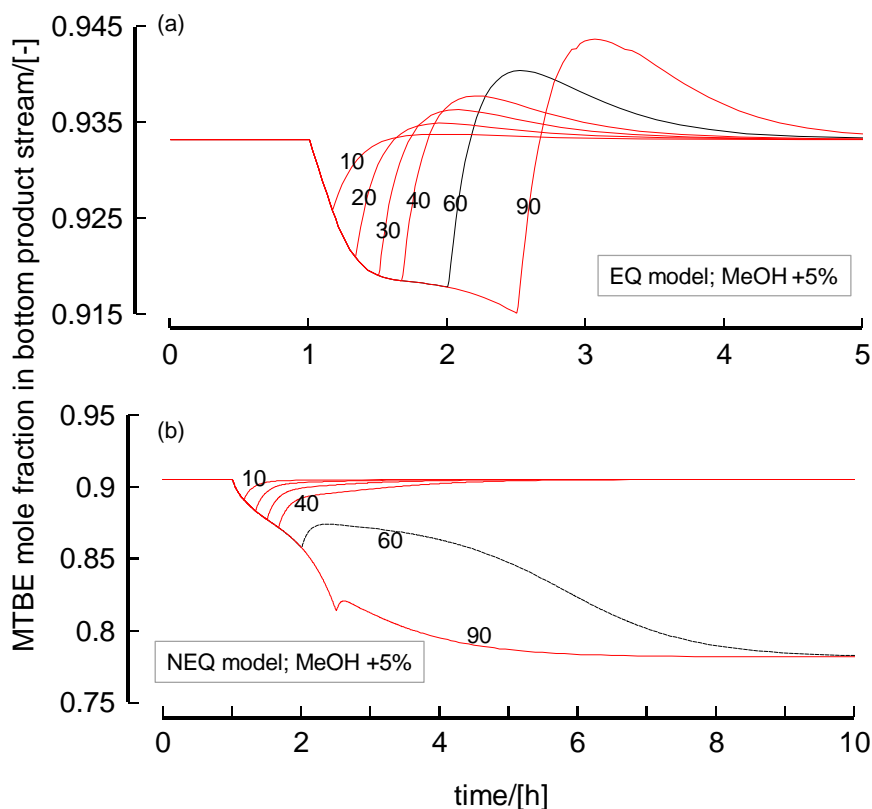


Figure 6. Dynamic response to a 5% increase in the MeOH feed flow, 1 h after column start-up. The perturbation period is varied from 10 to 90 minutes. (a) response of EQ model and (b) response of NEQ model.

implementations. Towards this end, in the EQ model implementation we have assumed a tray efficiency of 65% for the non-reactive rectifying stages and 58% for the non-reactive stripping stages; these values corresponded closely to the calculations of the NEQ model for the corresponding non-reactive rectifying and stripping sections using the *A.I.Ch.E.* calculation method for sieve tray mass transfer (for details of this model see Lockett, 1986). The interfacial area is estimated from the Hofhuis and Zuiderweg (1979) correlation and the fractional liquid hold-up on the tray is estimated from the correlation of Barker and Self (1962). Of course, in the NEQ model implementation of the non-reactive stages, efficiencies are not used in the calculations but can be calculated from the simulation results; these stage efficiencies vary for individual components. For the reactive section, the EQ model assumes vapour and liquid phases to be in equilibrium. We also carried out simulations for another variant of the EQ model in which all components were assumed to have identical efficiencies on every reactive stage. The value of this efficiency, 65%, was chosen to match the steady-state conversion of the NEQ model.

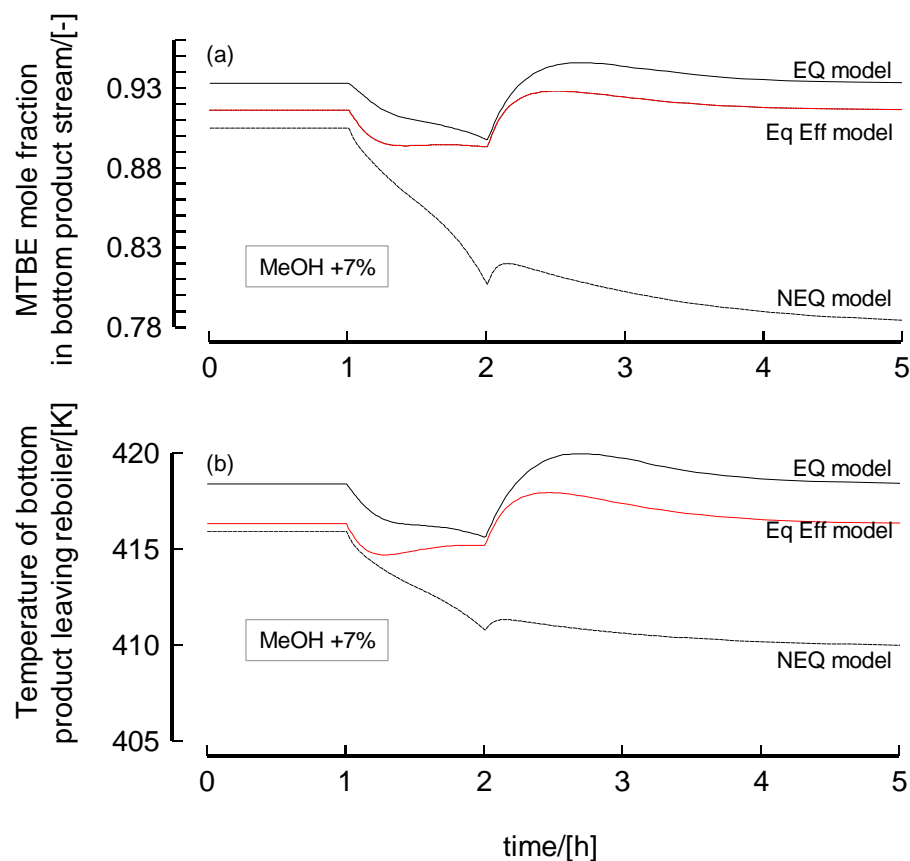


Figure 7. Dynamic response to a 5% increase in the MeOH feed flow, 1 h after column start-up and lasting for 1 h. (a) The MTBE mole fraction in the bottom stream obtained by EQ, NEQ and Equal Efficiency models and (b) The temperature in the bottom stream obtained by EQ, NEQ and Equal Efficiency models.

Before performing dynamic simulations we used the continuation method to investigate the steady-state behaviour of the MTBE synthesis configuration shown in Fig. 4 using the molar bottoms flow rate as continuation parameter. The bifurcation diagram for three different implementations of the model are shown in Fig. 5. At a bottoms flow rate of 205 mol/s both EQ (100% component efficiencies) and NEQ models show multiple steady-states. Interestingly, the Equal Efficiency model for the reactive section in which the component efficiencies were taken to be 0.65 on all stages does not show any multiplicity.

Taking the bottoms flow rate to be 205 mol/s, we performed dynamic simulations of the RD columns, starting with the high conversion steady-state situation, and introducing a +5% perturbation in the feed MeOH, 1 h after start-up. Fig. 6 (a) and (b) show the dynamic responses of the EQ and NEQ models for varying perturbation durations from 10 minutes to 90 minutes. For the EQ model, the system reverts back to the initial-steady

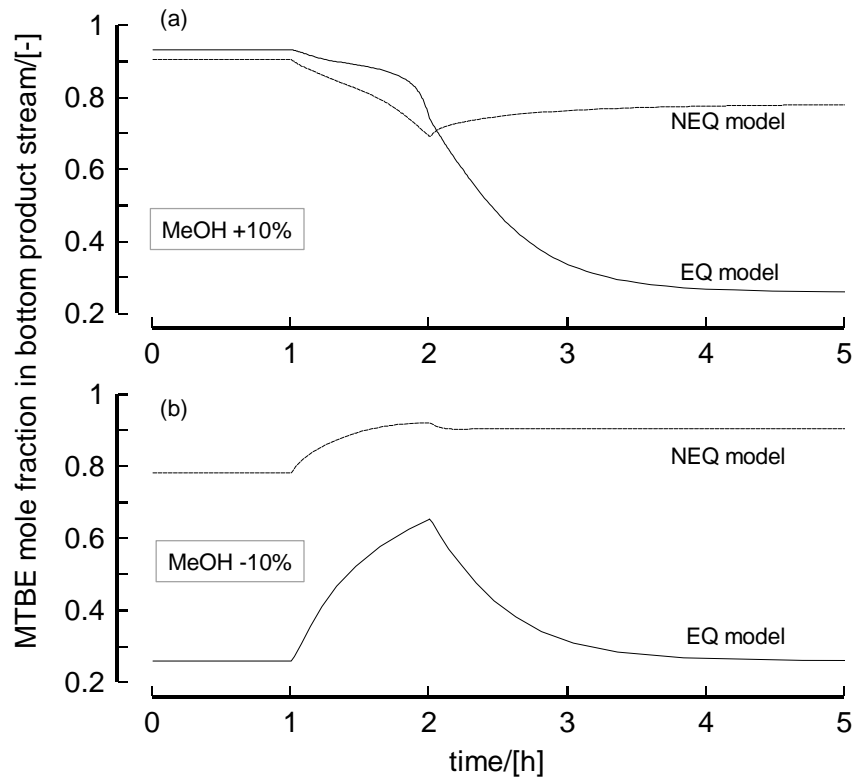


Figure 8. Dynamic response to a (a) 10% increase or (b) 10% decrease in the MeOH feed flow, 1 h after column start-up and lasting for 1 h.

state for all perturbation durations; see Fig. 6 (a). It is interesting to note the strong under- and over-shoots in the MTBE product compositions at the bottom of the column. The dynamic response of the NEQ model is qualitatively different. For perturbations smaller than 40 minutes in duration the system reverts back to the initial steady-state but with a much smaller under-shoot in the MTBE bottoms composition; see Fig. 6 (b). No composition overshoot is observed. For a MeOH feed perturbation lasting more than 60 minutes, the system suffers a steady-state transition from the high-conversion branch to the low-conversion branch of the bifurcation diagram shown in Fig. 5.

We now fix the period of perturbation to be 1 h and increase the magnitude of the perturbation to +7% in the MeOH feed. Fig. 7 (a) and (b) show the dynamic responses of the EQ, NEQ and Equal Efficiency models to the bottoms MTBE composition and bottoms temperature. The EQ and Equal Efficiency model revert back to the initial steady-state. It is interesting to note the strong under- and over-shoots in the MTBE product compositions and temperature at the bottom of the column. Both the EQ and Equal Efficiency models have similar dynamic characteristics. The dynamic response of the NEQ model is qualitatively different from that of the EQ and Equal Efficiency models. The system suffers a transition from the high-conversion branch to the low-

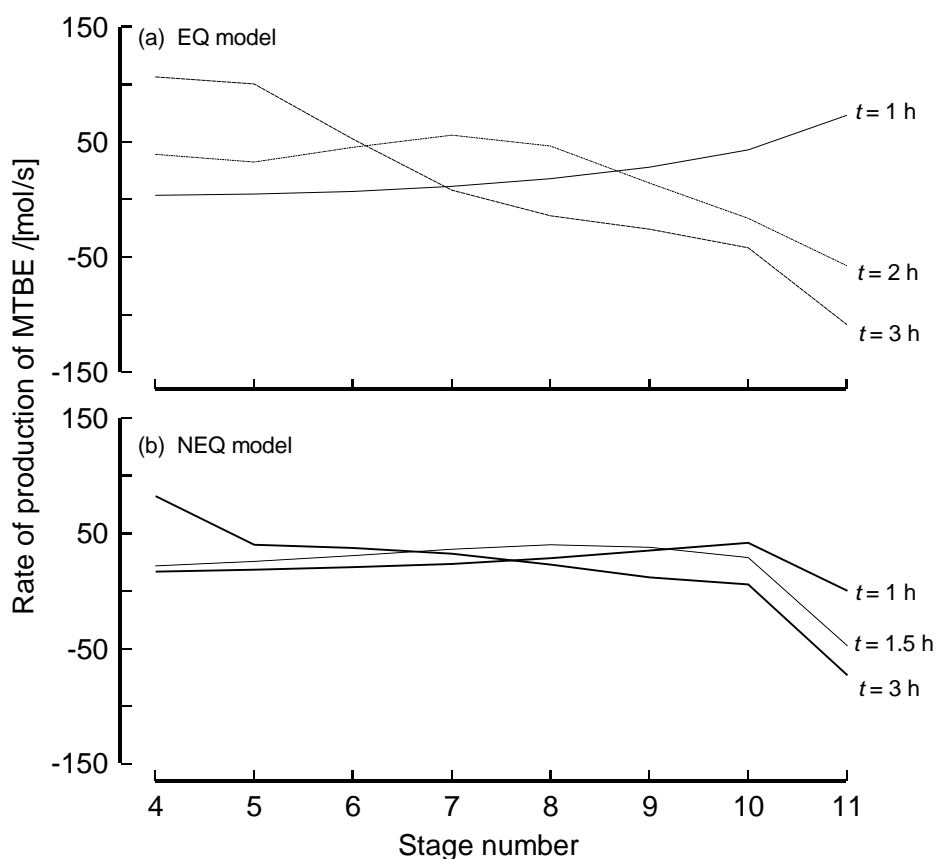


Figure 9. MTBE production rates for (a) EQ model and (b) NEQ model for +10 % MeOH feed flow perturbation. The variation along the height of the reactive stages is shown.

conversion branch of the bifurcation diagram shown in Fig. 5. Furthermore, it is interesting to note that the NEQ model does not show any prominent over- or under-shoots in composition or temperature.

Figure 8 (a) shows the RD column response to a +10% increase in the MeOH feed flow. Both the EQ and NEQ models “suffer” transitions to the low-conversion branch. Figure 8 (b) shows the response of the RD column to a 10% decrease in the MeOH feed flow, when starting at the low-conversion branches of the bifurcation diagram in Fig. 5. The EQ model returns to its initial (low-conversion) steady-state. The NEQ model, in sharp contrast, “enjoys” a transition to the high-conversion branch. The asymmetry in the responses of the two models to a +10% and –10% feed MeOH perturbation is worthy of note.

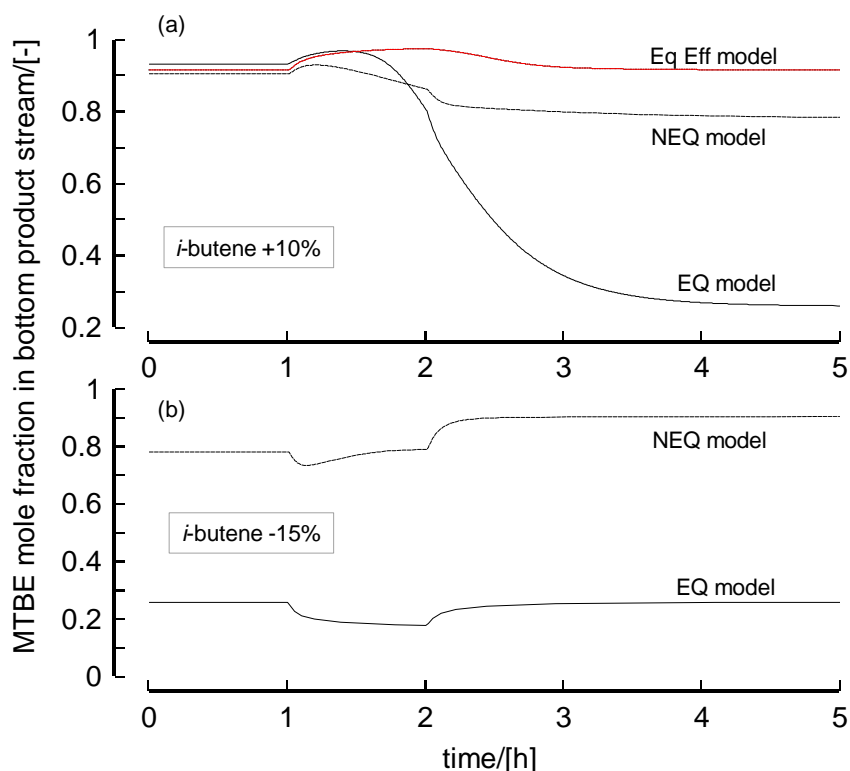


Figure 10. Dynamic response to a (a) 10% increase or (b) 15% decrease in the iso-butene feed flow, 1 h after column start-up and lasting for 1 h.

Some insights can be obtained into the differences of the EQ and NEQ models by considering the MTBE production rates in the reactive section at various time steps. Figure 9 (a) presents the reaction rate profiles along the height of the reactive section for the EQ model for the situation corresponding to that shown in Fig. 8 (a), i.e. with +10% MeOH feed perturbation. At $t = 1$ h, i.e. before the perturbation is introduced, the MTBE production rates are all positive in sign, i.e. the reaction is proceeding in the forward direction. At $t = 2$ h, the MTBE production rate is negative in the bottom portion of the reactive section, signifying that the reaction is proceeding in the reverse direction. This undesirable situation gets worse at $t = 3$ h, where the situation is close to the final low-conversion steady-state. Figure 9 (b) shows the MTBE production rates for the corresponding NEQ model. Again we see that at $t = 1.5$ and 3 h, MTBE production rates are negative in the bottom portion of the reactive section. Comparing Figs 9 (a) and (b) we observe that the reaction rate is less negative for then NEQ model. Introduction of mass transfer resistance helps to mitigate a bad situation.

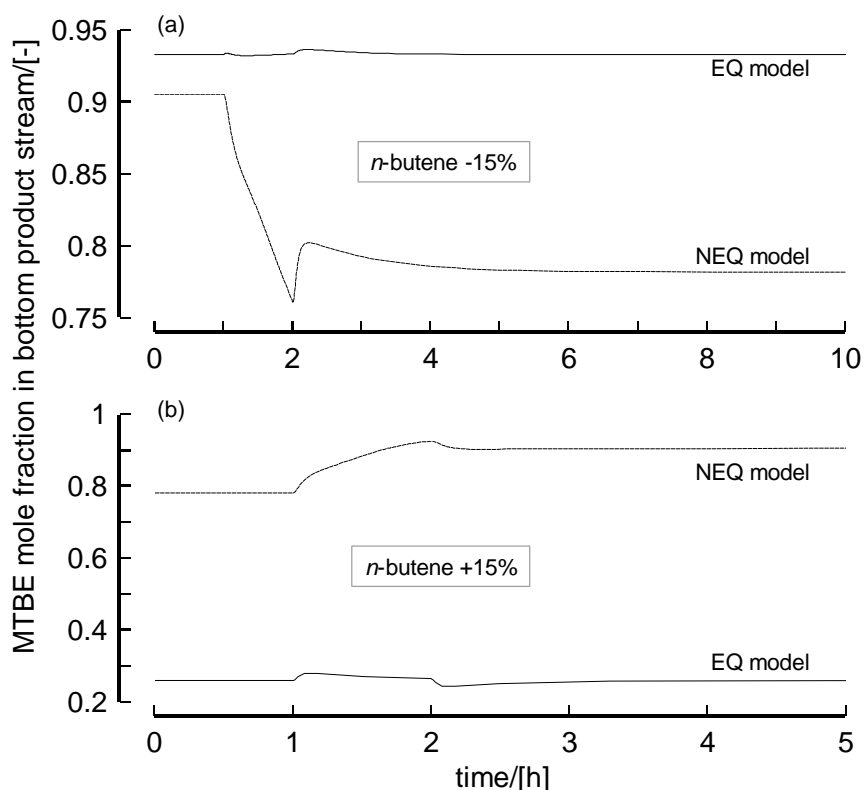


Figure 11. Dynamic response to a (a) 15% decrease or (b) 15% increase in the n-butene feed flow, 1 h after column start-up and lasting for 1 h.

Figure 10 (a) shows the RD column response to a +10% increase in the iso-butene feed flow. Both the EQ and NEQ models suffer transitions to the low-conversion branch. Intriguingly, the Equal Efficiency model recovers to the initial steady-state (recall from Fig. 5 that this model does not exhibit steady-state multiplicity). Figure 10 (b) shows the response of the RD column to a 15% decrease in the iso-butene feed flow, when starting at the low-conversion branch of the bifurcation diagram in Fig. 5. The EQ model returns to its initial (low-conversion) steady-state. The NEQ model, in sharp contrast, experiences a transition to the high-conversion branch.

Figure 11 (a) shows the RD column response to a 15% decrease in the n-butene feed flow. The EQ model is oblivious to this feed disturbance, whereas the NEQ model suffers a transition to the low-conversion steady-state. Figure 11 (b) shows the response of the RD column to a 15% increase in the n-butene feed flow, when starting at the low-conversion branch of the bifurcation diagram in Fig. 5. Once again, the EQ model is oblivious to this disturbance. The NEQ model shows a transition to the high-conversion branch.

Dynamics of Sieve Tray vs packed RD Configurations

We now study the influence of hardware configuration on RD column dynamics. The sieve tray configuration is compared with a column in which the reactive section is filled with catalytically active packing material in the form of ¼ inch Raschig ring shaped ion-exchange (Amberlyst 15) catalyst packing as described by Sundmacher and Hoffmann (1994). The specifications of the reactive section are: column diameter = 6 m, reactive packed zone height = 0.7 m, specific packing surface = $600 \text{ m}^2/\text{m}^3$, void fraction in the column = 0.72, packing density = $410 \text{ kg}/\text{m}^3$, catalyst pore voidage = 0.45, ion-exchange capacity of catalyst = 4.54 (meq H^+ /gram). The non-reactive rectifying and stripping sections are configured as sieve trays with exactly the same configuration as in the foregoing simulations. In the NEQ model for the reactive section the mass transfer coefficients are calculated using the Onda et al. (1968) correlation. The 0.7 m high packed reactive section needs to be divided into a sufficient number of “slices” (= stages) for accurate calculations. Our study shows that at least 88 slices are required for acceptable accuracy. Increasing the number of slices beyond 88 does not alter the results.

The bifurcation diagram corresponding to Fig. 5 for the sieve and packed column configurations are shown in Fig. 12. For a bottoms flow rate of 205 mol/s both configurations show steady-state multiplicity. The dynamic simulations reported below have been carried out with a bottoms flow rate of 205 mol/s with an initial steady state that is chosen to be either at the high- or low- conversion branches of the bifurcation diagrams.

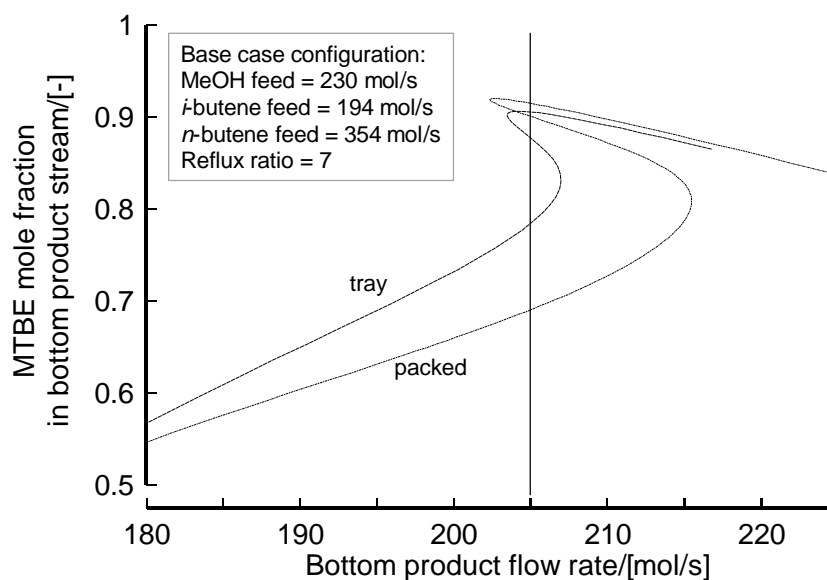


Figure 12. Bifurcation diagrams for sieve tray and packed column configurations for MTBE synthesis.

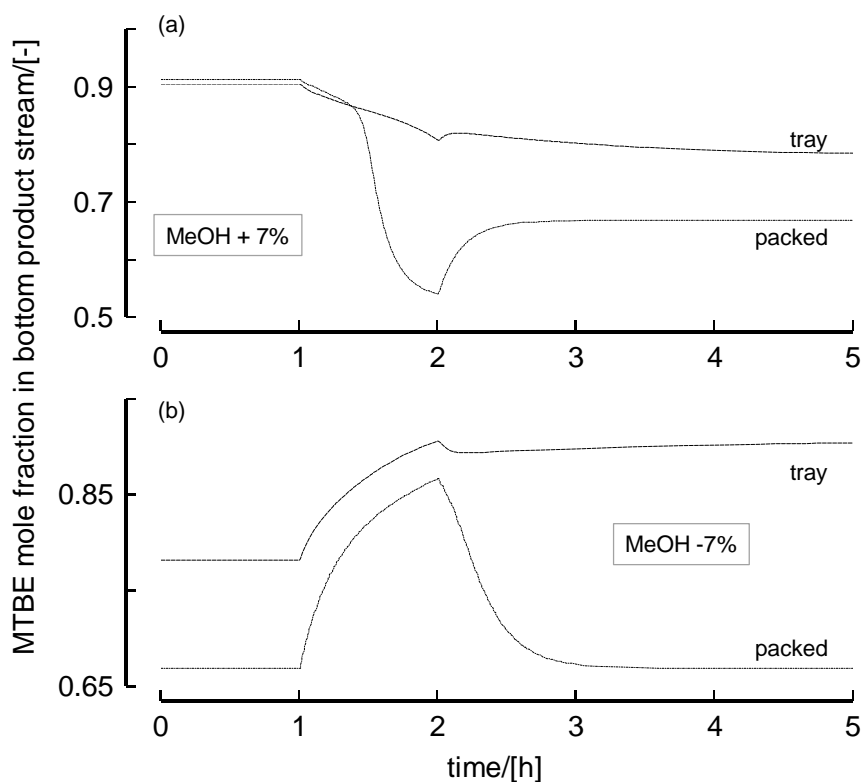


Figure 13. Dynamic response to a (a) 7% increase or (b) 7 % decrease in the MeOH feed flow, 1 h after column start-up and lasting for 1 h.

Figure 13 (a) shows the RD column response to a +7% increase in the MeOH feed flow. Both the tray and packed column configurations suffer transitions to the low-conversion branch. Figure 13 (b) shows the response of the RD column to a 7% decrease in the MeOH feed flow, when starting at the low-conversion branches of the bifurcation diagram in Fig. 12. The packed column returns to its initial (low-conversion) steady-state. The tray column, in sharp contrast, enjoys a transition to the high-conversion branch. The asymmetry in the responses of the two hardware configurations is worthy of note.

Figure 14 (a) shows the RD column response to a +3% increase in the iso-butene feed flow. We now note that the tray column returns to its initial state whereas the packed column stabilises to the low-conversion steady state. Figure 14 (b) shows the response of the RD column to a 15% decrease in the iso-butene feed flow, when starting at the low-conversion branch of the bifurcation diagram in Fig. 12. The packed column returns to its

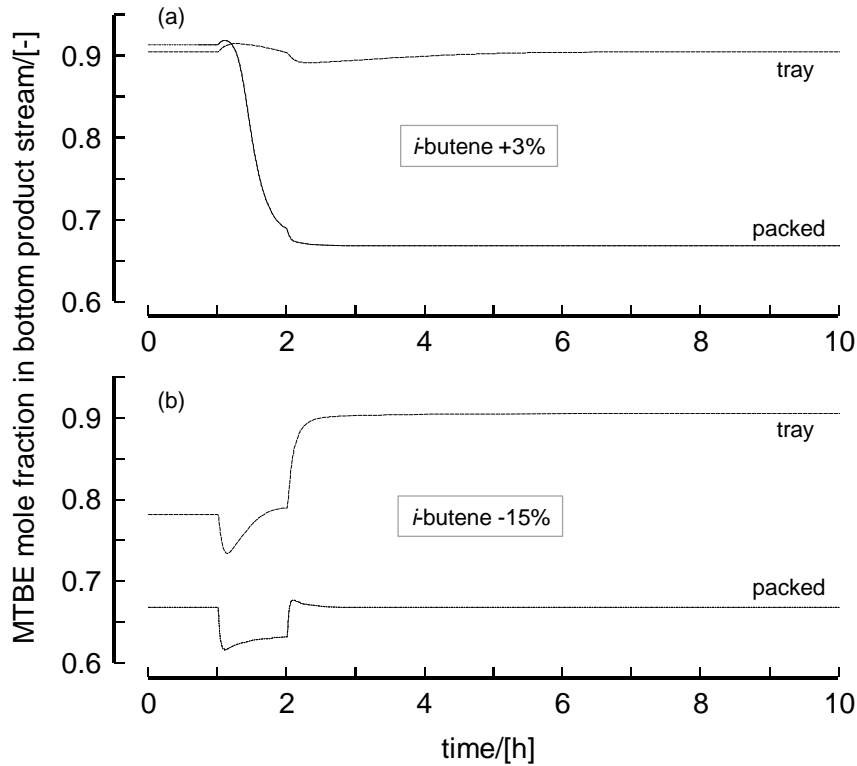


Figure 14. Dynamic response to a (a) 3% increase or (b) 15% decrease in the iso-butene feed flow, 1 h after column start-up and lasting for 1 h.

initial (low-conversion) steady-state. The tray column experiences a transition to the high-conversion branch.

Figure 15 (a) shows the RD column response to a 5% decrease in the n-butene feed flow. The tray column is almost insensitive to this feed disturbance. On the other hand, the packed column shifts to the low-conversion steady-state. Figure 15 (b) shows the response of the RD column to a 15% increase in the n-butene feed flow, when starting at the low-conversion branch of the bifurcation diagram in Fig. 12. Both the tray and packed column configurations experience transition to the high-conversion branch.

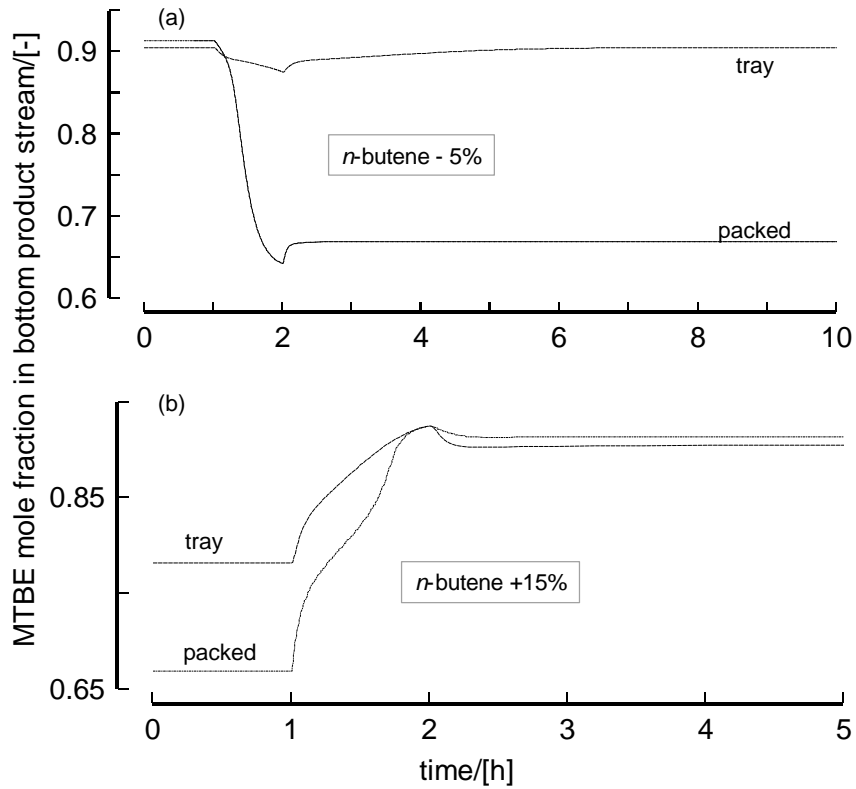


Figure 15. Dynamic response to a (a) 5% decrease or (b) 15% increase in the *n*-butene feed flow, 1 h after column start-up and lasting for 1 h.

Concluding Remarks

We have developed a dynamic NEQ stage model for RD columns. The rich dynamic features of RD columns have been illustrated by a case study for MTBE synthesis. The EQ and NEQ models show qualitatively different responses to feed flow disturbances of MeOH, iso-butene and n-butene. When the perturbation is long enough or the feed flow change is high enough, the NEQ model experiences a transition in steady-states. This transition could be from a high-conversion to a low-conversion level, or vice-versa. The EQ model is less prone to steady-state transitions and for perturbations in the n-butenes flow, it remains oblivious to the perturbations. A model, in which the component efficiencies are assumed to be equal to one another and equal for all stages, does not show any steady-state transitions. It is concluded that for proper description of the RD column dynamics, the NEQ model is essential.

The dynamic response of an RD column is also sensitive to the hardware choice. The packed column configuration and tray column configurations show different responses. It is clear that the control strategies to be adopted will also be determined by the precise configuration of the reactive section.

In Chapter 7 the dynamic NEQ stage model will be extended to include multiple cells per stage in both vapour and liquid phases in order to account for staging in the vapour and liquid phases.



Chapter 7

Development of a Dynamic Nonequilibrium Cell Model for Reactive Distillation Tray Columns

Abstract

In this chapter we develop a nonequilibrium (NEQ) cell model to describe the dynamic operation of reactive distillation (RD) tray columns. The features of our model are: (1) use of the Maxwell-Stefan equations for describing mass transfer between fluid phases, (2) chemical reactions are assumed to take place only in the liquid phase, (3) coupling between mass transfer and chemical reactions within the diffusion layer is accounted for, and (4) the use of multiple well-mixed cells in the liquid and vapour flow directions accounts for staging in either fluid phase. When the chemical reactions are suppressed, our model describes the dynamic behaviour of conventional distillation columns.

We demonstrate the utility of the dynamic NEQ cell model by means of three cases studies: (1) metathesis of 2-propene in an RD column, (2) distillation of methanol – *iso*-propanol – water, (3) synthesis of methyl tert-butyl ether (MTBE) in an RD column and (4) hydration of ethylene oxide to ethylene glycol in an RD column. For comparison purposes we have also carried out dynamic simulations using the equilibrium stage (EQ) model.

Introduction

The design and operation issues for reactive distillation (RD) systems are considerably more complex than those involved for either conventional reactors or conventional distillation columns. The introduction of an in-situ separation function within the reaction zone leads to complex interactions between vapour-liquid equilibrium, vapour-liquid mass transfer, intra-catalyst diffusion (for heterogeneously catalysed processes) and chemical kinetics. Such interactions have been shown to lead to the phenomena of multiple steady states and complex dynamics. In the literature, there has also been considerable attention to the phenomena of multiple steady states. Using the equilibrium (EQ) stage model, steady-state multiplicities have been reported for applications such as synthesis of methyl tert-butyl ether (MTBE) (Güttinger and Morari, 1999a, 1999b; Jacobs and Krishna, 1993; Mohl et al., 1999; Nijhuis et al., 1993; Hauan et al., 1995), synthesis of ETBE (Sundmacher, Uhde and Hoffmann, 1999), synthesis of TAME (Mohl et al., 1999; Rapmund et al., 1998) and for production of ethylene glycol (Ciric and Miao, 1994); Kumar and Daoutidis, 1999). More recent work presented in Chapter 2 and the work of Higler et al. (1999a) have used the nonequilibrium (NEQ) model to examine steady-state multiplicities in MTBE synthesis and for ethylene glycol production.

To describe the dynamics of RD columns, three types of models exist in the literature.

- (1) Equilibrium (EQ) stage model (Abufares *et al.*, 1995; Bartlett and Wahnschaft, 1998; Espinosa *et al.*, 1994; Grosser et al., 1987; Kumar and Daoutides, 1999; Moe et al., 1995; Perez-Cisneros et al., 1996; Scenna et al., 1998; Schrans *et al.*, 1996; Sneesby et al., 1998),
- (2) EQ stage model with fixed stage efficiencies (Alejski and Duprat, 1996; Ruiz *et al.*, 1995), and
- (3) Nonequilibrium (NEQ) stage model (Kreul et al., 1998, 1999).

Roat et al. (1986) integrate the control system equations with the EQ stage model equations and show, using the Eastman methyl acetate process, that control schemes with good steady-state characteristics may fail under unsteady-state conditions. Besides the methyl acetate process, there are other RD processes such as the synthesis of ethylene glycol that are carried out in tray columns in which the contacting pattern on any stage is cross-current. For large diameter columns used in industry there will be sufficient staging in both the vapour and liquid phases. Liquid phase staging is considerably more important for RD operations than for conventional distillation because of its influence on conversion and selectivity. The assumption of well-mixed vapour and liquid phases, made in all published EQ and NEQ models, does not hold for such RD tray columns. The primary objective of this chapter is to develop a rigorous dynamic NEQ model for RD columns, which would cater for cross-flow contacting of vapour and liquid phases by dividing the stage into a number of well-mixed cells in the liquid and vapour flow directions.

When the chemical reactions are suppressed, our model describes the dynamics of conventional multicomponent distillation tray column and extends the earlier work of Kooijman and Taylor (1995).

We underline the various features of the developed dynamic NEQ cell model by means of four cases studies: (1) metathesis of 2-propene in an RD column, (2) distillation of methanol – isopropanol – water, (3) synthesis of MTBE in an RD column and (4) hydration of ethylene oxide to ethylene glycol in an RD column.

Dynamic Nonequilibrium (NEQ) Cell Model Development

The basic idea of the NEQ cell model is shown in Fig. 1. Each stage is divided into a number of *contacting cells*; these cells describe just a small section of a single tray. The vapour entering a stage is divided into the cells, m in total, in the first horizontal row. The liquid entering the stage is, similarly, divided into the cells, n in total, in the first vertical column. Again, in all of our calculations the liquid flow is divided equally into the cells in a horizontal column. Any feed entering the stage is also apportioned in the same manner to the entering row, or column, of cells in the same manner. By choosing an appropriate number of cells in each flow direction, one can model the actual flow patterns on a tray. A column of cells can model plug flow in the vapour phase, and multiple columns of cells can model plug flow in the liquid phase. When the number of well

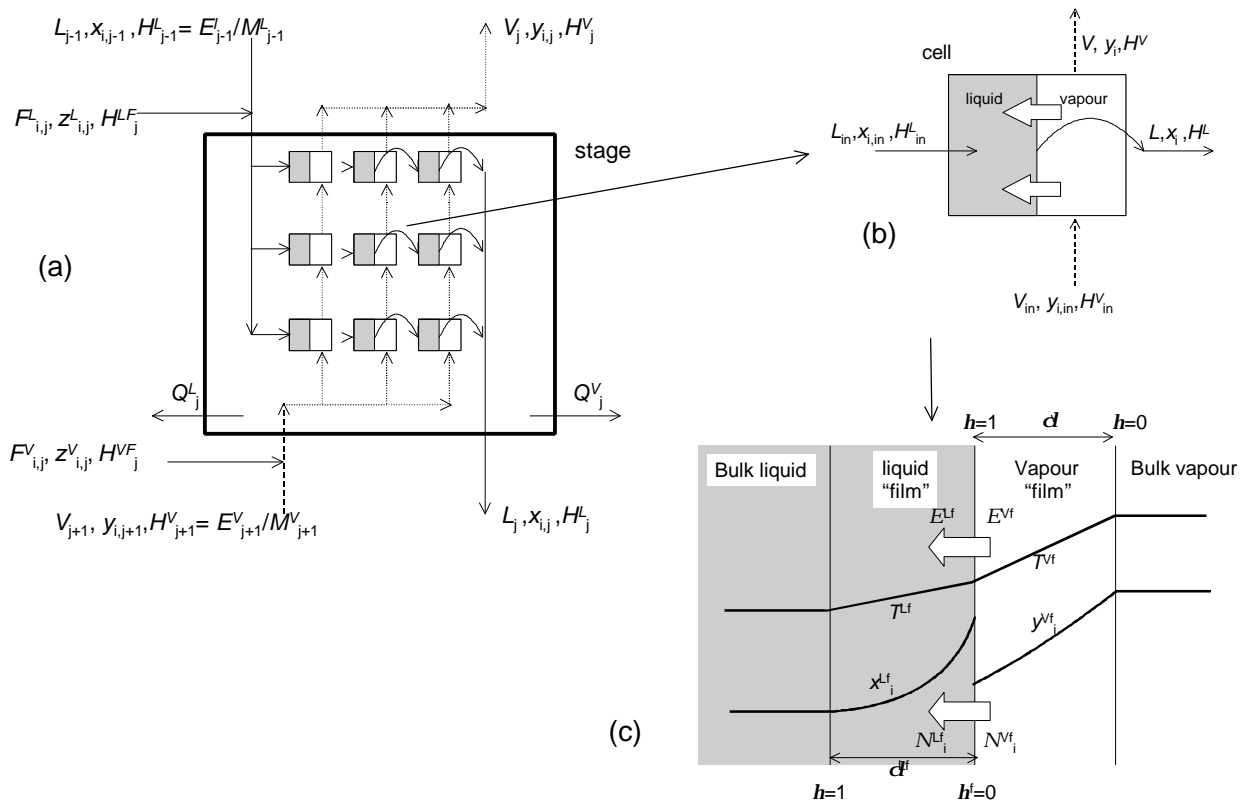


Figure 1. (a) Schematic representation of a NEQ cell model for a stage j . (b) Balance relations for a representative cell. (c) Composition and temperature profiles within the vapour and liquid "films"

mixed cells in any flow direction is four or more, we have essentially plug flow of that phase. Various degrees of backmixing in the vapour and liquid phases can be modelled by choosing the number of well-mixed cells to lie between 1 and 4. The precise estimate of the number of cells may be derived from eddy diffusion models for trays (Bennett and Grimm, 1991). Further details of the implementation of the cell model can be found in Higler et al. (1999b; 1999c) who have developed a steady-state version for RD columns. We first analyse the conservation relations for a typical cell on a tray (cf. Fig. 1 (b)).

Cell conservation relations

The dynamics of a well-mixed cell are determined, *inter alia*, by the storage capacity, or accumulation, of mass and energy in the vapour and liquid phase. The time rate of change of the number of moles of component i in the vapour (M_i^V) and liquid (M_i^L), are given by

$$\frac{dM_i^V}{dt} = V_{in} y_{i,in} - V y_i - N_i^V \quad (1)$$

$$\frac{dM_i^L}{dt} = L_{in} x_{i,in} - L x_i + N_i^L + \sum_{k=1}^r n_{i,k} R_k e^L \quad (2)$$

Allowance is made for a total of r (homogeneous) chemical reactions in the liquid phase with a reaction rate R_k . e^L represents the volumetric liquid hold-up in the cell. Heterogeneous chemical reactions taking place inside catalyst particles are modelled with a pseudo-homogeneous description and use of catalyst effectiveness factors and effective reaction rate constants. The overall molar balance for the cell is obtained by summing Eqs. (1) and (2) over the total number of components, c in the mixture

$$\frac{dM^V}{dt} = V_{in} - V - \sum_{k=1}^c N_k^V \quad (3)$$

$$\frac{dM^L}{dt} = L_{in} - L + \sum_{k=1}^c N_k^L + \sum_{i=1}^c \sum_{k=1}^r n_{i,k} R_k e^L \quad (4)$$

The mole fractions of the vapour and liquid phases are calculated from the respective phase molar hold-ups

$$y_i = M_i^V / M^V; \quad x_i = M_i^L / M^L \quad (5)$$

Only $c-1$ of these mole fractions are independent because the phase mole fractions sum to unity

$$\sum_{k=1}^c y_k = 1; \quad \sum_{k=1}^c x_k = 1 \quad (6)$$

In our model $c-1$ molar component balances (1) and (2) have been implemented along with eqs (3) - (6).

The phase energy balance is written in terms of the energy “hold-ups” in the cell

$$\frac{dE^V}{dt} = V_{in} \frac{E_{in}^V}{M_{in}^V} - V \frac{E^V}{M^V} - E^V - Q^V \quad (7)$$

$$\frac{dE^L}{dt} = L_{in} \frac{E_{in}^L}{M_{in}^L} - L \frac{E^L}{M^L} + E^L - Q^L \quad (8)$$

The heat removal from the liquid phase in each cell is simply the heat removal from stage divided by the total number of cells

$$Q^L = Q_j^L / (m \times n) \quad Q^V = Q_j^V / (m \times n) \quad (9)$$

The energy hold-ups are related to the corresponding molar hold-ups via the stage enthalpies

$$E^V = H^V M^V; \quad E^L = H^L M^L \quad (10)$$

There is no need to take separate account in Eqs (7) and (8) of the heat generated due to chemical reaction since the computed enthalpies include the heats of formation.

Interfacial mass and energy transfers

The resistance to mass and energy transfer is located in thin “films” adjacent to the vapour-liquid interface; see Fig. 1 (c). The liquid phase diffusion film thickness \mathbf{d}^l is of the order of 10 μm and the vapour phase diffusion film thickness \mathbf{d}^v is of the order of 100 μm . The storage capacity for mass and energy in these films is negligibly small compared to that in the bulk fluid phases and so the interfacial transfer rates can be calculated from quasi-stationary interfacial transfer relations. The molar component balances within the film are given by

$$\frac{\partial N_i^{Vf}(\mathbf{h}^{Vf})}{\partial \mathbf{h}^{Vf}} = 0 \quad (11)$$

$$\frac{\partial N_i^{Lf}(\mathbf{h}^{Lf})}{\partial \mathbf{h}^{Lf}} + \sum_{k=1}^r \mathbf{n}_{i,k} R_k(\mathbf{h}^{Lf}) A \mathbf{d}^l = 0 \quad (12)$$

In Eqs. (11) and (12), A represents the interfacial area and $A \mathbf{d}^l$ represents the volume available for liquid phase chemical reaction. The coupling of diffusion and chemical reaction within the liquid film is particularly important for fast chemical reactions (Hatta number exceeding unity). The molar transfer rate N_k is related to the chemical potential gradients by the Maxwell-Stefan equations (Krishna and Wesselingh, 1997; Taylor and Krishna, 1993)

$$\frac{y_i^{Vf}}{RT^{Vf}} \frac{\mathbf{Jm}_i^{Vf}}{\mathbf{Jh}} = \sum_{k=1}^c \frac{y_i^{Vf} N_k^{Vf} - y_k^{Vf} N_i^{Vf}}{c_i^{Vf} \mathbf{k}_{i,k}^{Vf} A} \quad (13)$$

$$\frac{x_i^{Lf}}{RT^{Lf}} \frac{\mathcal{J}m_i^{Lf}}{\mathcal{J}h} = \sum_{k=1}^c \frac{x_i^{Lf} N_k^{Lf} - x_k^{Lf} N_i^{Lf}}{c_t^{Lf} \mathbf{k}_{i,k}^{Lf} A} \quad (14)$$

The $\mathbf{k}_{i,k}$ represents the mass transfer coefficient of the i - k pair in the phase; this coefficient is estimated from information on the corresponding Maxwell-Stefan diffusivity $\mathcal{D}_{i,k}$ using the standard procedures discussed in Taylor and Krishna (1993). Only $c - 1$ of the Eqs (13) or (14) are independent. The following summation equations hold:

$$\sum_{k=1}^c y_{i,j}^{Vf} = 1; \quad \sum_{k=1}^c x_{i,j}^{Lf} = 1 \quad (15)$$

The energy balances within the diffusion film are given by

$$\frac{\partial E^{Vf}}{\partial h^{Vf}} = 0; \quad \frac{\partial E^{Lf}}{\partial h^{Lf}} = 0 \quad (16)$$

where the interfacial energy transfer rate E has both conductive and convective contributions

$$E^{Vf} = -h^{Vf} A \frac{\mathcal{J}T^{Vf}}{\mathcal{J}h} + \sum_{i=1}^c N_i^{Vf} H_i^{Vf}; \quad E^{Lf} = -h^{Lf} A \frac{\mathcal{J}T^{Lf}}{\mathcal{J}h} + \sum_{i=1}^c N_i^{Lf} H_i^{Lf} \quad (17)$$

At the vapour-liquid interface we assume phase equilibrium and the mole fractions in the vapour and liquid phases are related by

$$y_i \Big|_l = K_i x_i \Big|_l; \quad T^{Vf} \Big|_l = T^{Lf} \Big|_l \quad (18)$$

Furthermore the fluxes of mass and energy are continuous across the interface

$$N_i^{Vf} \Big|_l = N_i^{Lf} \Big|_l; \quad E^{Vf} \Big|_l = E^{Lf} \Big|_l \quad (19)$$

Link between cell variables and stage variables

The foregoing analysis pertains to each cell within the distillation tray "froth" region. We need to develop the inter-relation between the cell variables and the stage variables. The sum of the molar vapour flows leaving the top row of cells gives the total molar vapour flow leaving the stage j . A corresponding equation for last column of cells gives the total molar liquid flow leaving the stage j .

$$\sum_{mm=1}^m V_{mm,n} = V_j; \quad \sum_{nn=1}^n L_{m,nn} = L_j \quad (20)$$

The relations for the component molar flows are

$$\sum_{mm=1}^m y_{i,mm,n} V_{mm,n} = y_{i,j} V_j; \quad \sum_{nn=1}^n x_{i,m,nn} L_{m,nn} = x_{i,j} L_j \quad (21)$$

For the energy hold-ups we have

$$\sum_{mm=1}^m \frac{E_{mm,n}^V}{M_{mm,n}^V} V_{mm,n} = H_j^V V_j; \quad \sum_{nn=1}^n \frac{E_{m,nn}^L}{M_{m,nn}^L} L_{m,nn} = H_j^L L_j \quad (22)$$

The volumetric hold-ups per cell are – here – assumed to be a simple fraction $1/(m \times n)$ of the corresponding stage hold-ups

$$\mathbf{e}^V \equiv \frac{1}{c_{t,j}^V} M_j^V = \frac{1}{(m \times n)} \mathbf{e}_j^V; \quad \mathbf{e}^L \equiv \frac{1}{c_{t,j}^L} M_j^L = \frac{1}{(m \times n)} \mathbf{e}_j^L \quad (23)$$

A similar relation holds for the interfacial area:

$$A = \frac{1}{(m \times n)} A_j \quad (24)$$

Phase equilibrium and reaction rates are calculated per cell based on the local compositions and temperature prevailing. Hydrodynamics and mass transfer parameters are calculated using stage flows, compositions and temperatures. For example, for sieve tray columns the volumetric liquid hold-up on the stage can be calculated from knowledge of the active (or bubbling) tray area, A_{bub} , and estimation of the clear liquid height, h_{cl} (Bennett et al., 1983; Barker and Self, 1962).

$$\mathbf{e}_j^L = h_{cl,j} A_{bub,j} \quad (25)$$

From the chosen tray spacing, h_t , the corresponding volumetric vapour hold-up can be calculated

$$\mathbf{e}_j^V = (h_t - h_{cl,j}) A_{bub,j} \quad (26)$$

The liquid and vapour residence times on the stage can be calculated from knowledge of the volumetric hold-ups and flows on the stage. The liquid and vapour residence times for a particular cell is calculated as follows

$$\mathbf{t}_{mm,nn}^V = \frac{1}{n} \mathbf{t}_j^V; \quad \mathbf{t}_{mm,nn}^L = \frac{1}{m} \mathbf{t}_j^L \quad (27)$$

Although not done here, the hold-up in the vapour disengagement space between trays can be modelled by rows of cells containing only vapour. It would also be straightforward to use columns of liquid to model the hold-up in the downcomer of a tray column. The mass and energy transfer rate equations would not be needed for such cells.

Model System

As described above the model combines differential equations for the bulk dynamics, with differential equations for the transport through the film and algebraic equations for the vapour-liquid equilibrium at the interface. For the purposes of solving the transfer rate equations we divide the film into a number of slices (five in the calculations described

Table 1. Model equations for dynamic nonequilibrium cell model . The model equations are either ordinary differential equations (ODE), ordinary differential equations (PDE), or algebraic equations (AE). The number of discrete points in the liquid film is denoted with nL , and in the vapour film with nV , respectively.

Description of equation	Bulk Liquid Phase				Bulk Vapour Phase			
	Number of eqns	Type	Eq. (xx)	Var.	Number of eqns	Type	Eq. (xx)	Var.
Total molar balance	1	ODE	Eq. (4)	M^L	1	ODE	Eq. (3)	M^V
Molar component balance	$c-1$	ODE	Eq. (2)	M_i^L x_i	$c-1$	ODE	Eq. (1)	M_i^V y_i
Mole fractions	c	AE	Eq. (5)		c	AE	Eq. (5)	
Summation	1	AE	Eq. (6)		1	AE	Eq. (6)	
Energy balance	1	ODE	Eq. (8)	E^L	1	ODE	Eq. (7)	E^V
Energy hold-up	1	AE	Eq. (10)	T^L	1	AE	Eq. (10)	T^V
Residence time	1	AE	Eq. (27)	L	1	AE	Eq. (27)	V
“Film” Liquid Phase								
Molar component balance	$nL \times c$	PDE	Eq. (12)	N_i^{Lf}	c	PDE	Eq. (11)	N_i^{Vf}
Maxwell-Stefan equations	$nL \times (c-1)$	PDE	Eq. (14)	x_i^{Lf}	$nV \times (c-1)$	PDE	Eq. (13)	y_i^{Vf}
Summation	$nL \times 1$	AE	Eq. (15)		$nV \times 1$	AE	Eq. (15)	
Energy balance	$nL \times 1$	PDE	Eq. (16)	E^{Lf}	$nV \times 1$	PDE	Eq. (16)	E^{Vf}
Energy transfer rate	$nL \times 1$	PDE	Eq. (17)	T^{Lf}	$nV \times 1$	PDE	Eq. (17)	T^{Vf}
Total: $5c + 8 + nL \times (2c + 2) + nV \times (c + 2)$ implemented equations per cell								
Stage variables Liquid Phase								
Flow leaving the Stage	1	AE	Eq. (20)	L_j	1	AE	Eq. (20)	V_j
Component molar Flow	c	AE	Eq. (21)	x_{ij}	c	AE	Eq. (21)	y_{ij}
Enthalpy flow	1	AE	Eq. (22)	T_j^L	1	AE	Eq. (22)	T_j^V
Total: $(nn \times mm) (5c + 8 + nL \times (2c + 2) + nV \times (c + 2)) + 2c + 4$ implemented eqs. per stage								

below). The Maxwell-Stefan and energy transfer rate equations are written for each node with the derivative terms replaced by finite difference approximations. Central difference approximations should be avoided as they tend to lead to zigzag concentration profiles. The reboiler and condenser models have been presented in Chapter 6.

The resulting model is a set of differential-algebraic (DAE) equations and is summarised in Table 1, which also lists the variables computed by solving the model equations. The index of this DAE system is 1; the index being the minimum number of differentiations needed to obtain a system consisting only of ODE's (Unger et al. 1995, Mattsson et al. 1993). It is useful to know the index of a DAE system because some numerical integration methods cannot reliably solve systems with an index higher than one. A higher index was avoided by making the hydrodynamics depend explicitly on the flows leaving a stage or cell, Eqs. (25)-(27), by using steady-state mass and energy transfer rate equations, and by assuming the liquid residence time to be the same in each cell. An even distribution of molar hold-ups leads to an index greater than 1.

The DAE system is solved using BESIRK (Kooijman, 1995; Kooijman and Taylor, 1995b). BESIRK is a semi-implicit Runge-Kutta method originally developed by Michelsen (1976) and extended with an extrapolation scheme (Bulirsch and Stoer, 1966), improving the efficiency in solving the DAE problem. The evaluation of the sparse Jacobian required by this method is carried out primarily using analytical expressions. The exceptions include entries including derivatives of enthalpies, mass and heat transfer coefficients, hold-ups and pressure drop.

The initial condition is a solution to the steady state equations where all time derivatives are set to zero. Following the initialisation as described, the time-dependent equations are integrated for some predetermined time. The program stops the integration after a time-dependent discontinuity is reached and re-initialises the DAE system depending on the perturbation under consideration. Perturbations in the reboiler or condenser specifications, such as reboil ratio or reflux ratio, require a consistent re-initialisation of the flows in order to satisfy the algebraic constraints. In some cases it might also be required to define a continuous perturbation in order to maintain consistency and continuity of the solution (Kröner, et al. 1997). This is not necessary for the feed perturbation under consideration in this chapter. Our model also supports steady-state computations using Newton's method, as outlined in Taylor et al. (1994).

The simulations have been performed on a PC (Pentium II 286 MHz). A nonequilibrium model with 17 stages and 1 cell per stage contains approximately 2000 equations and requires about 30 minutes computing time to reach a new steady state following a perturbation. An equilibrium-stage model has about 300 equations, and needs only a couple of minutes for the same problem. The computational time increases significantly with increasing numbers of cells. A 3×3 cell model with 17 trays contains about 16000 equations and requires about 8 hours to compute the desired transient.

Case Study 1: Dynamics of Metathesis RD Column

Consider the reversible metathesis reaction of 2-pentene to 2-butene and 3-hexene:



The overall rate of reaction of 2-pentene is given by

$$R = 0.5c_{c5} \left(k_f x_{c5}^2 - x_{c4} x_{c6} / K_{eq} \right) \quad (29)$$

The forward reaction rate constant is

$$k_f = 78.2 \exp\left(-\frac{27600}{RT}\right) \quad [\text{s}^{-1}] \quad (30)$$

and the equilibrium reaction rate constant

$$K_{eq} = 0.25 \quad (31)$$

The metathesis reaction is most effectively carried out in a RD column in order to achieve highest possible conversions of 2-pentene (Higler et al., 1999c; Okasinski and Doherty, 1998). The RD column configuration chosen for study is essentially the same as that of Higler et al. (1999c) and consists of a 25-stage column with liquid feed of pure 2-pentene on stage 13; see Fig. 2. The feed flow rate is 10 mol/s. The condenser and top column pressures are fixed at 101.3 kPa. The RD column is constructed of sieve plates and the configuration details are given in Table 2. The pressure drop on each tray is

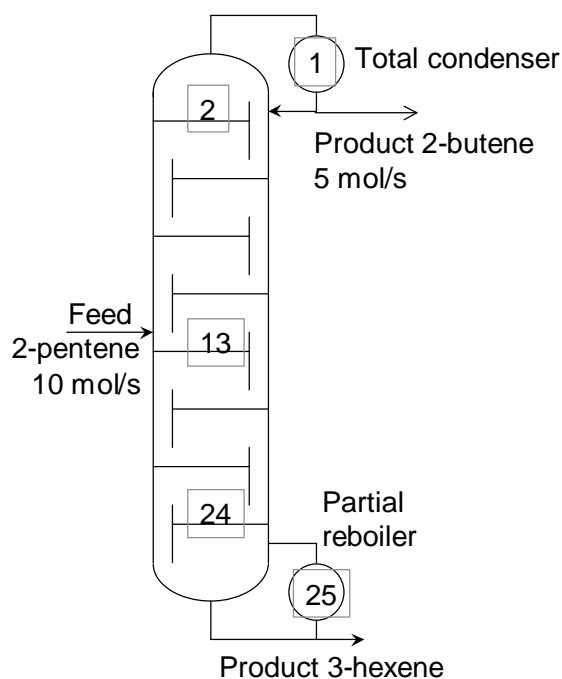


Figure 2. Configuration of the 2-pentene metathesis RD column.

Table 2. Specification of sieve tray columns used in the four case studies.

	Case study 1: Metathesis	Case study 2: MeOH-IPA- Water	Case study 3: MTBE	Case study 4: Ethylene Glycol
Type of tray	Sieve	Sieve	Sieve	Sieve
Column diameter /[m]	1.8	0.8	6	1.7
Total tray area /[m ²]	2.545	0.503	28.27	2.27
Number of liquid flow passes	2	1	5	1
Tray spacing /[m]	0.61	0.61	0.7	0.7
Liquid flow path length /[m]	0.62	0.52	0.97	1.283
Active area /total tray area	0.76	0.76	0.76	0.86
Hole diameter /[m]	0.0045	0.005	0.0045	0.0045
Total hole area /total tray area	0.1	0.11	0.1	0.1
Downcomer area /total tray area	0.12	0.12	0.12	0.07
Weir length /[m]	3.1	0.74	22	1.52
Weir height /[m]	0.08	0.05	0.05	0.08
Downcomer clearance /[m]	0.038	0.038	0.038	0.01
Reboiler hold-up/[m ³]	0.07	0.04	2.3	1.5 or 2.3
Reflux drum hold-up/[m ³]	0.07	None	1.3	0.7 or 1.3

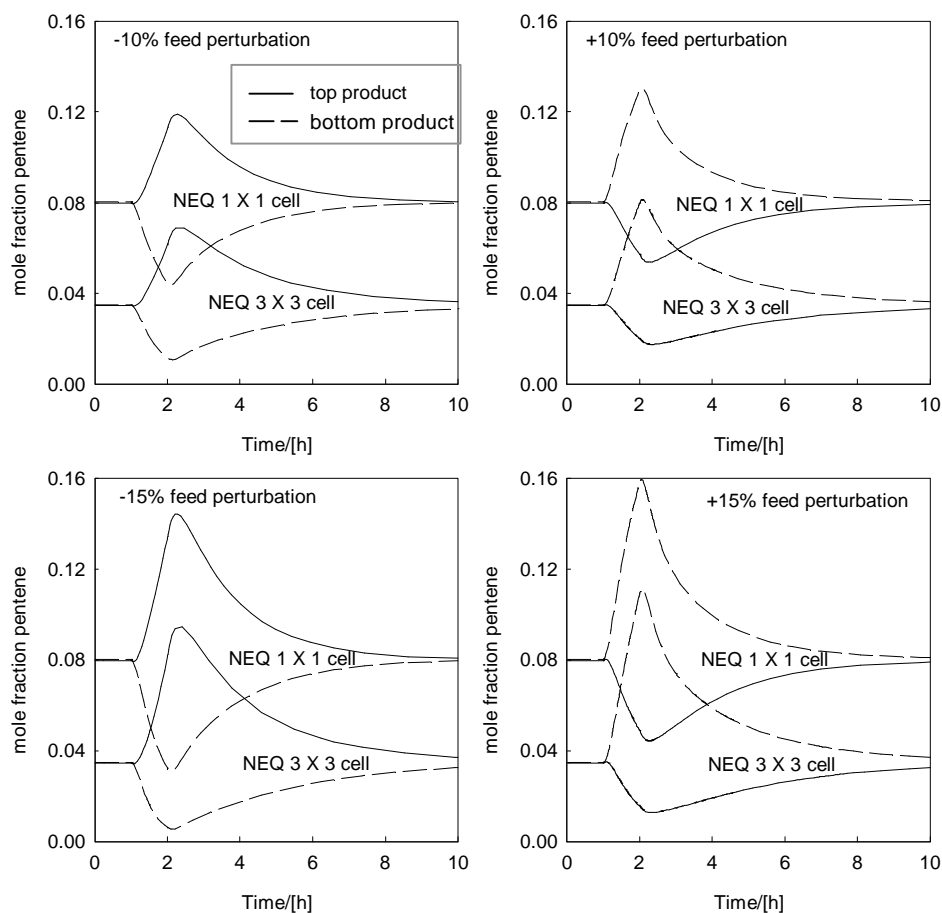


Figure 3. Dynamic response of metathesis RD column to feed perturbations. Comparison of the response of NEQ 1 \times 1 and NEQ 3 \times 3 models.

calculated using the Bennett et al. (1983) correlation. The top product flow rate is fixed at 5 mol/s. The boilup ratio is fixed at 8. For calculation of the thermodynamic properties the Peng-Robinson equation of state was used. The *A.I.Ch.E.* calculation method was used for estimation of the mass transfer coefficients in the vapour and liquid phases (for details of this model see Lockett, 1986)..

Two different NEQ model implementations were used to determine the column dynamics: the NEQ 1 \times 1 cell and NEQ 3 \times 3 cell models. The column was operated at the initial state for a period of 1 h and the 2-pentene flow to the column was perturbed by $\pm 10\%$ and $\pm 15\%$ for a period of 1 h. Figure 3 shows the influence of staging on the dynamic response of the 2-pentene mole fraction in the top and bottom products. Firstly, we note that the compositions of unreacted 2-propene in the top and bottom products at steady state is significantly lower for the NEQ 3 \times 3 cell model. This underlines the importance of vapour and liquid phase staging on conversion in RD columns. Secondly, we note that the amplitude of the over(under)shoot in the 2-pentene mole fraction of the

NEQ 3×3 cell model is almost as high as that of the NEQ 1×1 cell model, despite the base (steady-state) value being significantly lower. This means that the introduction of staging increases the sensitivity of the column to perturbations. This would need to be taken into account when designing controller strategies.

Case Study 2: Dynamics of Distillation of Methanol – Isopropanol - Water

We now examine the dynamics of a conventional distillation column separating the mixture: methanol (1) - *iso*-propanol (2) – water (3). Shown in Fig. 4 are the residue curve maps (described for example in Seader and Henley, 1998) for this system, calculated using the NRTL model (with parameters listed in Table 1; Chapter 5). The mixture has a binary minimum boiling azeotrope for *iso*-propanol-water. The distillation boundary splits the residue curve map into two regions. It can be seen that the residue curves, which originate along the distillation boundary, can choose two different paths ending up in different corners of the composition triangle. The residue curves coincide with the liquid composition trajectories during distillation at total reflux in a continuous contact device, such as a packed column, in which the liquid and vapour phases are in thermodynamic equilibrium.

Dynamic column simulations were carried out for a 13-stage sieve tray column, shown in Fig. 5, with the hardware specifications given in Table 2. The feed composition was chosen to lie in the distillation boundary: $x_1=0.5$, $x_2=0.35$, $x_3=0.15$. After steady operations for 1 h, the feed composition was perturbed to $x_1=0.5$, $x_2=0.38$, $x_3=0.12$. The

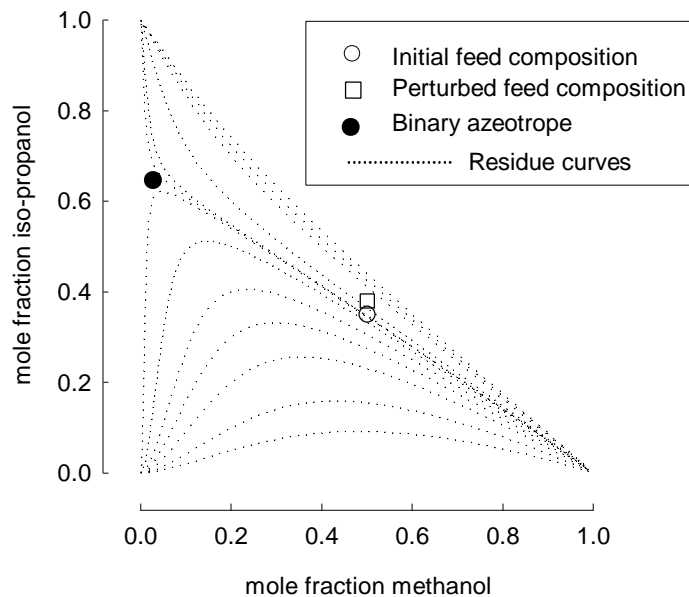


Figure 4. Residue curve map for methanol – iso-propanol - water.

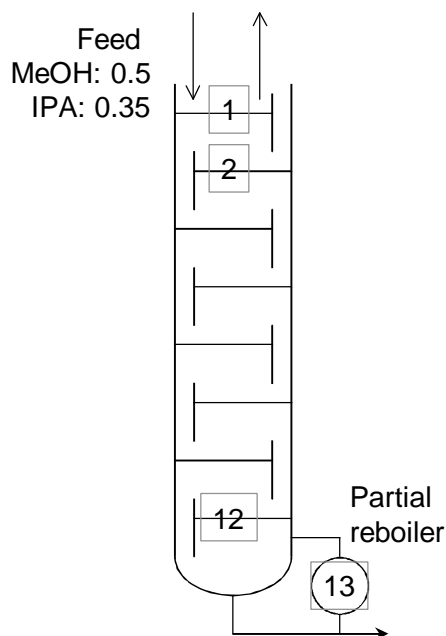


Figure 5. Configuration of sieve tray column for separating methanol – iso-propanol - water.

initial and perturbed feed compositions are indicated in Fig. 4. Two types of perturbations were examined: (a) a pulsed perturbation lasting 1 h, and (b) a step perturbation. Both types of perturbations were initiated after one hour of steady operation. The dynamic responses were calculated with three model implementations: (a) EQ model, (b) NEQ 1×1 cell model, and (c) NEQ 3×3 cell model. In the NEQ implementation the *A.I.Ch.E.* method was used for estimation of the mass transfer coefficients in the vapour and liquid phases.

The EQ and NEQ models even predict different initial steady states! The initial steady-state column composition profiles are shown in Fig. 6. The EQ model predicts that the reboiler would consist of pure *iso*-propanol. The NEQ 3×3 cell model, on the other hand, predicts a reboiler composition which is rich in water. The NEQ 1×1 cell model, as expected, has the poorest separation capability, but the composition trajectory follows the trend of the NEQ 3×3 cell model. Introducing more stages would make the NEQ 1×1 cell model approach the separation performance of the NEQ 3×3 cell model.

Experimental data reported by Pelkonen et al. (1997) for total reflux operation of methanol - *iso*-propanol - water in a 0.1 m diameter column packed with Sulzer BX packing, start at a composition $x_1=0.5$, $x_2=0.35$, $x_3=0.15$ at the top of the column and end up with virtually pure water in the reboiler. These experiments appear to verify the validity of the NEQ composition trajectories shown in Fig. 6.

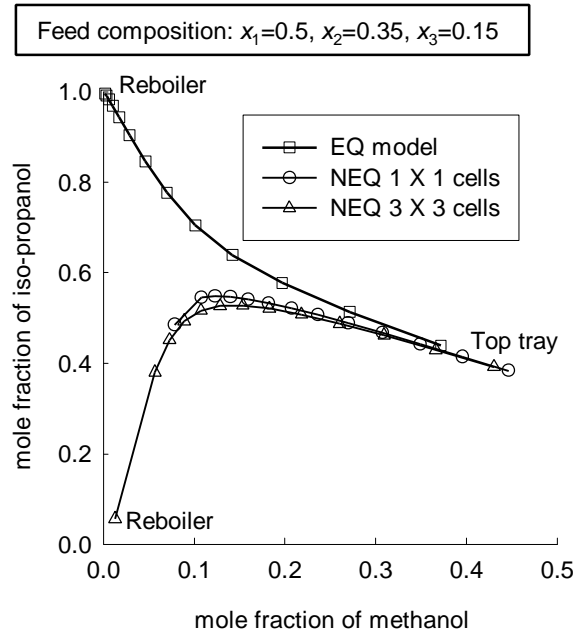


Figure 6. Steady state column composition trajectories for distillation of methanol (1) – iso-propanol (2) – water (3). Comparison of the response of EQ, NEQ 1 × 1 and NEQ 3 × 3 models.

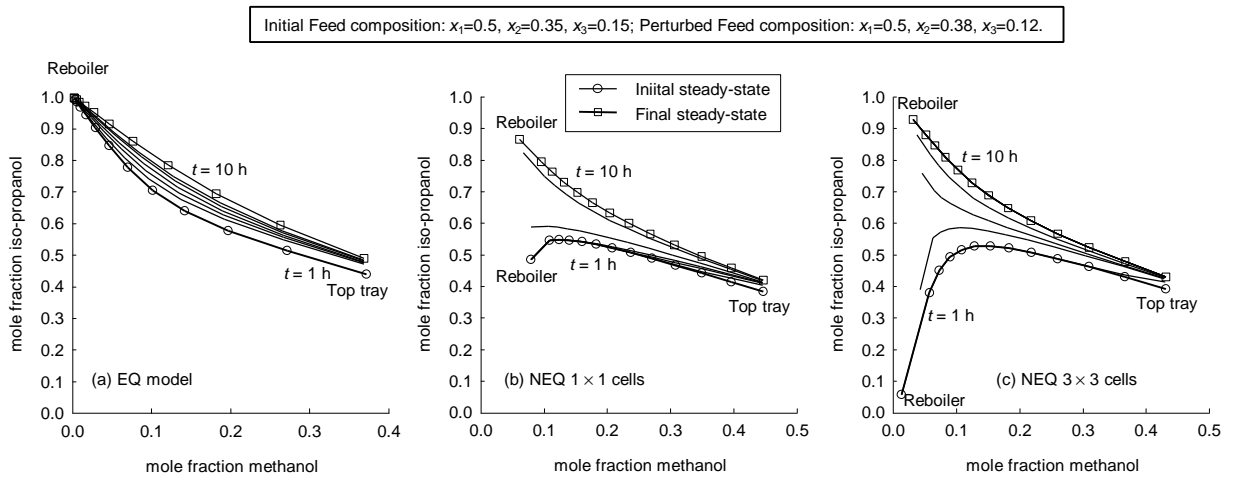


Figure 7. Response to step disturbance in feed composition for distillation of methanol (1) – iso-propanol (2) – water (3). Comparison of the responses of EQ, NEQ 1 × 1 and NEQ 3 × 3 models.

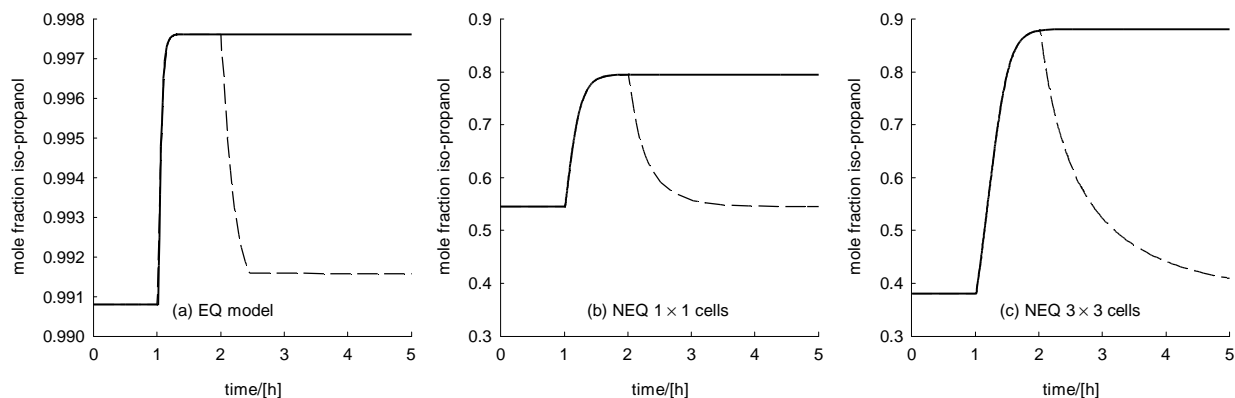


Figure 8. Tray-12 composition response to pulse and step disturbance in feed composition for distillation of methanol (1) – iso-propanol (2) – water (3). Comparison of the responses of EQ, NEQ 1 × 1 and NEQ 3 × 3 models.

The time-evolution of the column composition profiles responding to a step feed composition perturbation are shown in Fig. 7 for the three model implementations. The incorporation of mass transfer resistance and staging increases the sensitivity of the column response. For the NEQ 3 × 3 cell model the reboiler composition changes from water-rich state to *iso*-propanol rich state even for the small feed composition perturbation.

Figure 8 compares the tray-12 composition of *iso*-propanol for both step and pulse feed composition perturbations. Again, it is clear that the NEQ 3 × 3 cell model is the most sensitive one. It exhibits the highest amplitude of overshoot and takes the longest time to recover to the initial steady state.

The need for using proper control strategies (and proper models!) is underlined when operating close to the distillation boundary.

Case Study 3: Dynamics of Reactive Distillation Column for MTBE Synthesis

Consider the synthesis of MTBE in an RD column. The column configuration chosen for the simulations is shown in Figure 9; this is essentially the configuration described by Jacobs and Krishna (1993) in their simulation study using the EQ stage model. The total number of stages is 17, including a total condenser and a partial reboiler; the column pressure is 1115 kPa. Reactive stages are located in the middle of the column, stage 4 down to and including stage 11. The column has two feed streams: a methanol feed and a

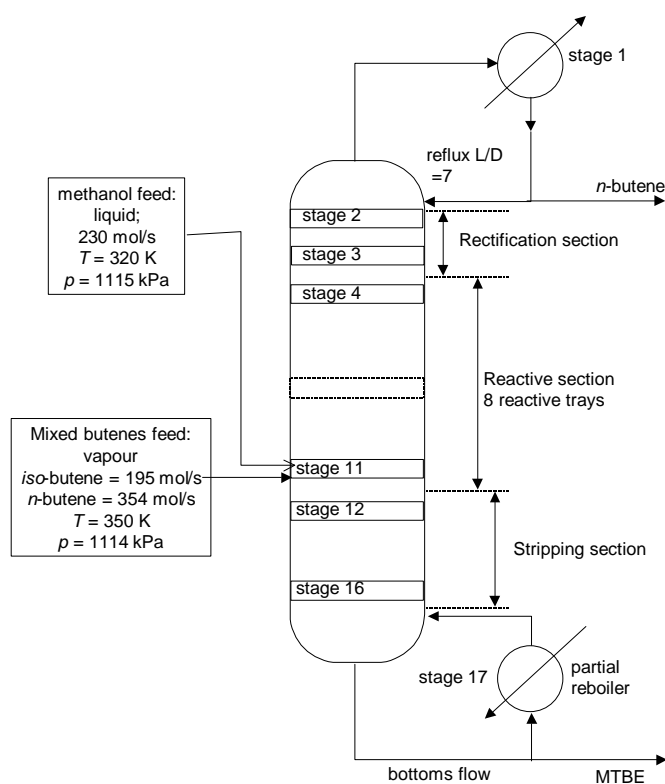


Figure 9. Configuration of the MTBE synthesis column, following Jacobs and Krishna (1993). The column consists of 17 stages. The reactive stages are configured as sieve trays (see Fig. 4 in Chapter 4).

mixed butenes feed. A small stoichiometric excess of methanol is used. The mixed butenes feed, to stage 11, contains a mixture of *iso*-butene, which is reactive, and *n*-butene, which is non-reactive or inert. The reflux-ratio is set to 7 and the bottom flow rate is either set to 211 mol/s or varied (as a continuation parameter). The product removed from the top of the column is predominantly the inert *n*-butene. The bottoms product consists predominantly of MTBE. For a properly designed and operated column it is possible to achieve close to 100% conversion of *iso*-butene. The tray hardware details are specified in Table 2. The total amount of catalyst in the reactive zone is 8000 kg. The ion exchange capacity of the catalyst is 4.54 meq H⁺/g.

The UNIQUAC model was used for description of liquid phase nonideality, while the Soave-Redlich-Kwong equation of state was used for the vapour phase. The extended Antoine equation was used for calculation of the vapour pressure. Thermodynamic and kinetic data are taken from Rehfinger and Hoffmann (1990a, 1990b).

The first objective of our dynamic simulations is to compare the results of EQ and NEQ multiple cell model. The separation capability of the non-reactive stripping and rectifying sections will also affect the overall column performance. We decided to focus on the

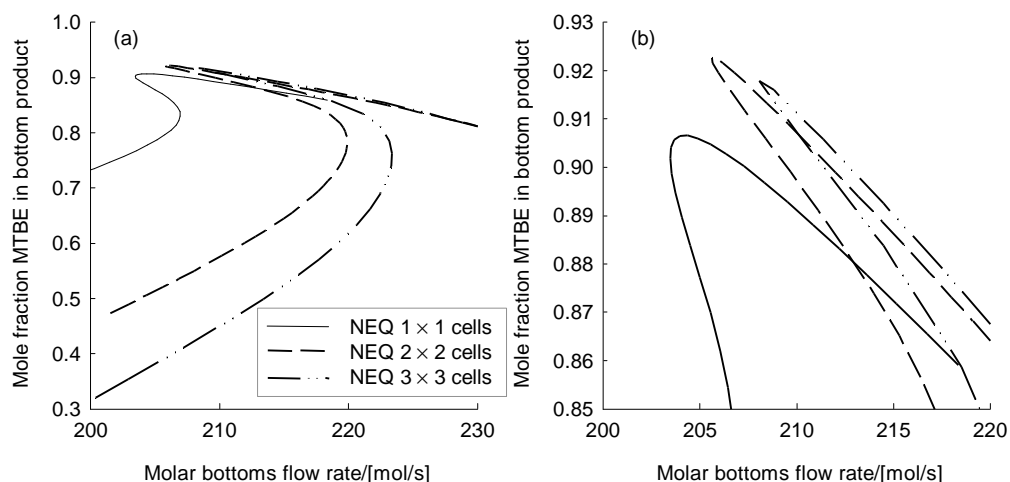


Figure 10. Bifurcation diagram for three different model implementations, NEQ 1×1 , NEQ 2×2 and NEQ 3×3 models. (a) and (b) are drawn to different scales.

differences of the EQ and NEQ modelling of the reactive section only and, therefore, assumed the non-reactive stages to have equal separation capability in both implementations. Towards this end, in the EQ model implementation we have assumed a tray efficiency of 65% for the non-reactive rectifying stages and 58% for the non-reactive stripping stages; these values corresponded closely to the calculations of the NEQ model for the corresponding non-reactive rectifying and stripping sections using the *A.I.Ch.E.* calculation method for sieve tray mass transfer. The interfacial area is estimated from the Hofhuis and Zuiderweg (1979) correlation and the fractional liquid hold-up on the tray is estimated from the correlation of Barker and Self (1962). Of course, in the NEQ model implementation of the non-reactive stages, efficiencies are not used in the calculations but can be calculated from the simulation results; these stage efficiencies vary for individual components. For the reactive section, the EQ model assumes vapour and liquid phases to be in thermodynamic equilibrium (however, not in reaction equilibrium).

Before performing dynamic simulations we used the continuation method to investigate the steady-state behaviour using the molar bottoms flow rate as continuation parameter. The bifurcation diagram for the NEQ model with 1×1 , 2×2 and 3×3 cells are shown in Fig. 10. All three configurations show steady-state multiplicity. Clearly it is desirable to operate on the high-conversion branch of these curves; as is to be expected the conversion levels on this branch increase with increasing degree of staging in the vapour and liquid phases. In fact, the bifurcation diagram for the NEQ 3×3 cell model coincides closely with that obtained by an EQ model; see Fig. 11.

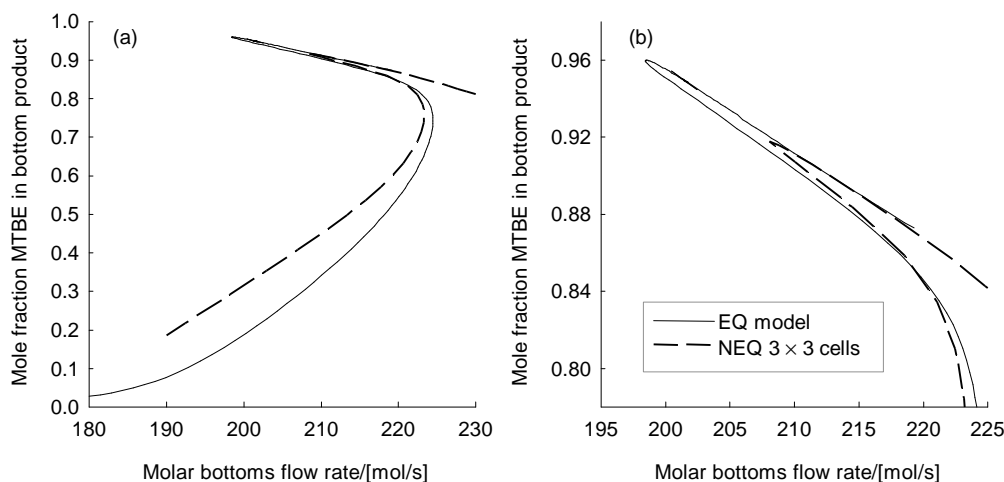


Figure 11. Comparison of the bifurcation diagram for NEQ 3×3 cell model with EQ model. (a) and (b) are drawn to different scales.

The implication of the results in Fig. 11 is that when there is sufficient degree of staging in the liquid and vapour phases (3 well mixed cells in either phases), the steady-state column performance corresponds to that of a column operating at thermodynamic equilibrium with the reaction rates determined by chemical kinetics. While the EQ model may be sufficient to describe the *steady-state* column performance under kinetically controlled conditions, we show below that the column *dynamics* could be significantly different when calculated with an NEQ model.

Taking the bottoms flow rate to be 211 mol/s, we performed dynamic simulations, starting with the high conversion steady-state situation, and introducing a +3%, +5% and +7% perturbation in the feed MeOH, 1 h after start-up. Fig. 12 shows the dynamic responses of the NEQ 3×3 model for the MTBE bottom production composition and temperature. It is interesting to note that for the +5% and +7% perturbations in the feed MeOH, the system suffers an (undesirable) transition from the high steady state to the lower one. Figure 13 compares the response of the NEQ 2×2 and NEQ 3×3 models with the EQ model for (a) +3%, (b) +5% and (c) +7% perturbation in the feed MeOH. From Fig. 13 (a) we see that the responses of the EQ and NEQ 3×3 models are close to each other. However, when the magnitude of the perturbation is increased we see in Figs 13 (b) and (c) that the EQ and NEQ 3×3 model behave differently, both *quantitatively* and *qualitatively*. The NEQ 3×3 cell model suffers steady-state transitions whereas the EQ model recovers its initial high steady-state conversion.

For a -15% perturbation in the inert n-butene feed to the column, the dynamic responses are shown in Fig. 14. The EQ model is practically oblivious to this perturbation in the inert feed, whereas the NEQ 3×3 suffers transition from the high conversion steady-state to the lower one.

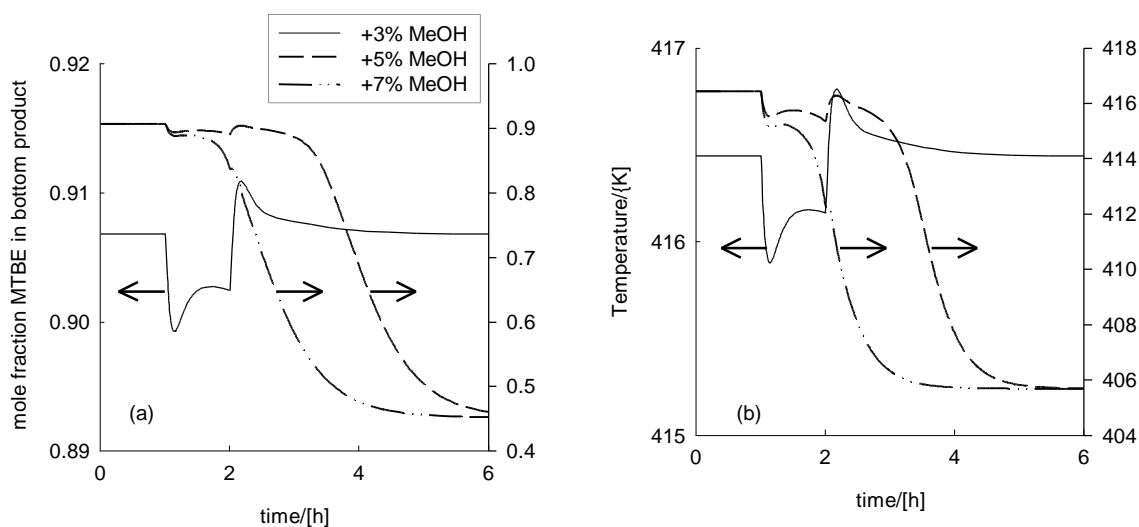


Figure 12. Dynamic response obtained with the NEQ 3×3 cell model for MeOH feed flow perturbations (+3%, +5% and +7%), 1 h after column start-up. The perturbation period is 1 h. (a) response of MTBE bottom product composition and (b) response of bottom product temperature.

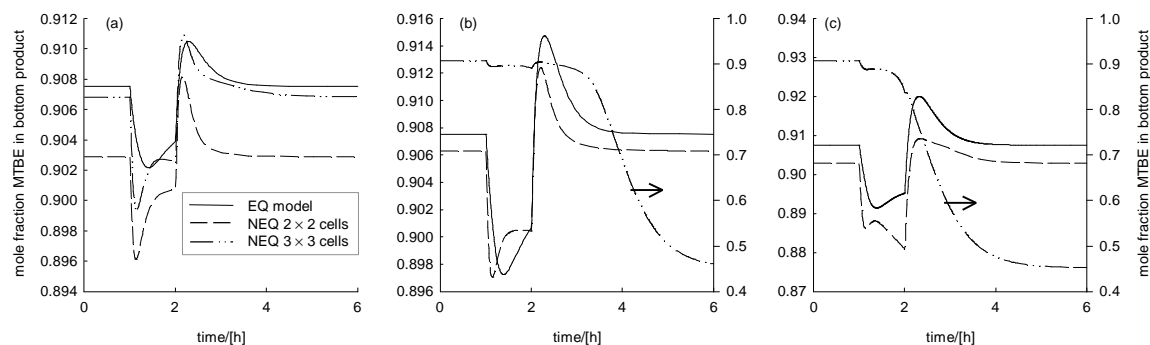


Figure 13. Dynamic response obtained with the EQ, NEQ 2×2 and NEQ 3×3 models to MeOH feed flow perturbations of (a) +3%, (b) +5% and (c) +7%, 1 h after column start-up. The perturbation period is 1 h.

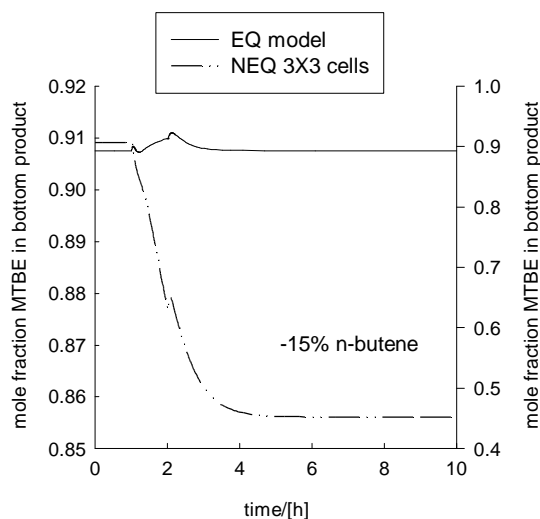


Figure 14. Dynamic response obtained with the EQ and NEQ 3 × 3 models to a -15% feed flow perturbations of n-butene, 1 h after column start-up. The perturbation period is 1 h.

Case Study 4 Dynamics of Reactive Distillation Column for Ethylene Glycol

We consider the reaction of ethylene oxide (EO) with water to produce ethylene glycol (EG) in a reactive distillation column. The reaction is irreversible and proceeds in the presence of a catalyst: $\text{EO} + \text{H}_2\text{O} \rightarrow \text{EG}$. In addition we have an unwanted side reaction in which ethylene glycol reacts with ethylene oxide to di-ethylene-glycol $\text{EO} + \text{EG} \rightarrow \text{DEG}$. The reaction rate constant of the second reaction is, under reaction conditions, about three times as large as the rate constant of the first reaction. Therefore, in a conventional reactor with equimolar feed, a considerable amount of DEG is produced. Furthermore, the reactions are both highly exothermic requiring good temperature control. A reactive distillation column offers both the advantages of heat integration and in-situ separation of the desired product, EG, preventing further reaction to DEG. By choosing total reflux operation, one can ensure that the water mole fraction in the liquid phase on all the trays in the reactive section is close to unity (EO is considerably more volatile than water). The ethylene oxide that is supplied to the column reacts with water to form EG and because of the high surplus of water in the liquid, the concentrations of

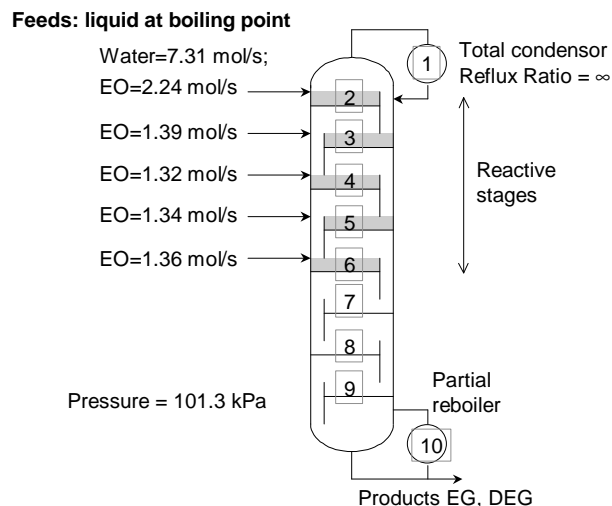


Figure 15. Configuration of RD column for hydration of ethylene oxide to ethylene glycol. Further details to be found in Ciric and Miao (1994) and Chapter 2.

ethylene oxide and ethylene glycol will be very low. This results in a low production rate of DEG. Furthermore, the distillation process provides direct temperature control, since the temperature of the liquid phases will always be at boiling point. Hot spot formation and the danger of runaway reactions are non-existent in reactive distillation.

The column configuration chosen for case study is similar to the set up of Ciric and co-workers (Ciric and Gu, 1994; Ciric and Miao, 1994), details of which are given in Fig. 15. This is a 10-stage sieve tray column (including total condenser and partial reboiler). Water is supplied to the top of the column, while the EO feed is distributed along the top section of the column. Reactions are assumed to take place only on stages 2 to 6 because catalyst is considered to be present only on these stages. The column is operated at total reflux, while in the bottom a boilup ratio of 24 is maintained. The reaction kinetics and thermodynamics data are the same as those reported in the paper by Ciric and Miao (1994). Since the NEQ model calculations require the estimation of heat and mass transfer coefficients, we need to specify the tray configuration and layout. The configuration of the sieve trays are the same as in our early study of steady-state operation (see Chapter 2) and is summarised in Table 2. The volumetric liquid hold-up in the reflux drum is 0.700 m^3 and in the reboiler is 1.5 m^3 .

The dynamic simulations were performed as follows. The earlier developed steady-state version of the NEQ model (see Chapter 2) was first used to determine the steady-state conditions. Using this steady-state solution as a starting basis, the simulations were run in the dynamic mode and at $t = 1 \text{ h}$, disturbances in the feed flows of EO or H_2O are introduced to study the column response. These disturbances lasted for 1 h.

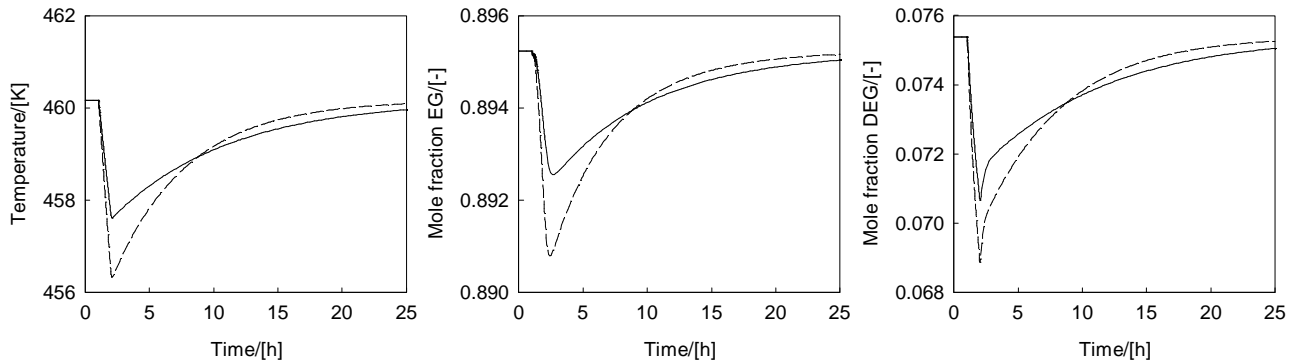


Figure 16. Dynamic response to a 10% increase in the water feed flow to stage 2, 1 h after column start-up. Number of cells in vapour and liquid flow directions are $m = 1$, $n = 1$. The continuous lines — denotes the case in which the condenser and reboiler hold-ups are 1300 L and 2300 L respectively. The dashed lines ----- represent the case in which the condenser and reboiler hold-ups are 700 L and 1500 L respectively.

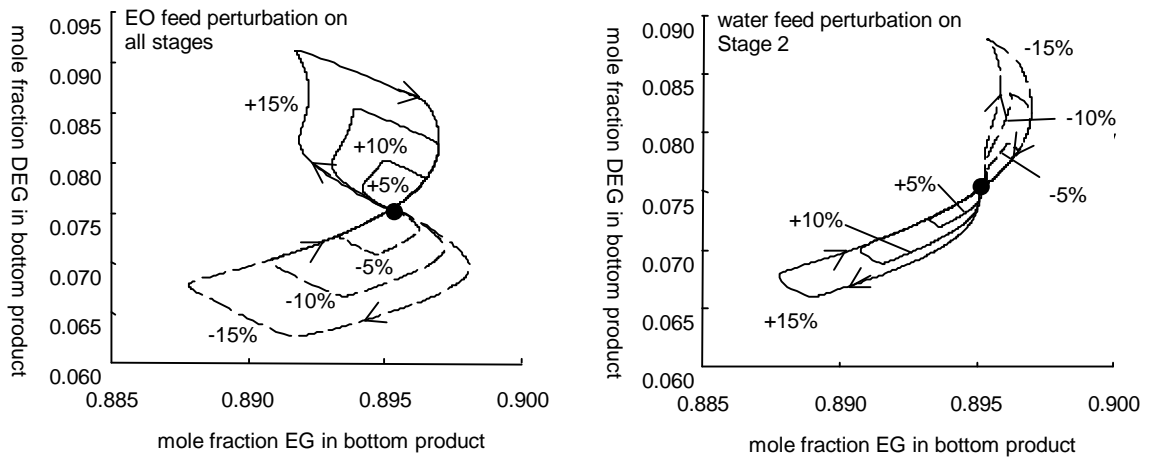


Figure 17. Composition phase portraits obtained during feed perturbations of EO (to all stages 2,3,4,5,6) and H₂O (to stage 2) to various extents, 1 h after column start-up. Number of cells in vapour and liquid flow directions are $m = 1$, $n = 1$. The large black dot represents the initial (and final) steady-state. The arrows indicate the direction of the transient composition trajectories.

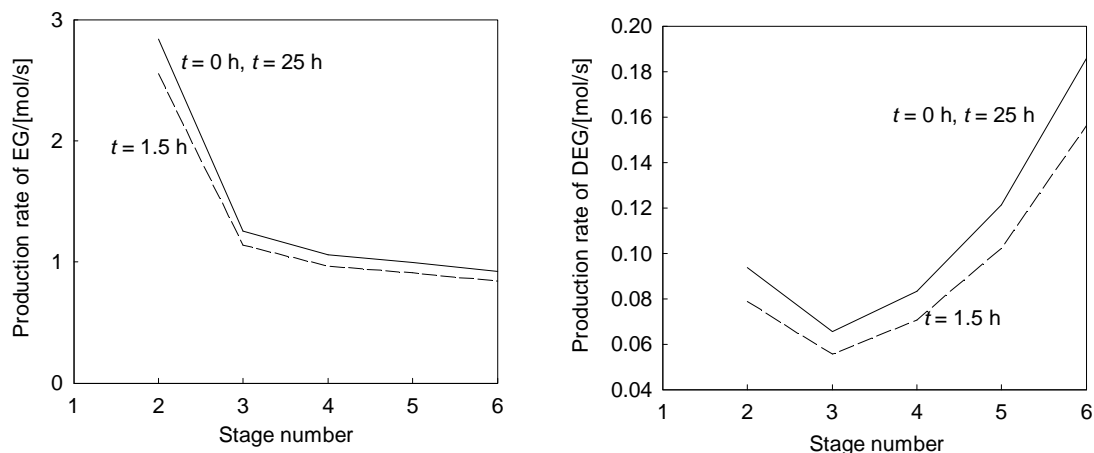


Figure 18. Production rates of EG and DEG along the reactive stages at time $t = 0$ and $t = 1.5$ h. Response to a -10% perturbation of EO feed to all reactive stages. NEQ model with $m = 1$ and $n = 1$.

Let us first consider the influence of the reboiler and condenser hold-ups on the column responses. Simulations using the NEQ cell model taking $m = 1$, $n = 1$ are shown in Fig. 16 for a 10% increase in the water feed to stage 2. Increased buffer capacities (1.3 m^3 and 2.3 m^3 in condenser and reboiler) leads to a slower approach to steady-state than for the base case configuration (0.7 m^3 condenser and 1.5 m^3 reboiler). However we note the higher under-shoots in the temperature and mole fractions of EG and DEG in the bottom product stream with lower buffer capacities. All other simulations reported below are with the base case buffer capacities.

Figure 17 shows the dynamic composition phase portrait (DEG vs. EG mole fractions in the bottom product) obtained after perturbations in the EO and H_2O feed flows to various extents. A positive EO perturbation feed leads to substantial unwanted DEG production during the transient. Similarly, a positive H_2O feed perturbation has the opposite, beneficial, effect. It is interesting to note that the all feed perturbations lead to substantial changes in the DEG composition and have only a minor influence on the EG product composition. This point is further emphasised in Fig. 18 which shows the production rates of EG and DEG on the reactive stages for a -10% perturbation to EO feed on stages 2,3,4,5 and 6. It is interesting to note the significant decrease in the DEG production rate on all stages during the transient (see the reaction rate profiles at $t = 1.5$ h after start-up). This decrease in DEG production rate is more pronounced than the decrease in the EG production rate. A proper control of feed flows is therefore essential to preserve reaction selectivity in the column.

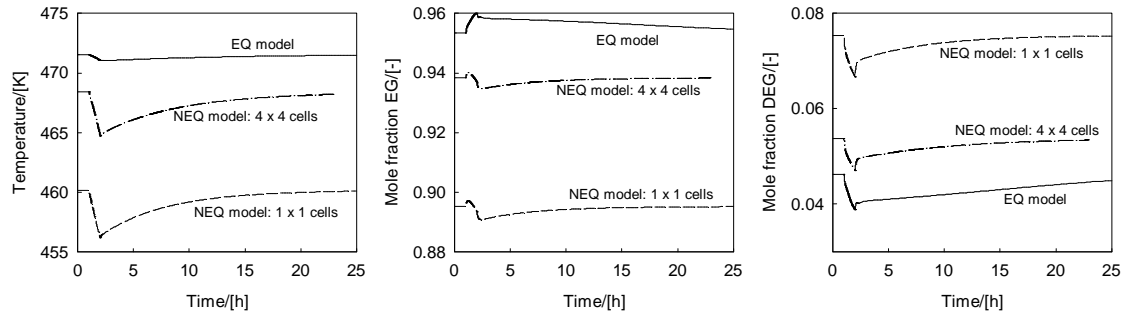


Figure 19. Dynamic responses of the temperature, EG mole fraction, DEG mole fraction of the bottom product stream to a 10% decrease in the EO feed flow (to stages 2,3,4,5,6), 1 h after column start-up. Comparison of NEQ cell models ($m = 1$, $n = 1$ and $m = 4$, $n = 4$) with EQ model.

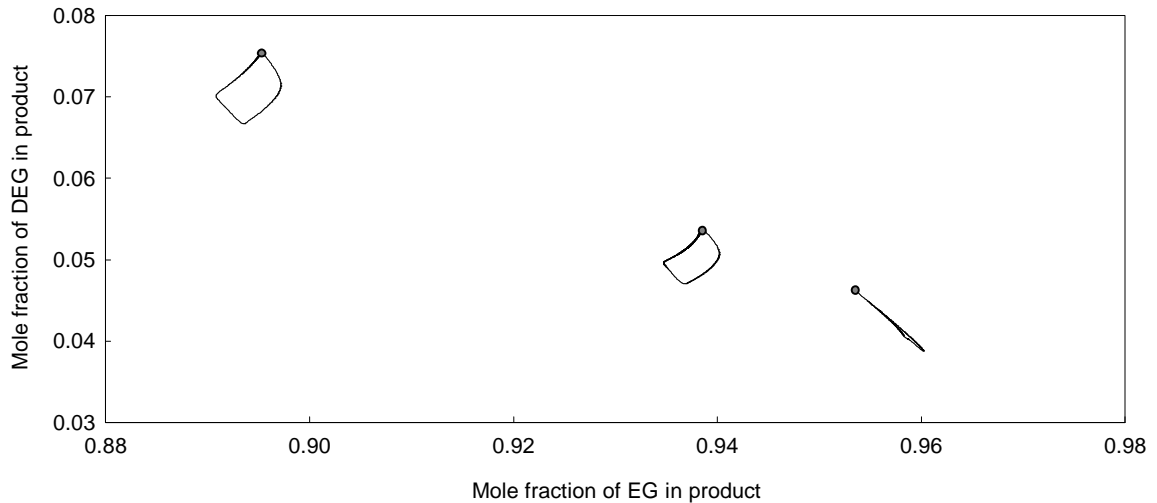


Figure 20. Composition phase portraits (DEG vs EG composition in bottom product) during transient response to a 10% decrease in the EO feed flow (to stages 2,3,4,5,6), 1 h after column start-up. Comparison of NEQ cell models ($m = 1$, $n = 1$ and $m = 4$, $n = 4$) with EQ model. The large black dots denote the initial (and final) steady-state values.

For the 1.7 m diameter column, with a weir height of 80 mm, existing correlations would anticipate a substantial degree of staging in the liquid and vapour phases. In Fig. 19 we compare the transient responses to a 10% decrease in the EO feed (to all reactive stages) for three cases: (1) NEQ cell model with 1×1 cells, (2) NEQ cell model with 4×4 cells (which would correspond roughly with plug flow of both phases on a tray), and (3) EQ model. As anticipated, the EQ model anticipates the best RD performance with respect to conversion and selectivity, i.e. the highest EG and the lowest DEG composition in the bottom product. The 4×4 cell NEQ model is considerably superior to the 1×1 cell NEQ model in this respect. The corresponding composition phase portraits in Fig. 20 illustrate this more clearly. The EQ model covers a much smaller composition space during transient than either of the two NEQ cell models.

Concluding Remarks

We have developed a rigorous dynamic NEQ cell model for RD columns. The cell model becomes necessary in order to take account of staging of the vapour and liquid phases on a tray of an RD column.

The results presented in Figs 11 - 14 provide convincing evidence to support the contention of Doherty and Buzad (1992) who wrote “...*steady state simulations are inadequate for assessing the effectiveness of operability and control schemes for reactive distillation columns... control schemes with good steady-state measures frequently fail under dynamic conditions, and that the failure was discovered only by using the full nonlinear dynamic simulation.There are good opportunities for productive research in this area, including such effects as the existence of multiple steady-states in reactive distillation and strategies for operating at the desired one.*”

We add one rider to the remark of Doherty and Buzad (1992) that *nonequilibrium* dynamic models, such as that described in this chapter, taking proper account of interphase mass transfer and of liquid and vapour staging on a tray, are essential for developing the proper control strategies for RD columns.

Conclusions

The major objective of this thesis, as stated in the Introduction, was to develop a dynamic NEQ cell model for RD columns.

In order to appreciate better the column dynamics, it is necessary to have a better feel for the steady-state performance. In Chapters 2, 3, 4 and 5, we gained some new insights into the steady-state design and operation aspects of RD columns. The major findings are given below.

1. The “window” of realisation of multiple steady-states is much smaller when using the NEQ model. The EQ model tends to exaggerate the phenomenon of multiple steady-states. Some of the steady states cannot be realised in practice because of flooding and weeping considerations. Overdimensioning of the column might ensure that only the low-conversion steady state is realised! This conclusion is not sufficiently realised in the literature.
2. The *conversion* and *selectivity* can be positively influenced by proper hardware design. For RD columns we would generally like to use larger weir heights than in conventional distillation. Also, the operating regime for RD columns is preferably in the froth regime rather than in the spray regime.
3. In Chapter 3 we had compared the steady-state performance of tray and packed column configurations for RD operations. In a tray column we have cross-flow contact of vapour and liquid phases. Also, for long liquid flow paths and high weirs (desirable for RD operations), there is sufficient degree of staging in the vapour and liquid phases in order to approach plug flow conditions. This leads to improved conversions when compared to packed columns.
4. For design of RD columns, use is often made of an EQ model with estimated component efficiencies. In Chapter 4 we have brought out the problems of estimation of component efficiencies in RD columns. Component efficiencies are strongly influenced by chemical reaction. Whether a component is a reactant or product influences the component efficiency. When the RD column exhibits steady-state multiplicity, each of these steady-states yields significantly different component efficiency values. Component efficiencies in RD are also influenced significantly by the degree of staging in the vapour and liquid phases. *A priori* estimation efficiencies in RD columns is well nigh impossible.
5. When operating close to the distillation boundary for non-reactive, conventional, distillation, the use of the rigorous Maxwell-Stefan diffusion equations to describe mass transfer can result in completely different composition trajectories from that predicted by an EQ model.

The development of the dynamic NEQ model is outlined in Chapters 6 and 7. On the basis of a variety of case studies performed the following conclusions can be drawn.

1. For a process exhibiting multiple-steady state, the EQ and NEQ models could lead to *qualitatively* different responses to feed flow disturbances. In general the EQ model is less sensitive to feed disturbances than the NEQ model. The NEQ model can suffer transition from the high conversion steady-state to the lower one while the EQ model regains its initial steady state.
2. The EQ model generally tends to underestimate the role of “inerts” in the feed stream.
3. The dynamic response of an RD column is also sensitive to the hardware choice. Due to differences in the hold-up of packed and tray columns, their response to feed disturbances could even be *qualitatively* different.
4. The introduction of staging in the liquid and vapour phases not only influences the steady state performance, by increasing reaction conversion and separation capability, but also has an influence on column dynamics.
5. With the NEQ multiple-cells-per-stage model the column dynamics becomes more sensitive to perturbations when compared to the EQ stage model.
6. When operating close to the distillation boundary for non-reactive, conventional, distillation, even small feed composition perturbations could lead to completely different compositions of products.
7. Even when the NEQ multiple-cell and EQ stage models exhibit almost identical *steady-state* characteristics, the *dynamic* responses of an RD column to perturbations could be significantly different.
8. For complex reaction schemes, feed flow perturbations affect by-product formation to a significant extent.

The overall conclusion of this thesis is that nonequilibrium dynamic model, taking proper account interphase mass transfer and of liquid and vapour staging in a column, are essential for developing the proper description of RD column dynamics and for developing appropriate control strategies.

References

- Abufares, A.A. and Douglas, P.L. (1995) Mathematical modeling and simulation of an MTBE catalytic distillation process using SPEEDUP and AspenPlus, *Chem. Eng. Res. & Design., Trans I.Chem.E., Part A*, **73**, 3 - 12
- Agreda, V.H., Partin, L.R. and Heise, W.H. (1990) High-purity methyl acetate via reactive distillation, *Chem. Eng. Progress*, **2**, 40 - 46.
- A.I.Ch.E. Bubble Tray Design Manual, A.I.Ch.E., New York (1958)
- Alejski, K., J. Szymanowski and M. Bogacki, (1988) The application of a minimization method for solving reactive distillation problems, *Comput. Chem. Engng.*, **12**, 833 – 839.
- Alejski, K. and Duprat, F. (1996) Dynamic simulation of the multicomponent reactive distillation, *Chem. Eng. Sci.*, **51**, 4237-4252
- Allgor, R.J., Berrera, M.J., Barton, P.I., and Evans, L.B. (1996) Optimal batch process development, *Comput. Chem. Eng.*, **20**, 885-896
- Asselineau, L., Mikitenko, P., Viltard, J.C., Zuliani, M. (1994) U.S. Patent 5368691: Reactive distillation process and apparatus for carrying it out
- Barbosa, D. and Doherty, M.F. (1987) A new set of composition variables for the representation of reactive phase diagrams, *Proc. Roy. Soc. Lond. A*, **413**, 459-464
- Barker P.E., Self, M.F. (1962) The evaluation of liquid mixing effects on a sieve plate using unsteady and steady state tracer techniques. *Chem. Eng. Sci.*, **17**, 541-554.
- Bart, H.-J. and Landschützer, H., (1996) Heterogene Reaktivdestillation mit axialer Rückvermischung, *Chem. Ing. Tech.*, **68**, 944-946 (1996)
- Bartlett, D.A. and Wahnschafft, O.M. (1998) Dynamic simulation and control strategy evaluation for MTBE reactive distillation, in *Foundations of computer-aided process operation* (Pekny, J.F. and Blau, G.E., editors), AIChE Symp. Series, **320**, 315-321
- Bennett, D.L. and Grimm, H.J. (1991) Eddy diffusivity for distillation sieve trays. *A.I.Ch.E.J.*, **37**, 589-596.
- Bennett D.L., Agrawal R., Cook P.J. (1983) New pressure drop correlation for sieve tray distillation columns. *A.I.Ch.E.J.*, **29**, 434 - 442.
- Bezzo, F., Bertucco, A., Forlin, A., and Barolo, M., (1999) Steady-state analysis of an industrial reactive distillation column, *Separation and Purification Technology*, **16**, 251-260
- Bravo, J.L., A. Pyhalathi and H. Jaervelin (1993) Investigations in a catalytic distillation pilot plant: Vapour/ liquid equilibrium, kinetics and mass transfer issues, *Ind. Eng. Chem. Res.* **32**, 2220 - 2225
- Bulirsch, R. and Stoer, J. (1966) Numerical treatment of ordinary differential equations by extrapolation methods, *Numerical Math.*, **8**, 1-13
- Buchholz, M., Pinaire, R., Ulowitz, M.A. (1995) European Patent 448884B1: Structure and method for catalytically reacting fluid streams in mass transfer apparatus
- Castillo, F.J.L. and Towler, G.P. (1998) Influence of multicomponent mass transfer on homogeneous azeotropic distillation, *Chem.Eng.Sci.*, **53**, 963-976.
- Carland, R.J. (1994) Fractionation tray for catalytic distillation, U.S. Patent 5,308,451

- Carra, S., E. Santacesaria, M. Morbidelli and L. Cavalli (1979a) Synthesis of propylene oxide from propylene-chlorohydrins - I Kinetic aspects of the process, *Chem. Eng. Sci.*, **34**, 1123 - 1132
- Carra, S., M. Morbidelli, E. Santacesaria and G. Buzzi (1979b) Synthesis of propylene oxide from propylene chlorohydrins - II. Modeling of the distillation with chemical reaction unit, *Chem. Eng. Sci.*, **34**, 1133 - 1140
- Chan, H. and Fair, J.R. (1983), Prediction of Point Efficiencies on Sieve Trays. 1. Binary Systems, *Ind. Eng. Chem. Proc. Des. Dev.*, **23**, 814-819
- Ciric, A.R. and P. Miao (1994) Steady state multiplicities in an ethylene glycol reactive distillation column. 1994, *Ind. Eng. Chem. Res.*, **33**, 2738 - 2748
- Ciric, A.R., and D. Gu. (1994), Synthesis of nonequilibrium reactive distillation by MINLP optimization, *A.I.Ch.E.J.*, **40**, 1479 - 1487
- Crossland, C.S., Gildert, G.R., Hearn, D. (1995) U.S. Patent 5431890: Catalytic distillation structure
- Danner, R.P. and Daubert, T.E., Manual for predicting chemical process design data, A.I.Ch.E., New York (1983).
- DeGarmo, J.L., V.N. Parulekar and V. Pinjala (1992) Consider reactive distillation, *Chem. Eng. Progress*, **3**, 43 - 50
- Doherty, M.F. and G. Buzad (1992) Reactive Distillation by Design, *Chem. Eng. Res. & Design., Trans I.Chem.E., Part A*, **70**, 448-458
- Eldarsai, H.S. and Douglas, P.L. (1998) Methyl-tert-butyl ether catalytic distillation column. Part I: Multiple steady states, *Trans.I.Chem.E., Part A*, **76**, 509 - 516
- Ellenberger, J. and Krishna, R., Counter-current operation of structured catalytically packed distillation columns: pressure drop, holdup and mixing, *Chem. Eng. Sci.*, **54**, 1339-1345 (1999)
- Espinoza, J., E. Martinez and G.A. Perez (1994), Dynamic behavior of reactive distillation columns, Equilibrium systems, *Chem. Eng. Commun*, **128**, 19 - 42
- Fair, J.R., Steinmeyer, D.E., Penney, W.R. and Croker, B.B. (1997) Gas absorption and gas-liquid system design, Section 14 in Perry's Chemical Engineers' Handbook, D.W. Green and J.O. Maloney (editors), 7th Edition, McGraw-Hill, New York
- Fair, J.R., (1998), Design aspects for reactive distillation - Columns for simultaneous reaction and separation need skillful planning, *Chemical Engineering (New York)* **105** (11) 158
- Flato, J. and Hoffmann, U. (1992) Development and start-up of a fixed bed reaction column for manufacturing antiknock enhancer MTBE, *Chem. Eng. Technol.*, **15**, 193-201
- Frey, T. and Stichlmair, J. (1999a) Thermodynamic fundamentals of reactive distillation, *Chemical and Engineering Technology*, **22**, 11-18
- Gani, R., Jepsen, T.S., and Perez-Cisneros, E. (1998) A generalized reactive separation unit model. Modelling and simulation aspects, *Comput. Chem. Eng.*, **22**, S363-S370
- Gelbein, A.P. and Buchholz, M. (1991) U.S. Patent 5073236: Process and structure for effecting catalytic reactions in distillation structure
- Gorak, A., 1995, Simulation thermischer Trennverfahren fluider Vielkomponentengemische. In Prozeßsimulation, H. Schuler (editor), VCH Verlagsgesellschaft mbH, Weinheim, pp. 349-408.

- Grosser, J.H., Doherty, M.F. and Malone, M.F. (1987) Modeling of reactive distillation systems, *Ind. Chem. Eng. Res.*, **26**, 983-989.
- Grosser, J.H., Doherty, M.F. and Malone, M.F. (1987) Modeling of reactive distillation systems, *Ind. Chem. Eng. Res.*, **26**, 983-989.
- Groten, W.A., Booker, D., Crossland, C.S. (1998) U.S. Patent 5730843: Catalytic distillation structure
- Güttinger, T.E. and Morari, M. (1999a), Predicting multiple steady states in equilibrium reactive distillation. 1. Analysis of nonhybrid systems, *Ind. Chem. Eng. Res.*, **38**, 1633-1648
- Güttinger, T.E. and Morari, M. (1999b), Predicting multiple steady states in equilibrium reactive distillation. 2. Analysis of hybrid systems, *Ind. Chem. Eng. Res.*, **38**, 1649-1665.
- Van Gulijk, C. (1998) Using computational fluid dynamics to calculate transversal dispersion in a structured packed bed, *Comput. Chem. Eng.*, **22**, S767-S770
- Van Hasselt, B., 1999, The three-levels-of-porosity reactor, Ph.D. dissertation in Chemical Engineering, Delft University of Technology
- Hauan, S., Hertzberg, T. and Lien, K.M. (1995) Why Methyl-*tert*-butyl-ether production by reactive distillation may yield multiple solutions, *Ind. Chem. Eng. Res.*, **34**, 987-991
- Hearn, D. (1993) U.S. Patent 5266546: Catalytic distillation machine
- Higler A.P., Taylor, R. and Krishna, R. (1998) Modeling of a reactive separation process using a nonequilibrium stage model, *Comput. Chem. Engng.* **22**, Supplement, S111 - S118
- Higler, A., Taylor, R. and Krishna, R., (1999a) Nonequilibrium Modelling of Reactive Distillation: Multiple steady states in MTBE synthesis, *Chem. Eng. Sci.*, **54**, 1389-1395
- Higler A.P., Taylor, R. and Krishna, R. (1999b) The influence of mass transfer and liquid mixing on the performance of reactive distillation tray column, *Chem. Eng. Sci.*, **54**, 2873-2881
- Higler, A., Krishna, R., Ellenberger, J. and Taylor, R., (1999c) Counter-current operation of a structured Catalytically Packed Bed Reactor: Liquid phase mixing and mass transfer, *Chem. Eng. Sci.*, in press
- Higler, A., Krishna, R. and Taylor, R. (1999d) A nonequilibrium cell model for multicomponent (reactive) separation processes, *A.I.Ch.E.J.*, **45**, 2357-2370
- Higler, A., Krishna, R. and Taylor, R. (1999e) A non-equilibrium cell model for packed distillation columns. The influence of maldistribution, *Ind.Eng.Chem. Res.*, **38**, 3988-3999
- Higler, A., Krishna, R. and Taylor, R. (2000a) Non-equilibrium modelling of reactive distillation: A dusty fluid model for heterogeneously catalysed processes, *Ind.Eng.Chem. Res.*, accepted
- Higler, A., Krishna, R. and Taylor, R. (2000b) Non-equilibrium modelling of reactive distillation: The influence of maldistribution, *Ind.Eng.Chem. Res.*, under review
- Hofhuis P.A.M, Zuiderweg F.J., 1979, Sieve plates: dispersion density and flow regimes. *Inst. Chem. Engrs. Symp. Series No 56*, pp. 2.2/1 – 2.2/26.
- Jacobs, R. and Krishna, R. (1993) Multiple Solutions in reactive distillation for methyl-*tert*-butyl ether synthesis, *Ind. Eng. Chem. Res.* **32**, 1706 - 1709

- Johnson, K.H. (1993) U.S. Patent 5189001: Catalytic distillation structure,
- Johnson, K.H. and Dallas, A.B. (1994) U.S. Patent 5348710: Catalytic distillation structure
- Jones, E.M., Jr. (1985) Contact structure for use in catalytic distillation, U.S. Patent 4536373
- Jones, E.M., Jr. (1992) U.S. Patent 5130102: Catalytic distillation reactor
- Jones, E.M., Jr. (1992) Distillation column reactor, European Patent 0 402 019 A3
- Kooijman, H.A. (1995) Dynamic Nonequilibrium Column Simulation, Ph.D. Dissertation, Clarkson University, Potsdam, USA.
- Kooijman, H.A. and Taylor, R. (1995) A Dynamic Nonequilibrium Model of Tray Distillation Columns, *AIChEJ*, **41**, 1852-1863
- Kreul, L.U., Gorak, A., Dittrich, C. and Barton, P.I. (1998) Dynamic catalytic distillation: Advanced simulation and experimental validation, *Comput. Chem. Engng.* **22**, S371-S378
- Kreul, L.U., Gorak, A., and Barton, P.I. (1999) Dynamic rate-based model for multicomponent batch distillation, *AIChE J.*, **54**, 1953-1962
- Krishna, R. and Sie, S.T. (1994) Strategies for Multiphase Reactor Selection, *Chem. Engng Sci.*, **49**, 4029-4065
- Krishna, R. and Wesselingh, J.A. (1997) The Maxwell-Stefan Approach to Mass Transfer, *Chem. Eng. Sci.*, **52** 861-911
- Krishna, R., Van Baten, J.M., Ellenberger, J., Higler, A.P. and Taylor, R. (1999) CFD simulations of sieve tray hydrodynamics, *Chem. Eng. Research & Design, Trans.I.Chem.E.*, **77**, 639 - 646
- Krishnamurthy, R. and Taylor, R. (1985) Nonequilibrium stage model of multicomponent separation processes, *A.I.Ch.E.J.*, **32**, 449 - 465
- Kröner, A, Marquardt, W, and Gilles, E.D. (1997), Getting around consistent initialization of DAE systems?, *Comput. Chem. Eng.*, **21**, 145 - 158
- Kubicek, M., (1976) Algorithm 502, dependence of a solution of nonlinear systems on a parameter., *ACM Trans. Math. Softw.* **2**, 98-107.
- Kumar, A. and Daoutidis, P. (1999) Modeling, analysis and control of ethylene glycol reactive distillation column, *A.I.Ch.E.J.*, **45**, 51 - 68
- Lee J.H. and Dudukovic, M.P., (1998) A comparison of the equilibrium and nonequilibrium models for a multicomponent reactive distillation column, *Comput. Chem. Eng.*, **23**, 159-172
- Lebens, P.J.M., Kapteijn, F., Sie, S.T., and Moulijn, J.A. (1999) Potentials of internally finned monoliths as a packing for multifunctional reactors, *Chem. Eng. Sci.*, **54**, 1359 – 1365
- Lockett, M.J. (1986) Distillation tray fundamentals, Cambridge University Press, Cambridge, UK.
- Majer, C, Marquardt, W, and Gilles, E.D. (1995), Reinitialization of DAE's after discontinuities, *Comput. Chem. Eng.*, **19**, S507 – S512
- Marion, M.C., Viltard, J.C., Travers, P., Harter, I., Forestiere, A. (1998) U.S. Patent 5776320: Process and apparatus for reactive distillation with a particular distribution of liquid and vapour phases
- Mattsson, S.E. and Sönderlind, G (1993) Index-reduction using dummy derivatives, *SIAM J. Sci. Statist. Comput.*, **14**, 677-692 .

- Michelsen, M. (1976) An efficient general purpose method of integration of stiff ordinary differential equations, *A.I.Ch.E.J.*, **22**, 594-597 .
- Mohl, K.D., Kienle, A., and E.D. Gilles (1998) Multiple steady states in a reactive distillation column for the production of the fuel ether TAME I. Theoretical Analysis, *Chem. Eng. Technol.*, **21**, 133-136
- Mohl, K.D., Kienle, A., Gilles, E.D., Rapmund, P., Sundmacher, K. and Hoffmann, U., (1999), Steady-state multiplicities in reactive distillation columns for the production of fuel ethers MTBE and TAME: theoretical analysis and experimental verification, *Chem. Eng. Sci.* **54**, 1029-1043
- Moe H.I., Hauan, S., Lien, K.M., and Hertzberg, T. (1995) Dynamic model of a system with phase and reaction equilibrium, *Comput. Chem. Eng.*, **19**, S513-S518
- Moritz, P. and Hasse, H. (1999) Fluid dynamics in reactive distillation packing Katapak[®]-S, *Chem. Eng. Sci.*, **54**, 1367-1374
- Nijhuis, S.A., Kerkhof, F.P.J.M. and Mak, A.N.S. (1993) Multiple steady states during reactive distillation of Methyl-*tert*-butyl-ether., *Ind. Eng. Chem. Res.* **32**, 2767 - 2774
- Nocca, J.L., J. Leonard, J.F. Gaillard, and P. Amigues (1989) Process for manufacturing a tertiary alkyl ether by reactive distillation, U.S. Patent 4847431
- Nocca, J.L, Leonard, J., Gaillard, J.F., Amigues, P. (1991) U.S. Patent 5013407: Apparatus for reactive distillation
- Onda, K., Takeuchi, H. and Okumoto, Y., (1968) Mass transfer coefficients between gas and liquid phases in packed columns, *J. Chem. Eng. Japan*, **1**, 56-62.
- Pelkonen, S., Kaesemann, R. and Gorak, A., (1997), Distillation lines for multicomponent separation in packed columns: Theory and comparison with experiments, *Ind. Eng. Chem. Research*, **36**, 5302-5398.
- Pelkonen, S., Gorak, A. and Ohligschläger, A, (1999), Experimental study on multicomponent distillation in packed columns, *Chemical Engineering and Processing*, under review
- Pelkonen, S., Gorak, A., Kooijman, H.A., and Taylor, R. (1997) Operation of a Packed Distillation Column: Modelling and Experiments distillation, *Distillation and Absorption '97, I. Chem. E. Symp. Ser.*, **142**, 269-277
- Perez-Cisneros, E., Schenk, M., Gani, R., and Pilavachi, P.A. (1996) Aspects of simulation, design and analysis of reactive distillation operations, *Comput. Chem. Eng.*, **20**, S267 - S272
- Perez-Cisneros, E., Gani, R. and Michelsen, M.L. (1997a) Reactive separation systems. Part I: Computation of physical and chemical equilibrium, *Chem. Eng. Sci.*, **52**, 527-543
- Perez-Cisneros, E., Schenk, M., and Gani, R. (1997b) A new approach to reactive distillation simulation, *Distillation and Absorption '97, I. Chem. E. Symp. Ser.*, **142**, 715-724
- Pilavachi, P.A., Schenk, M., Perez-Cisneros, E. and Gani, R. (1997) Modeling and simulation of reactive distillation operations, *Ind. Eng. Chem. Res.*, **36**, 3188-3197
- Podrebarac, G.G., Ng, F.F.T, and Rempel, G.L. (1998a) The production of diacetone alcohol with catalytic distillation – Part I: Catalytic distillation experiments, *Chem. Eng. Sci.*, **53**, 1067-1075

- Podrebarac, G.G., Ng, F.F.T, and Rempel, G.L. (1998b) The production of diacetone alcohol with catalytic distillation – Part II: A rate-based catalytic distillation model for the reaction zone, *Chem. Eng. Sci.*, **53**, 1077-1088
- Rapmund, P., Sundmacher, K. and Hoffmann, U., (1998), Multiple steady states in a reactive distillation column for the production of the fuel ether TAME part II: Experimental validation, *Chemical Engineering and Technology*, **21**, 136 - 139
- Rehfinger, A. and Hoffmann, U., (1990a) Kinetics of methyl-*tert*-butyl ether liquid phase synthesis catalyzed by ion exchange resin. I - Intrinsic rate expression in liquid phase activities, *Chem. Eng. Sci.*, **45**, 1605 - 1616
- Rehfinger, A. and Hoffmann, U., (1990b) Kinetics of methyl-*tert*-butyl ether liquid phase synthesis catalyzed by ion exchange resin, II - Macropore diffusion of MeOH as rate controlling step. *Chem. Eng. Sci.*, **45**, 1619 - 1626
- Reid, R.C., Prausnitz, J.M. and Poling, B.M., The properties of gases and liquids, Fourth Edition, McGraw-Hill, New York (1988)
- Roat, S.D., Downs, J.J., Vogel, E.F., and Doss, J.E. (1986) The integration of rigorous dynamic modeling and control system synthesis for distillation columns: an industrial approach, in *Chemical Process Control – CPC III*, Morari, M. and McAvoy, T.J. (Eds.) Elsevier, New York
- Ronge, G., 1995, Überprüfung unterschiedlicher Modelle für den Stoffaustausch bei der Rektifikation in Packungskolonnen. Fortschritt-Berichte VDI Verfahrenstechnik No. 390, Düsseldorf.
- Ruiz, C.A., M.S. Basualdo and N.J. Scenna (1995), Reactive distillation dynamic simulation, *Chem. Eng. Res. & Design., Trans.I.Chem.E. Part A*, **73**, 363 - 378
- Sawistowski, H and P.A. Pilavakis (1979), Distillation with chemical reaction in a packed column. *I.Chem.E Symp Series No. 56*, 49 - 63.
- Savkovic-Stevanovic, J. (1982) Mathematical model of unsteady state distillation column with association reaction, *Proc. 3rd Austrian-Italian-Yugoslav Congress on Chemical Engineering*, Graz, Austria, **I**, 326-332
- Scenna, N.J., Ruiz, C.A. and Benz, S.J., (1998) Dynamic simulation of startup procedures of reactive distillation columns, *Comput. Chem. Engng.* **22**, S719-S722
- Schrans, S., S. de Wolf and R. Baur (1996), Dynamic simulation of reactive distillation, An MTBE case study, *Comput. Chem. Eng.*, **20**, Supplement, S1619 - S1624
- Seader, J.D. and Henley, E.J. (1998) Separation process principles, John Wiley, New York.
- Shoemaker, J.D. and E.M. Jones (1987), Cumene by catalytic distillation, *Hydrocarbon Processing*, June 1987, 57 - 58
- Siirola, J.J. (1995) An Industrial Perspective on Process Synthesis, *A.I.Ch.E. Symposium Series No. 304*, **91**, 222 - 233
- Simandl, J. and W.Y. Svrcek (1991), Extension of the simultaneous solution and inside-outside algorithms to distillation with chemical reactions, *Comput. Chem Engng.*, **15**, 337 - 348
- Smith Jr., L.A. (1984) U.S. Patent 4443559: Catalytic distillation structure
- Smith Jr., L.A. (1985) European Patent 008860B1: Catalytic distillation process and catalyst

- Sneesby, M.G., Tadó, M.O., Datta, R., and Smith, T.N. (1997a) ETBE synthesis via reactive distillation. 1. Steady-state simulation and design aspects, *Ind. Eng. Chem. Res.*, **36**, 1855-1869
- Sneesby, M.G., Tadó, M.O., Datta, R. and Smith, T.N. (1997b) ETBE synthesis via reactive distillation. 2. Dynamic simulation and control aspects, *Ind. Eng. Chem. Res.*, **36**, 1870-1881
- Sneesby, M.G., Tadó, M.O., Datta, R. and Smith, T.N. (1997c) ETBE synthesis via reactive distillation. 2. Dynamic simulation and control aspects, *Ind. Eng. Chem. Res.*, **36**, 1870-1881
- Sneesby, M.G., Tadó, M.O., Datta, R. and Smith, T.N. (1998a) Detrimental influence of excessive fractionation on reactive distillation, *A.I.Ch.E.J.*, **44**, 388-393
- Sneesby, M.G., Tadó, M.O., and Smith, T.N. (1998d) Steady-state transitions in the reactive distillation of MTBE, *Comput. Chem. Eng.*, **22**, 879-892
- Sneesby, M.G., Tadó, M.O., and Smith, T.N. (1998c) Multiplicity and pseudo-multiplicity in MTBE and ETBE reactive distillation, *Chem.Eng. Res. Des.*, **76** 525-531
- Stichlmair, J.G. and Fair, J.R. (1998) *Distillation Principles and Practice*, Wiley-VCH, New York
- Stichlmair, J.G. and Frey, T., 1999, Reactive distillation processes, *Chemical and Engineering Technology*, **22**, 95-103
- Stringaro, J.P. (1991) European Patent 433222A1: Reactor including a catalyst body for performing a heterogeneous reaction
- Stringaro, J.P. (1995) U.S. Patent 5470542: Catalyzing fixed bed reactor
- Subawalla, H., Gonzalez, J.C., Seibert, A.F., and Fair, J.R. (1997) Capacity and Efficiency of Reactive Distillation Bale Packing: Modeling and Experimental Validation, *Ind. Eng. Chem. Res.*, **36**, 3821-3832
- Sundmacher, K. and Hoffmann, U. (1994), Multicomponent mass transfer and energy transport on different length scales in a packed reactive distillation column for heterogeneously catalyzed fuel ether production, *Chem. Eng. Sci.* **49**, 4443 - 4464
- Sundmacher, K (1995) Reaktivdestillation mit katalytischen fuellkoerperpackungen - ein neuer Process zur Herstellung der Kraftstoffkomponente MTBE, Ph.D thesis, Universität Clausthal
- Sundmacher, K., Hoffmann. U., (1996) Development of a new catalytic distillation process for fuel ethers via a detailed nonequilibrium model, *Chem. Eng. Sci.* **51**, 2359-2368
- Sundmacher, K., Uhde , G. and Hoffmann, U., (1999) Multiple reactions in catalytic distillation processes for the production of the fuel oxygenates MTBE and TAME: Analysis by rigorous model and experimental validation, *Chem. Eng. Sci.* **54**, 2839-2847
- Suzuki, I., Yagi, H., Komatsu, H., and Hirata, M. (1971) Calculation of multicomponent distillation accompanied by chemical reaction, *J. Chem. Eng. Jap.*, **4**, 26-33
- Taylor, R. and Krishna, R. (1993) *Multicomponent mass transfer*, John Wiley, New York.
- Taylor, R., Kooijman, H.A., and Hung, J.S. (1994) A second generation nonequilibrium model for computer simulation of multicomponent separation processes, *Comput. Chem. Engng.* **18**, 205 - 217

- Towler, G.P. and Frey, S.J. (2000) Reactive Distillation, Chapter 2 in *Reactive Separation Processes* (ed. S. Kulprathipanja), Taylor & Francis, Philadelphia
- Trambouze, P., 1990, Countercurrent two-phase flow fixed bed catalytic reactors, *Chem. Eng. Sci.*, **45**, 2269-2275
- Wayburn, T.L., and Seader, J.D., (1987) Homotopy continuation methods for computer aided process design, *Comput. Chem. Engng.* **11**, 7 - 25
- Xu, X., Zhao, Z. and Tian, S.-J. (1997) Study on catalytic distillation processes, Part III. Prediction of pressure drop and holdup in catalyst bed, *Chem. Eng. Res. & Design., Trans.I.Chem.E. Part A*, **75**, 625 – 629.
- Xu, X., Zhao, Z., and Tian, S. (1999) Study on catalytic distillation processes, Part IV: Axial dispersion of liquid in catalyst bed of catalytic distillation column, *Chem. Eng. Res. & Design, Trans. I. Chem. E. Part A*, **77**, 16-20
- Zheng, Y. and Xu, X. (1992a) Study on catalytic distillation processes, Part I: Mass transfer characteristics in catalyst bed within the column, *Chem. Eng. Res. & Design, Trans. I. Chem. E. Part A*, **70**, 459-46
- Zheng, Y. and Xu, X. (1992b) Study on catalytic distillation processes, Part II: Simulation of catalytic distillation processes, Quasi homogeneous and rate based model, *Chem. Eng. Res. & Design, Trans. I. Chem. E. Part A*, **70**, 465-470
- Zuideweg, F.J. (1982) Sieve trays - A view on the state of art. *Chem. Eng. Sci.* **37**, 1441-1461

